FINAL TECHNICAL REPORT

EQUIPMENT SPECIFICATION FOR A SPACE RATED RADAR ALTIMETER

By

T. W. Godbey
B. N. Keeney
W. J. Kelly
F. H. Klauser
L. A. McLaren
W. A. Reynolds
S. L. Slusarczyk

January 1969

Prepared under Contract No. NAS 12-683 by
AEROSPACE ELECTRONICS
GENERAL ELECTRIC COMPANY
Utica, New York

Electronics Research Center
NATIONAL AERONAUTICS AND SPACE ADMINISTRATION

ERRATA SHEET

FINAL TECHNICAL REPORT

FTR

EQUIPMENT SPECIFICATION FOR A SPACE RATED RADAR ALTIMETER

PREPARED UNDER CONTRACT NO. NAS 12-683 by

AEROSPACE ELECTRONICS

GENERAL ELECTRIC COMPANY

UTICA, NEW YORK

18 MARCH 1969

NI

PAGE	LOCATION	CORRECTION
49	Table IX	Line 1, Column 2: S/B Pulse Rate/Pulse Width Line 2, Column 2: S/B (PPS/N sec)
55	Figure 16	COVER MRG. HOLES: S/B COVER MTG. HOLES (abbreviation for mounting)
A-2	Last equation	$\frac{1}{\frac{1+h}{r_e}}$ S/B $\frac{1}{1+\frac{h}{r_e}}$
A-7	Figure A-5	First equation S/B $A(t') = \pi ct'h \left(\frac{1-ct'}{4h}\right)\left(\frac{1}{1+h/r_e}\right)$
A-7	Figure A-5	Third equation S/B $A(nT) = \pi cTh \left(1-\frac{2cT}{h}\right)\left(\frac{1}{1+h/r_e}\right)$
B-6	Figure B-2	$N_0 N_R$ S/B $\frac{N_0}{N_R}$
D-5	Figure D-2	Seventh line down, AGG S/B AGC
	Figure D-3	Fourth line, AGG S/B AGC
D-7	Figure D-6	Last line, 40 N SEC/CM S/B 20 N SEC/CM
D-9	Fourth line down	40 SEC/CM S/B 40 N SEC/CM
D-10	Third line down	50 PU.SES S/B 50 PULSES
	Fourth line down	40 SEC/CM S/B 40 N SEC/CM

PAGE	LOCATION	CORRECTION
E-6	Figure E-1	VAGC appearing on ordinate scale S/B Vagc
	Figure E-2	Ordinate scales S/B $+\frac{Vagc}{2}$ and $-\frac{Vagc}{2}$
E-7	Figure E-3	VAGC S/B Vagc
	Figure E-4	The ordinate scales should be $+\frac{Vagc}{3}$ and $-2\ \frac{Vagc}{3}$
E-8	Figure E-5	VAGC S/B Vagc
F-2		Equation F-3 S/B $\sigma = \pi R^2\theta^2 \frac{cT_p}{2} \sum_1 \sigma_i$

ADD PAGE F-8 ATTACHED

REFERENCES

1. M. I. Skolnik, Introduction to Radar Systems, McGraw-Hill, New York, New York. 1962

2. D. K. Barton, Radar System Analysis, Prentice-Hall, Englewood Cliffs, New Jersey. 1964

3. A Benoit, "Signal Attenuation Due to Neutral Oxygen and Water Vapor, Rain and Clouds", Microwave Journal, Horizon House, Dedham, Mass. November, 1968.

Gerald L. Pucillo

Technical Monitor

NAS 12-683

Electronics Research Center
575 Technology Square
Cambridge, Massachusetts 02139

Requests for copies of this report should be referred to:

NASA Scientific and Technical Information Facility
P. O. Box 33, College Park, Maryland 20740

FINAL TECHNICAL REPORT

EQUIPMENT SPECIFICATION FOR A SPACE RATED RADAR ALTIMETER

By

T.W. Godbey
B.N. Keeney
W.J. Kelly
F.H. Klauser
L.A. McLaren
W.A. Reynolds
S.L. Slusarczyk

January 1969

Prepared under Contract No. NAS 12-683 by
AEROSPACE ELECTRONICS
GENERAL ELECTRIC COMPANY
Utica, New York

Electronics Research Center
NATIONAL AERONAUTICS AND SPACE ADMINISTRATION

TABLE OF CONTENTS

Section		Page
1.0	SUMMARY	1
2.0	INTRODUCTION	3
3.0	SYMBOLS	5
4.0	RECOMMENDED EQUIPMENT SPECIFICATIONS	9
5.0	TECHNICAL DESCRIPTION	19
5.1	The Ocean Model	19
5.2	The Signal Detection Problem	20
5.2.1	Averaging	21
5.2.2	Pulse width	21
5.2.3	Accuracy	21
5.2.4	Detectors	22
5.2.5	Waveform distortion	22
5.2.6	Range processors	22
5.2.7	Acquisition	23
5.2.8	Candidate designs	24
5.3	High Speed Counters	27
5.4	Synthesized Designs	28
5.4.1	Transmitters	33
5.4.2	Duplexer	40
5.4.3	Preamplifier	41
5.4.4	Detector and range tracker	41
5.4.5	Local oscillator and IF amplifier	46

TABLE OF CONTENTS (Continued)

Section		Page
5.4.6	AFC and AGC	46
5.4.7	Reference frequency synthesizer	47
5.4.8	Power supply and power budget	47
5.5	Output Data Requirements	47
5.5.1	Altitude data	47
5.5.2	Housekeeping data	51
5.6	Mechanical Design	52
5.6.1	Structural	52
5.6.2	Component packaging	54
5.6.3	Module description	54
5.6.4	Vehicle mounting	56
5.6.5	Environmental performance	[illegible]
5.6.6	Vibration	57
5.6.7	Shock	57
5.6.8	Thermal	58
5.6.9	Pressure	58
5.6.10	Other environments	59
5.6.11	Summary	59
6.0	REFERENCES	61
7.0	BIBLIOGRAPHY	63
Appendix		
A	THE CHARACTERISTIC OCEAN RADAR RETURN AT SATELLITE ALTITUDES	A-1
B	THE OCEAN RADAR RETURN NOISE CHARACTER AND SIGNAL PROCESSING	B-1

TABLE OF CONTENTS (Continued)

Appendix		Page
C	PROPAGATION ERRORS	C-1
D	SEA RETURN PULSE SIMULATOR	D-1
E	EARLY/LATE GATE TRACKING	E-1
F	METEOROLOGICAL ECHOES AND ATTENUATION	F-1

LIST OF ILLUSTRATIONS

Figure		Page
1	MECL High Frequency Counter	29
2	High Frequency Counter Test Configuration	30
3	MECL Operation Profiles	31
4	High Frequency Counter Waveforms	32
5	Pulse Radar Altimeter Block Diagram	34
6	Magnetron Transmitter (High and Low Power)	35
7	Traveling Wave Tube Transmitter (High Power)	35
8	TWT Transmitter (Low Power For High Repetition Rate)	35
9	CFA Transmitter	36
10	Chirp Transmitter	36
11	Early/Late Gate Tracking Loop	43
12	Threshold Tracking Loop	44
13	Voltage Controlled Oscillator Tracking Loop	45
14	Power Supply Block Diagram	48
15	Radar Altimeter Isometric View	53
16	Radar Altimeter - Cover Removed	55

LIST OF ILLUSTRATIONS (Continued)

Figure		Page
A-1	Radar Power Return From a Flat, Lambertian Scattering Ocean	A-4
A-2	Geometry of Radar Target Area, A(t), Build Up as a Function of Time, t, from Radar Transmission	A-5
A-3	Characteristic Radar Altimeter Return From Flat, Lambertian Scattering Ocean (Square Law Detection No AGC)	A-6
A-4	Characteristic Radar Altimeter Return From Flat, Lambertian Scattering Ocean (Envelope Detection No AGC)	A-6
A-5	Geometry of Satellite Radar Altimeter Return From Spherical Ocean Surface	A-7
A-6	Characteristic Radar Altimeter Return From Spherical Lambertian Scattering Ocean (Square Law Detection, No AGC)	A-8
A-7	Characteristic Radar Altimeter Return From Spherical Lambertian Scattering Ocean (Envelope Detection, No AGC)	A-8
A-8	Characteristic Radar Altimeter Return From Spherical Lambertian Scattering Ocean (Square Law Detection, AGC On Return)	A-9
A-9	Characteristic Radar Altimeter Return From Spherical Lambertian Scattering Ocean (Envelope Detection, AGC On Return)	A-9
A-10	Illustration of Real Ocean as a Radar Scattering Cross Section Generator	A-10
A-11	Probability Density Function of Sea Area (S) as a Function of Distance (Z) From Mean Sea Level for a Significant Wave Height $H_{1/3}$	A-11

LIST OF ILLUSTRATIONS (Continued)

Figure		Page
A-12	Effect of Large Sea State ($H_{1/3}$ = 55 ft) Upon Transmitted Pulse Width for Square Law Detected Sea Returns	A-12
B-1	Probability Density Functions of Noise and Signal Plus Noise (Envelope Detection) The Classical Radar Problem	B-5
B-2	Probability Density Functions of Noise and Ocean Return Plus Noise (Envelope Detection) the Satellite Radar Altimeter Problem	B-6
D-1	Sea Return Pulse Simulator Block Diagram	D-4
D-2	Detector Output (No Bias)	D-5
D-3	Detector Output (No Bias)	D-5
D-4	Detector Output (No Bias)	D-6
D-5	Detector Output (With Bias)	D-6
D-6	Detector Output (With Bias)	D-7
D-7	Integrator Output	D-7
D-8	Threshold Circuit Output	D-8
D-9	Threshold Circuit Output	D-8
D-10	Square Law Detector Output Waveforms - N_o/N_r = 30 db	D-9
D-11	Square Law Detector Output Waveforms - N_o/N_r = 20 db	D-9
D-12	Square Law Detector Output Waveforms - N_o/N_r = 10 db	D-10
E-1	Characteristic Ocean Return with Square Law Detection Low Sea State (Solid Line) High Sea State (Dashed Line)	E-6

LIST OF ILLUSTRATION (Continued)

Figure		Page
E-2	Early/Late Gate Control Function Square Law Detection Low Sea State (Solid Line) High Sea State (Dashed Line)	E-6
E-3	Characteristic Ocean Return with Envelope Detection Low Sea State (Solid Line), Sea States from $H_{1/3}$ = 3 to 18.5 Meters (Dashed Line)	E-7
E-4	Early/Late Gate Control Function, Envelope Detection Low Sea State (Solid Lines), High Sea State $H_{1/3}$ = 18.5 Meters (Dashed Lines)	E-7
E-5	Effect of Sea State Up to $H_{1/3}$ = 18.5 Meters on Early/ Late Gate, Envelope Detection Control Function Zero Crossing Point	E-8
E-6	Average Volt - nsec Energy in Sea State Gate Versus Significant Wave Height ($H_{1/3}$) in Meters	E-9
F-1	Geometry of the Ocean Return	F-5
F-2	Cross Section of the Volume of the Resolution Cell for a Storm Return	F-6
F-3	Return from a Heavy Storm Center	F-7

LIST OF TABLES

Table		Page
I	Equipment Specification, Space Rated Radar Altimeter Type 1 (Unambiguous PRF)	11
II	Error Budget (1 Sigma in Meters) Space Rated Radar Altimeter Type 1 (Unambiguous PRF)	13
III	Equipment Specification, Space Rated Radar Altimeter Type 2 (Ambiguous PRF)	14
IV	Error Budget (1 Sigma in Meters) Space Rated Radar Altimeter Type 2 (Ambiguous PRF)	15
V	Equipment Specification, Space Rated Radar Altimeter Type 3 (Ambiguous PRF)	16
VI	Error Budget (1 Sigma in Meters) Space Rated Radar Altimeter Type 3 (Ambiguous PRF)	17
VII	Candidate Designs Characteristics	25
VIII	Transmitter/Modulator Configurations	38
IX	Power Budget	49
X	Size, Weight and Power Characteristics	56

ACKNOWLEDGEMENTS

During this study and over the past several years we have been encouraged and supported by many people. The most significant and continuous contributions have come from a variety of sources.

Professor R. K. Moore and his many associates who over the years have contributed much to the special literature of radar returns at vertical incidence from all manner of terrain.

Professor W. J. Pierson, whose special competence in the accurate prediction of sea state from apparently inadequate data, gives us daily proof of the power of a good theory properly applied and inspires us to obtain accurate synoptic coverage of all oceans so that this benefit can be extended to all mankind.

Professor W. S. von Arx, whose measurement of the profile across the Puerto Rico Trench gave us the first real evidence of the kind of geoidal feature which must be eventually measured and mapped.

Dr. C. A. Lundquist, who showed how altitude data fit easily and naturally into present geodetic data reduction programs, specified upper bounds on altitude accuracy requirements for geodesy, and provided information, insight and encouragement when it was needed.

Dr. Gordon de Quincy Robin, Director of Scott Polar Research Institute, Cambridge, England, one of the first scientists to request altimeter data from satellites and a continuing supporter of all satellite altimeter proposals.

Professors J. V. Harrington and E. J. Frey, who with Professor W. S. von Arx, studied in depth the ultimate limitations on satellite altimetry, and proposed ways by which this ultimate might be obtained.

General acknowledgement is due all of the oceanographers, geodesists, radar and laser instrumentation scientists who have demonstrated by their concern, studies, committee activities and publications their continuing interest and the genuine need for accurate altitude data from satellites.

Finally, a study of the comparative merits of Laser versus Radar altimetry for satellite application has recently been completed by the Raytheon Company for NASA.

This study was conducted with the help of many contributors from various departments of the General Electric Company. The major contributors were William J. Kelly, Thomas W. Godbey and Fred H. Klauser. Mr. Kelly performed most of the technical analysis, directed the circuit design and test evaluation effort during the study and also wrote most of the technical material in this report. T.W. Godbey prepared the material on the ocean model and related subjects, the equipment specifications and error budgets and with Mr. Kelly selected the recommended design and wrote all the associated material. F.H. Klauser managed the study effort and organized and edited this final report.

Able assistance in the areas of analysis, circuit design, test evaluation, vendor surveys and report writing was provided by Messrs. B.N. Keeney, L.A. McLaren, W.A. Reynolds, S.L. Slusarczyk, M.L. Marietta and F.K. Paul.

1.0 SUMMARY

This report presents three Equipment Specifications which describe the capabilities of altimeters suitable for the Geos C Mission, as it is understood by the General Electric Company. The fact that three designs were synthesized to meet the mission requirements emphasizes the conclusion that the construction of an altimeter suitable for orbital use over ocean is feasible.

Calculations presented in the body of this report indicate that an ultimate accuracy on the order of one meter is feasible for altitudes up to 850 nautical miles for the Geos C Mission. In addition useful measurement of sea state can be obtained employing both AGC and sea state gate information in the altimeter receiver. This has been achieved with designs that consume a maximum power of 34 watts, weigh a maximum of 26 pounds, and otherwise meet the restrictions of the Geos C spacecraft.

Analysis of the altimeter performance over ocean was greatly enhanced through laboratory tests of receiver circuits using the Sea Return Pulse Simulator, devised during this study. The simulator also served to provide a valuable human insight into the signal detection problem faced by the altimeter.

The weakest link in the altimeter designs, from a reliability point of view, is the transmitter tubes which have an unproven life beyond 500 or 1000 hours. Reliability calculations, based on generic type components, indicate an expected probability of success of .9 for three months altimeter operation with 30% duty cycle.

Consequently it is recommended that a transmitter tube evaluation be undertaken before, or in parallel with, an altimeter development, to gather more concrete data on expected performance.

It is also recommended that the high altitude, over ocean aircraft tests, presently being explored by NASA, be carried out to gain confidence in the ultimate performance of a spaceborne altimeter.

2.0 INTRODUCTION

The purpose of this report is to present a Space Rated Radar Altimeter Equipment Specification capable of development within an elapsed time of one year. The study results are a result of experience gained over the past seven years analyzing and devising altimeter designs for use in space systems. This experience was applied to a study of the specific Geos C problem, from July to December of 1968, for the Electronics Research Center of the National Aeronautics and Space Administration.

The one year delivery restriction evolved from the tentative program planning schedule information for Geos C, supplied by Mr. Jerome Rosenberg, NASA's Geos Program Manager.

A detailed examination of all the parameters affecting the design of an over ocean satellite altimeter is presented in Section 5.0 of this report.

The design bounds imposed to restrict the final choices were:

1. A maximum weight of 25 pounds.

2. A maximum volume and form factor dictated by the space available from the removal of an optical beacon from the Geos B spacecraft design.

3. An average power of 35 watts.

4. A maximum energy drain of 72 watt hours during a single operating interval.

5. A delivery time, for a flight model, of one year after receipt of an order.

The equipment specifications for the candidate designs essentially meet all of the above criteria. In some cases encouraging prospects, such as the chirp modulation approach, were dismissed because of the limit imposed by the expected delivery time. Some of the high peak power designs considered were eliminated because of power and weight limitations.

Hence it is essential that the candidate design choices be reexamined if any of the bounds are changed.

Equipment Specifications for three candidate designs are presented in Section 4.0 of this report, along with the associated error budgets. Justification for the conclusions reached in the equipment specifications are found in the Technical Description, Section 5.0, and in the appendices. The Technical Description is organized to concur with the work items outlined in the study Work Statement.

In conducting the study, a mathematical analysis of the ocean model and the signal detection problem was made to define the parameters affecting the altimeter design. As a result, a number of candidate designs were defined, based mostly upon mathematical considerations. An in depth design study was then made to fit the components, characteristics and capabilities of the real world to the candidate design requirements. The results are the synthesized designs, discussed in Section 5.4. Particular problems common to all designs are discussed in Section 5.3 and 5.5 titled High Speed Counters and Output Data Requirements respectively.

The design requirements outlined in the Recommended Equipment Specifications result from applying the five design bounds to the Synthesized Designs.

During the course of the study a Sea Return Pulse Simulator was devised, designed and built, using components and equipment available in the laboratory. This simulator, described in detail in Appendix D, generates a controllable noise spectrum which approximates the noise type signal expected from the ocean return. Various ocean return pulse signal to receiver noise ratios were applied to candidate receiver designs to determine performance under near actual conditions. As a result the receiver design approaches suggested were authenticated under simulated ocean return conditions as well as by mathematical analysis. Photographs shown in Appendix D visually present the noisy return signal expected from the ocean. Some of the statistics used in the analysis were derived from these and similar photographs of laboratory tests.

Finally, much of the information presented in this final report has already been presented in the August, September, October, and November 1968 Monthly Reports already submitted as part of this study. It will be found that some items studied, such as chirp radar, are treated in greater depth in the Monthly Reports, because they were disqualified from consideration under the ground rules of the study. As a result, they were not emphasized in this report.

3.0 SYMBOLS

A	Unit Surface Area
A_T	Ocean Area Intercepted
B_n	Receiver Noise Bandwidth
C	Ocean Surface Correlation Distance
E	RMS Ocean Surface Deviation from the Mean
E_y	Young's Modulus
F_e	Emissivity Factor
F_a	View Factor
G	Antenna Gain
G_{CF}	Control Function Gain at and Near Zero Error Position
$H_{1/3}$	Ocean Significant Waveheight
K	Boltzmann's Constant
L	Radar System Losses
$M(\ )$	Mean of a Rayleigh Noise Distribution ( )
N	Any Integer
N_o	Ocean Return Signal
N_r	Receiver Noise Power
P_R	Peak Power Received
P_T	Peak Transmitted Power

Q	Power Dissipation
R	One Way Radar Range
$S^2(\ )$	Variance of a Rayleigh Noise Distribution ( )
S	Sine Wave Signal
T_c	Temperature of Ambient Surroundings
T_e	Effective Receiver Noise Temperature
T_g	Early/Late Gate Pulse Width
T_p	Pulse Width
T_r	Temperature of Radiating Surface
V_R	Detector Output Signal
$V(t')$	Ocean Return, an Increasing Function of Time
V_{agc}	Detected Signal Standard Deviation
a_k	Normally Distributed Constant with a Mean of Zero and a Variance of One
a	Base Plate Width
b_k	Normally Distributed Constant with a Mean of Zero and a Variance of One
c	Speed of Light
d	Base Plate Thickness
e	Natural Logarithm Base
f_n	Resonant Frequency
f_p	Shock Pulse Frequency
h	Altitude

n	A Real Number, Greater than 1, Determined by the Antenna Beamwidth for the Pulse Width Limited Return Case
$p(\ )$	Probability Density Function of ( )
r_e	Earth Radius
t'	Time Measured from t_o
t_r	Rise Time of the Shock Pulse
t	Time Measured from Start of Transmitted Pulse
t_o	Time of Start of Ocean Reflected Pulse
x	Linearly Detected Signal
y	Square Law Detected Signal
α	Mechanical Parameter Determined by Edge Restraint and Mode Shape
γ	Poisson's Ratio
σ_s	Stefan-Boltzmann Constant
σ_o	Radar Cross Section per Unit Area (Radar Scattering Cross Section)
σ_T	Radar Scattering Cross Section
σ	Standard Deviation of Normal Distribution (White Noise)
σ_{VRMS}	RMS Error Voltage
σ_{tRMS}	RMS Time Error of Tracking Loop
σ_{VSS}	Measured Sea State Error Voltage
ρ	Material Density
λ	Radio Frequency Wavelength
θ_i	Angle of Reflection from Normal Incidence
ω_c	Transmitted Carrier Radial Frequency

4.0 RECOMMENDED EQUIPMENT SPECIFICATIONS

Three radar altimeter candidate systems fall within the constraints imposed by this study. Equipment descriptions and specifications for all three Space Rated Radar Altimeters are listed in Tables I through VI.

The first recommended altimeter, Type 1, is a high peak power, unambiguous pulse repetition frequency, gated threshold, range averaging altimeter. The equipment specification and error budget for the Type 1 altimeter are presented in Tables I and II respectively. The features of this altimeter design which make it an attractive candidate for the Geos C Radar Altimeter experiment are:

Minimum complexity: the design requires only the bare essentials to altitude track the ocean return pulse, and then process and transfer the data to the satellite memory storage or telemetry subsystems.

Fast acquisition: threshold acquisition of the first detected returns is certain.

Large signal to noise ratio: the minimum ocean return signal is at all times large enough to override the receiver noise by a significant margin.

Acceptable accuracy: the total RMS error budget for altitude approaches one meter.

The equipment specification and error budget for the Type 2 altimeter are presented in Tables III and IV respectively. The Type 2 is an ambiguous pulse repetition frequency, Early/Late Gate tracking, range averaging altimeter. This design performs Early/Late Gate tracking of square law detected ocean returns and is expected to track mean sea level independent of ocean wave buildup. The characteristics of the Type 2 altimeter design which make it a good candidate for the Geos C Radar Altimeter experiment are:

Good control of transmitted pulse characteristics: obtaining and controlling short pulses with fast rise and fall times is easier with low peak power magnetrons.

Inherent mean sea level tracking capability: as is shown in Appendix E, Early/Late Gate tracking of square law detected ocean returns has the

property of tracking to mean sea level without developing the bias errors due to sea state.

High input data rate: averaging of a large number of altitude measurements which result from the high transmitted pulse repetition frequency is the primary method used to obtain an accurate estimate of the mean sea level altitude once every second.

Acceptable acquisition time: the acquisition time will not exceed five seconds.

Adequate accuracy: the RMS error on one second altitude estimates improves as the square root of the data rate and approaches one meter.

The third candidate system, Type 3, is a medium peak power, ambiguous pulse repetition frequency, Early/Late Gate tracking, range averaging altimeter. Examination of the Type 3 equipment specification, listed in Table V, shows that the primary differences between the Type 3 and the Type 2 altimeters are:

Medium peak pulse power; 20 to 25 kilowatts for Type 3 compared to 4 kilowatts for Type 2.

Medium input data rate; about 1000 radar ocean returns per second for the Type 3 compared to about 5000 per second for Type 2.

Expected accuracy; the error budget of the Type 3 design has increased over Type 2 as a direct consequence of the difference in the input data rate. The random errors are just the square root of 5 larger than the Type 2 errors.

TABLE I
EQUIPMENT SPECIFICATION
SPACE RATED RADAR ALTIMETER TYPE 1 (UNAMBIGUOUS PRF)

Transmitter	Pulsed Magnetron
Peak power	100 KW
Center frequency	X Band
Pulse width	100 N Sec
Pulse rise time	15 N Sec nominal
Pulse fall time	25 N Sec nominal
Pulse repetition frequency	100 Hz
Receiver	Heterodyne
Local oscillator	Solid state (with AFC)
IF amplifier	Solid state
Sensitivity	8 db noise figure
Detectors	Solid state
Transmitted pulse	RF diode
Ocean return	Envelope
Tracking Loop	Hybrid or analog servo
Range gated threshold	Detection level proportional to automatic gain controlled ocean return
Sea state gate	One second average of signal received in sea state gate (see Appendix E)
Altitude Measurement	Digital counting of a frequency reference
Reference frequency	200 MHz, derived from external source
Frequency stability	One part in 10^8 at 5 MHz
Input/Output Logic	
Altitude word	22 binary bits, one word per second
Format	Serial or parallel
External signals for readout	Enable gate plus 22 clock pulses for serial readout required
Altitude readout gate	Altimeter generated digital signal for external data memory use
Altimeter acquisition command	Externally supplied digital signal which turns transmitter high voltage on

TABLE I
EQUIPMENT SPECIFICATION
SPACE RATED RADAR ALTIMETER TYPE 1 (UNAMBIGUOUS PRF)
(Continued)

Telemetry Outputs	Zero to five volts dc, analog and digital form
Digital outputs	Altitude, digital logic signals
Analog outputs	Temperatures, AGC, AFC, transmit pulse, sea state gate, housekeeping data
Power Required	34 watts. Altimeter turn on to be controlled by turn on of dc bus power
Antenna	4° parabolic, aligned with the spacecraft nadir
Size	1100 cubic inches
Weight	26 pounds

TABLE II
ERROR BUDGET (1 SIGMA IN METERS)
SPACE RATED RADAR ALTIMETER TYPE 1 (UNAMBIGUOUS PRF)

Error Source	Random	Bias	Remarks
Sea Return Noise	0.54	0.50	Calculated in Appendix B
Sea State	----	0.50	After correction by sea state gate data or sea state history (see Appendix E)
Propagation	0.10	----	Refer to Appendix C
Transmitter Pulse Variations	0.21	0.45	Rise time, 15 ±5 nsec; fall time, 25 ±7 nsec; pulse width, 100 ±10 nsec; peak power, ±20% jitter
Receiver/ Detection	0.04	0.48	AFC, AGC, and temperature corrected bias errors. Random errors include all pulse to pulse errors in the receiver/detector
Logic	0.10	0.20	Includes logic delays, gate duration errors, range counting quantization, clock stability, averaging by 100 counts
RSS	0.60	0.85	
Combined RSS*	1.04		Input data error to geodetic and oceanographic programs

*Best estimate of residual errors after all available corrections are made.

TABLE III
EQUIPMENT SPECIFICATION
SPACE RATED RADAR ALTIMETER TYPE 2 (AMBIGUOUS PRF)

Transmitter	Pulsed magnetron
Peak power	4 KW
Center frequency	X Band
Pulse width	100 N sec
Pulse rise time	15 N sec
Pulse fall time	20 N sec
Pulse repetition frequency	Approximately 5000 Hz, proportional to altitude (see Section 5.4)
Receiver	Heterodyne
Local oscillator	Solid state (with AFC)
IF amplifier	Solid state
Sensitivity	8 db noise figure
Detectors	Solid state
Transmitted pulse	RF diode
Ocean return	Square law
Tracking Loop	Analog servo
Early/Late gate	See Appendix E
Altitude Measurement	Same as Type 1
Input/Output Logic	Same as Type 1
Telemetry Outputs	Same as Type 1, except no sea state gate output
Power Required	Same as Type 1
Antenna	Same as Type 1
Size	Same as Type 1
Weight	22 pounds

TABLE IV
ERROR BUDGET (1 SIGMA IN METERS)
SPACE RATED RADAR ALTIMETER TYPE 2 (AMBIGUOUS PRF)

Error Source	Random	Bias	Remarks
Sea Return Noise	0.15	----	Calculated in Appendix E
Sea State	----	----	Calculated in Appendix E
Propagation	0.10	----	Refer to Appendix C
Transmitter Pulse Variations	0.05	0.22	Rise time, 15 ±5 nsec; fall time, 20 ±5 nsec; pulse width, 100 ±10 nsec; peak power, ±20% jitter
Receiver/ Detection	0.04	0.48	AFC, AGC, and temperature corrected bias errors. Random errors include all pulse to pulse errors in the receiver/detector.
Logic	0.10	0.20	Includes logic delays, gate duration errors, range counting quantization, clock stability, averaging by 100 counts
RSS	0.22	0.66	
Combined RSS*	0.70		Input data error to geodetic and oceanographic programs.

*Best estimate of residual errors after all available corrections are made.

TABLE V
EQUIPMENT SPECIFICATION
SPACE RATED RADAR ALTIMETER TYPE 3 (AMBIGUOUS PRF)

Transmitter	Pulsed magnetron
Peak power	20 to 25 KW
Center frequency	X Band
Pulse width	100 N sec
Pulse rise time	15 N sec
Pulse fall time	20 N sec
Pulse repetition frequency	Approximately 1000 Hz proportional to altitude (see Section 5. 4)
Receiver	Same as Type 2
Detectors	Same as Type 2
Tracking Loop	Same as Type 2
Altitude Measurement	Same as Type 2
Input/Output Logic	Same as Type 2
Telemetry Outputs	Same as Type 2
Power Required	Same as Type 2
Antenna	Same as Type 2
Size	Same as Type 2
Weight	24 pounds

TABLE VI
ERROR BUDGET (1 SIGMA IN METERS)
SPACE RATED RADAR ALTIMETER TYPE 3 (AMBIGUOUS PRF)

Error Source	Random	Bias	Remarks
Sea Return Noise	0.34	----	All random errors are the square root of five larger than Type 2
Sea State	----	----	Same as Type 2
Propagation	0.10	----	Same for all types
Transmitter Pulse Variations	0.11	0.22	
Receiver/ Detection	0.09	0.48	All bias errors are the same as Type 2
Logic	0.22	0.20	
RSS	0.45	0.66	
Combined RSS*	0.80		Input data error to geodetic and oceanographic programs

*Best estimate of residual errors after all available corrections are made.

5.0 TECHNICAL DESCRIPTION

5.1 The Ocean Model

The mechanism by which electromagnetic radiation is reflected from the ocean surface has been demonstrated by Schooley[1] to be mirror-like reflections from nearly flat (flatness being a function of RF wavelength where $\lambda/10$ is flat enough), approximately circular reflecting surfaces. For any given sea state and wind condition there will be an average number of these reflectors per unit area and an average diameter for the reflectors. The distribution of these reflectors along the slopes, peaks and troughs of the large waves encountered in open ocean is not known but since a single reflector with diameter larger than ten wavelengths is rare, they are very small with respect to the ocean wave dimensions and there is no reason to believe that the reflector distribution is not uniform across the ocean surfaces.

Each round flat reflector exhibits roughly the gain characteristics of a flat plate antenna of the same dimensions; thus the reflectors do not have to be pointing directly at the satellite to return radar signals. Small reflectors which have low gain but a large beamwidth are nearly randomly distributed in orientation between ±40° of the horizontal plane. Large reflectors have high gain and tend to be oriented more closely about the horizontal.

As the wind field across the ocean gets stronger the number of large reflectors decreases. It is probable that there is a limit, imposed by surface tension, to this process so that above certain wind speeds the surface will consist of only small scatterers uniformly distributed and oriented with respect to the horizontal. When these statistical characteristics of the ocean surface are considered they explain the observed behavior of the radar reflections from the ocean at and near vertical incidence.[2]

Statistical stability of the radar returns from satellite altitudes can be appreciated by the following example.

From an altitude of one million meters the area illuminated by a 100 nanosecond pulse is 94 million square meters for the pulse width limited case. If there is only one reflector per square meter this means that 94 million reflectors have been acquired in one tenth microsecond and furthermore during the next one tenth microsecond there will be a completely new set of 94

million reflectors acquired. Thus the average acquisition of new signals would be about 10^{15} per second. Each signal having a different amplitude and phase. This situation is completely analogous to thermal noise and has the same result, i.e., the radar returns will look like noise with a Rayleigh distributed envelope at the carrier frequency.

A different model for the ocean based on antenna tolerance theory leads to the same results.

Consider the ocean surface to be a large reflecting antenna with Gaussian distributed surface deviations. According to Ruze[3] and Zucker[4], the expected value of the gain of this antenna is a function of the transmitted wave length, λ, the RMS surface deviation E, and the correlation distance C, of the surface. In particular Zucker finds that for values of E larger than λ the expected gain is:

$$G = \left(\frac{C}{2E}\right)^2 \qquad (1)$$

Ruze states that under these conditions the distribution of gain is Rayleigh. *

Thus both models concur that the radar return will look like noise with a Rayleigh distribution of the amplitude envelope at the carrier frequency.

The characteristics of radar signals expected from the ocean from satellite altitudes were discussed in the fourth monthly report of this study and comprise Appendix A. The noise character and statistics of the return are discussed in Appendix B.

5.2 The Signal Detection Problem

In the determination of the altimeter specification, a study of several equipment configurations was made to determine the optimum hardware approach for the size, power, weight and delivery requirements of Geos C. The following discussion outlines the primary detection considerations and the resulting candidates.

*The apparent stability of the average radar cross-section of the ocean for high wind seas might therefore be explained by a limiting ratio of correlation distance to RMS deviation.

The signal detection problem can be considered as a combination of a pair of detection problems. First, it has been shown in the previous section that the ocean return pulse is essentially a pulsed noise process. The leading edge has an average power that varies with time as the integral of the transmitted pulse plus some rounding effects caused by significant wave heights. Since the envelope of this noise signal has a Rayleigh distribution, the detection process must determine the average position of the leading edge in the presence of the signal noise as well as in the presence of receiver noise.

The maximum altitude of 850 nautical miles and the weight and power limitations on the altimeter for Geos C prohibit the use of extremely short pulses of high peak power. Since the desired accuracy of the equipment is on the order of 1 to 2 meters (RMS), the position of the leading edge must be determined by taking the average of several pulse returns.

5.2.1 Averaging. - A good averaging time for the geodetic requirements is 1 second based on reference 5 and discussions with C. A. Lundquist. Then the number of returns averaged would be equal to the pulse repetition frequency. This would be approximately 100 for the maximum unambiguous repetition rate. However, the altitude is known from ground tracking data with sufficient accuracy to permit a high repetition frequency with only the fine grain measurement being supplied by the altimeter. For this reason, altimeter designs with pulse rates from 100 to 5000 pps were considered. For a prf in the 100 to 5000 pps range, there is negligible correlation of the noise from pulse to pulse so the reduction in RMS error would then be equal to the square root of the prf.

5.2.2 Pulse width. - The rise time of the return pulse is determined by the pulse width transmitted, hence the use of a pulse as long as 100 nanoseconds seems to be inconsistent with the 6 nanoseconds RMS ultimate ranging accuracy desired (1 meter RMS). Increased pulse width does provide a greater advantage over the receiver noise. For example, doubling the pulse width provides a 6 db gain in signal to noise ratio since the received power doubles and the required bandwidth is halved. The penalty for this improvement is an increase in the value of inherent bias delay. Hence equivalent pulse widths greater than 100 nanoseconds were not given serious consideration.

5.2.3 Accuracy. - The candidate designs considered have pulse characteristics such that the one second average of the ocean returns will reduce the random error to a value approaching one meter RMS. The equipment bias error of almost 30 meters can be calibrated with respect to temperature, AGC and AFC variation before flight. During the orbital mission ground tracking stations can monitor transmitter pulse trends to allow correction of bias errors from that source. It is estimated that the total delay will then be

known to ±10 ns (3σ). This estimate is based on the assumption that the test program will characterize the receiver with a 5% accuracy.

Most emphasis was given to designs that approached the 1 meter RMS error. This does not include the propagation errors of thirteen to fourteen meters which can be corrected to approximately ±0.1 meters (see Appendix C).

5.2.4 Detectors. - Square law and half wave linear detectors were treated from an analytical point of view. In addition to these, the peak detector (i.e., fast charge - slow discharge) and logarithmic detector were subjected to laboratory experiments.

The square law detector provides a mean voltage output that is proportional to its power input. This characteristic may be useful for constructing a receiver that is immune to sea state effects. For example, the analysis supplied by Pierson in Reference 6 indicates that the leading edge of the power return retains its area under the influence of wave effects. The square law detector would preserve this characteristic. Since the signal input is equivalent to a narrowband noise process, it can be shown that the mean and standard deviation of the output are equal.

The linear detector responds to the envelope of the signal input and therefore distorts the power return. With the Rayleigh distributed envelope, the output signal to noise ratio is calculated to be 5.7 db.

5.2.5 Waveform distortion. - There are several sources of error that cause the waveform shape to depart from the idealized ramp most treated in the literature. Some of these are the transmitter, IF filter, detector, output filter and sea state effects.

Several of these practical aspects can be quickly evaluated by means of a laboratory test set such as the Sea Return Pulse Simulator described in Appendix D. Some photographs of receiver waveforms are also provided there. This testing technique proved to be a powerful aid to the synthesis of the candidate designs.

5.2.6 Range processors. - Several types of range processors were given preliminary consideration. They can be placed in the following three basic categories:

1. Ambiguous PRF
2. Unambiguous PRF
3. Modulated pulse

Variations of two basic types of tracking loops were detailed. These were the Leading Edge Threshold tracker and the Early/Late Gate tracker. It was found that selection of a range processor is influenced by the choice of a transmitter. For example, a 2 to 10 KW transmitter does not provide a sufficiently high signal to noise ratio per pulse for good threshold detection, hence an Early/Late Gate tracker with multiple pulse averaging is required. On the other hand, a high power transmitter does provide an adequate signal to noise ratio for gated threshold detection (the tracking gate is used to reduce the false alarm probability to an acceptable level). Because of waveform stability, a high power transmitter that will fit in Geos C does not take full advantage of the waveform matching characteristics of an Early/Late Gate tracker. Also, an Early-Late Gate servo performs best at higher repetition rates where a reasonable loop bandwidth for tracking altitude rate of change can be employed.

A comparison of the two basic approaches was made analytically using results from References 7, 8, and 9. Supporting experiments with the two approaches were also made using the Sea Return Pulse Simulator to build confidence in the candidate designs. The basic principle involved is simply to average enough pulses to reduce the random error to an acceptable level. Also, it is important to use a range processor that does not add significant noise to the process. Both the Threshold and Early-Late Gate tracker fit this criterion. For the case of uncorrelated pulses, the signal to noise ratio increases by the square root of the number averaged. The resulting error magnitude can be estimated using the results of References 8 and 9. For a 100 ns pulse, the following time errors per pulse result from the sea noise in one assumed Early/Late Gate tracker design.

σ = 140 nanoseconds Square law detector

σ = 74 nanoseconds Linear detector

After averaging 100 pulses, these RMS errors are reduced to 14 and 7.4 nanoseconds respectively. The range error in feet is one half of these values.

5.2.7 Acquisition. - The details for acquiring the return pulse in the range gate were developed for the two types of trackers. It was found that for all the systems considered, the signal could be acquired in less than 5 seconds. Advantage can be taken of the fact that the received pulse remains at its maximum level for several microseconds. By matching a coarse acquisition circuit to this relatively long pulse, the total search time is greatly reduced. At high signal to noise ratios, threshold acquisition can be used. At low signal to noise ratios, comparison gates integrating several pulses are required. With the constraints imposed by Geos C, the altimeter will either have a low repetition rate with high signal to noise per pulse or a high repetition rate with

low signal to noise per pulse. Obviously, the threshold is compatible with the former and the comparison gates are compatible with the latter.

5.2.8 Candidate designs. - As a result of the detection study, coupled with the transmitter survey, three major candidate designs were initially defined for further investigation; an unambiguous pulse repetition frequency design, an ambiguous pulse repetition frequency design and a chirp modulation design. The characteristics of each are listed in Table VII.

The major factor in any of the designs relates to concentrating a sufficient amount of power on the ocean target in a short period of time.

The unambiguous designs require high power magnetrons to transmit a short duration pulse at X or Ku band to achieve a satisfactory return signal to noise ratio. Significantly greater transmit power is required at Ku band to obtain an equivalent return pulse signal to noise ratio, because of increased losses due to weather.

Because the Geos satellite coarse ephemeris will be known, it is possible to operate the altimeter pulse repetition frequency in an ambiguous range. This mode of operation permits the designer to concentrate the same effective power on the target by trading increased PRF for reduced peak transmitted power. Of course the receiver must assume part of the trade-off penalty because of the additional electronics required to integrate a number of received pulses. Improved accuracy can be achieved by narrowing the pulse width to 50 nanoseconds and compensating for the energy loss on target by doubling the PRF. This approach has a disastrous effect upon the signal to noise ratio per pulse, where 6 db is lost because of the increased receiver bandwidth required and the reduced energy per pulse. The poor signal to noise ratio per pulse limits consideration to the Early/Late Gate tracker.

A chirp radar system satisfactorily solves the energy on target problem through its ability to transmit a long, low power, modulated pulse which can be resolved to a 25 nanosecond accuracy by virtue of the coherent modulation on the pulse. A preliminary analysis of the chirp radar altimeter developed power, weight and performance estimates indicating that this approach might fit within the bounds established for this study. As such it is a strong contender for the "ultimate" satellite altimeter design.

As a result of the one year delivery requirement, however, the chirp approach is not considered a candidate design for this study because of the lack of sufficient information about the expected ocean return and the chirp modulation processing assemblies[10]. Thus the General Electric Company concurs with NASA's decision to undertake an additional study of chirp radar altimetry to determine its applicability.

TABLE VII
CANDIDATE DESIGNS - CHARACTERISTICS

Parameters	Unambiguous Pulse Repetition Frequency #1	#2	#3	Ambiguous Pulse Repetition Frequency #1	#2	Chirp Modulation
Peak Power	25 KW	100 KW	100 KW	5 KW	5 KW	2 KW
Pulse Width	100 ns	100 ns	100 ns	100 ns	50 ns	10 usec
Compression Ratio	-	-	-	-	-	400
Antenna Gain	32 db	34 db	32 db	32 db	32 db	32 db
Beamwidth	4°	3°	4°	4°	4°	4°
Pulse Repetition Rate	100	100	100	2500-5000	5000-10,000	100
Tracker	Threshold or Early/Late Gate			Early/Late Gate		Consider Both
Frequency	9 GHz	15 GHz	9 GHz	9 GHz	9 GHz	9 GHz
S/N per Pulse	+12 db	+17 db	+18 db	+5 db	-1 db	+15 db
Pulses Averaged	100	100	100	2500	5000	100

Using the information developed here, more detailed altimeter designs were synthesized and examined. This information is provided in Section 5.4 of this report.

The signal to noise ratio results found in Table VII were computed from the following range equation and receiver characteristics.

$$P_R = \frac{P_t G^2 \lambda^2 \sigma_o c T_p}{4(4\pi)^2 h^3 L} \qquad (2)$$

where:

P_R = Maximum received power
G = Antenna gain
λ = Wavelength of the transmit signal
σ_o = Radar cross section per unit area
c = Speed of light
T_p = Pulse width
h = Altitude
L = System losses

The noise power is:

$$N_r = K T_e B_n \qquad (3)$$

where

T_e = Effective noise temperature
B_n = Noise bandwidth

For the systems under consideration:

σ_o = 10 db (rough water)
h = 850 nautical miles
L = 3 db
T_e = 1900° (Pessimistic Value)
B_n = T_p^{-1}

5.3 High Speed Counters

Accurate measurement of range and generation of precise range gates are best accomplished by digitally counting a stable clock signal. The reference frequency, which is assumed to be supplied from an external source, must be counted in a manner to minimize bias errors caused by time delays through the digital logic and counting circuits.

In order to reduce the quantization error in the range measurement to an acceptable value, it is necessary to clock the range counter at a rate of 200 MHz. This results in a minimum range increment measurement of 2.5 feet. Various approaches can be employed to operate at this clock rate. The three most promising techniques are:

1. Direct counting

2. Two phase counting operating at 100 MHz

3. Vernier counting techniques

The first approach, direct counting, is selected as the approach to use because it is simpler and less complex than the other two. In addition, micro-electronic logic circuits now available, that allow direct counting at well over 200 MHz, have been evaluated satisfactorily over the satellite temperature profile.

The most flexible direct counter design which best fulfills this requirement is a parallel carry type which reduces the accumulated time delays to a minimum. In a parallel carry counter each stage changes at the same time, thus eliminating the propagation delay inherent in ripple counters. Since the required counter contains twenty-two stages, the interconnections in a parallel carry configuration are more involved than a ripple counter.

One way to overcome the long delays in the simple ripple counter is to preset the counter and decode it in the all ones state. In reaching the all ones state the ripple counter fills the most significant bit with a one first and then fills the next lower bit positions in sequence. When the least significant bit changes to a one, the all ones state is decoded. Thus the ripple delay is limited to that produced by one gate and one flip-flop. The counter off time, determined by the pulse repetition rate, allows sufficient time for information readout and presetting for the next counting interval. The preset counter approach also readily adapts to the generation of a digitally timed range gate.

In order to conserve power, the ripple counter described is implemented using a combination of Emitter Coupled Transistor and Diode Transistor logic

circuits. The first six high speed stages are of the Emitter Coupled type, using the MC 1070 flip-flop and the MC 1062S gate manufactured by Motorola Semiconductor Corporation, shown in Figure 1. Tests in the laboratory environment using the test configuration shown in Figure 2, yielded satisfactory operation up to an input frequency of 400 MHz. Temperature testing of these high frequency counter stages was completed at 256 MHz and operation profiles as a function of bias voltage, input signal level and power supply voltage are shown in Figure 3. Photographs of the waveforms at a 256 MHz counting rate are shown in Figure 4.

The test results indicate that a power supply voltage of 5.75 volts is required to guarantee reliable performance over a temperature range of -30° C to +85° C. This voltage grants satisfactory immunity to changes in all of the variables involved. The first six high speed stages consume 1.6 watts when counting an input clock at 256 MHz. The resulting 4 MHz output can be handled with low speed, low power diode transistor logic.

The subsequent stages are broken up into sections and appropriate logic circuits are used. The type required is dictated by the operating frequency in question. Power dissipation and maximum frequency of operation are generally directly proportional. For this reason a savings in dc power can be realized by matching the logic type to the operating frequency. To assure high reliability in the newly developed high speed stages, they can be wired in a redundant configuration operated by command, with power applied only to the stages in use.

5.4 Synthesized Design

Size, weight and power estimates of several equipment configurations were made to insure an optimum choice for the Geos C mission. In addition, approximate cost and reliability estimates were made. As a result of discussions with Dr. George Weiffenbach and Mr. George Bush of Johns Hopkins University's Applied Physics Laboratory it was assumed that the antenna, data memory, command programmer, telemetry, time reference generator and stable reference frequency source will be supplied by the spacecraft.

The primary constraints on the altimeter are a weight of 25 pounds, an average power of 35 watts, a maximum energy drain of 72 watt hours during a single operating interval and a one year delivery time of a flight model. The reduction in output data resulting from a low duty cycle can be traded for an increased dc operating power to maintain the energy consumption per orbit within limits. Equipment configurations that did not reasonably approach the primary constraints listed above were not given serious consideration. As

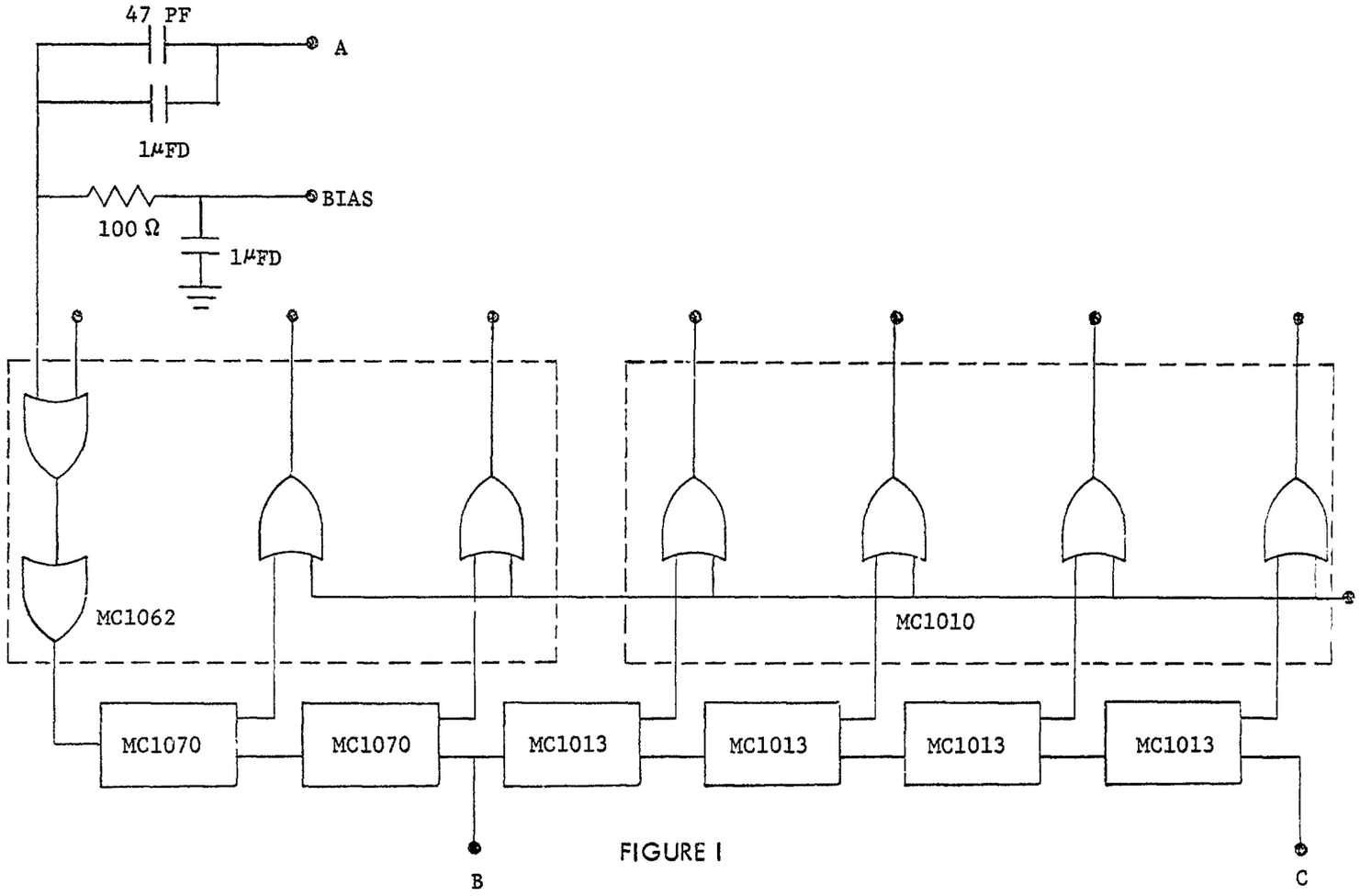

FIGURE I

MECL HIGH FREQUENCY COUNTER

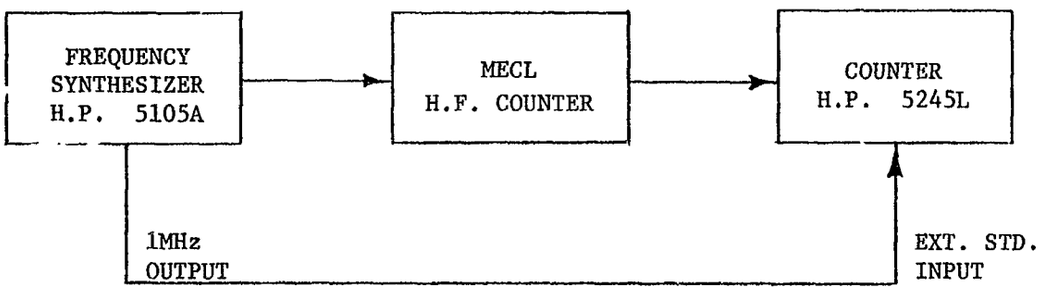

FIGURE 2

HIGH FREQUENCY COUNTER
TEST CONFIGURATION

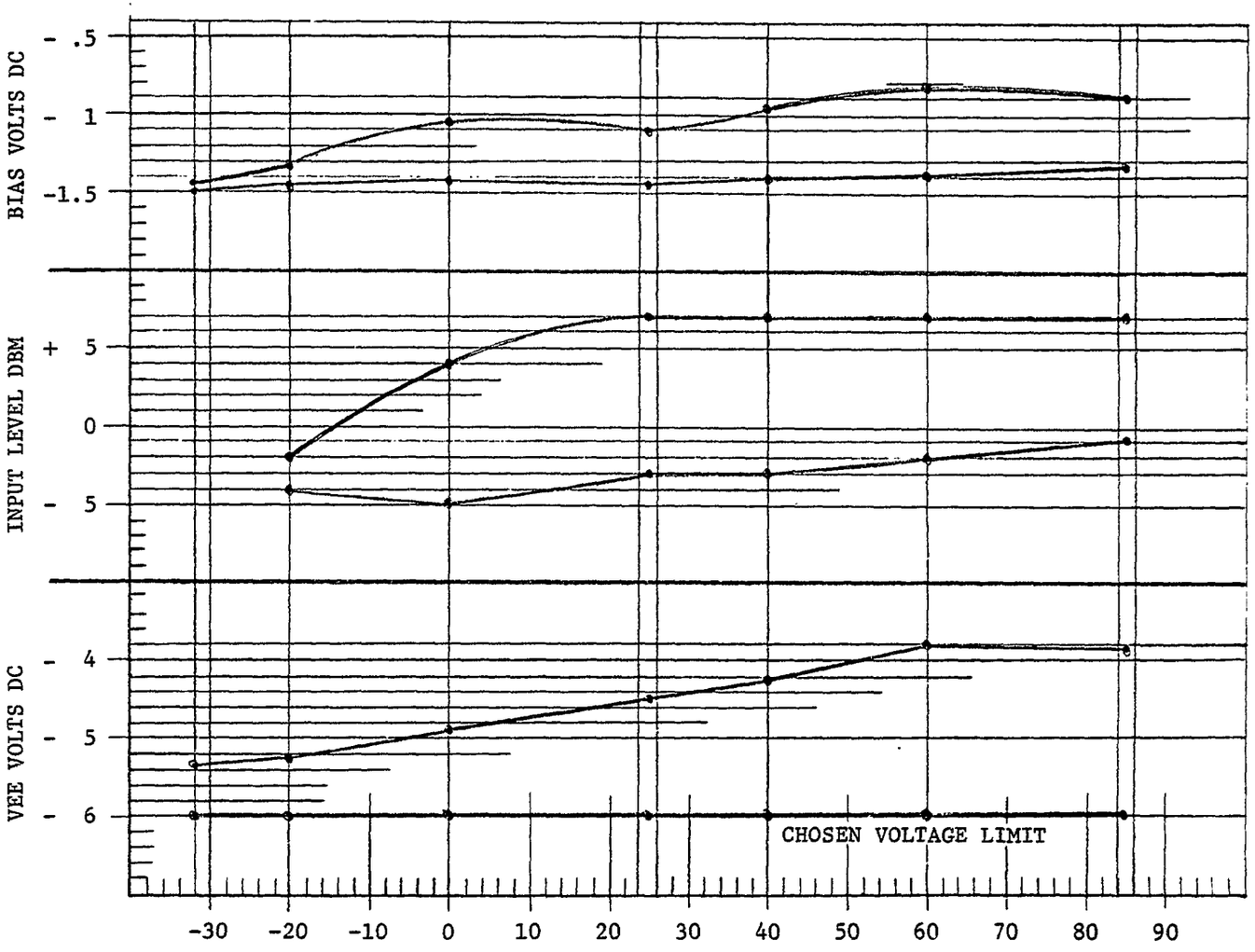

FIGURE 3 MECL OPERATION PROFILES

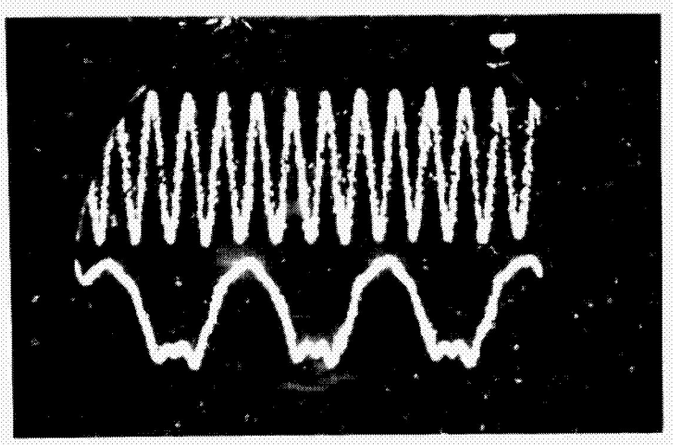

A 256 MHZ INPUT
B ÷4 OUTPUT

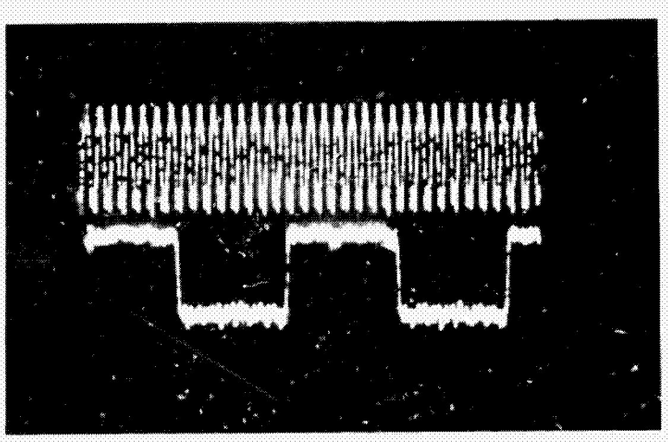

B ÷4 OUTPUT
C ÷64 OUTPUT

Tektronix Type 661 Oscilloscope

HIGH FREQUENCY COUNTER WAVEFORMS
FIGURE 4

can be expected the transmitter has the greatest impact on the design. It dominates the size, weight, power, and to a large extent the type of range tracker to be used.

The basic altimeter block diagram is provided in Figure 5. A pulse radar approach is used for practical reasons. That is, a CW radar requires a prohibitive value of transmitter-receiver isolation and an "almost CW" approach, compatible with the Geos C objectives and one year delivery, is not available at this time due to the complete lack of supporting data. The basic altimeter approach is compatible with Leading Edge Threshold or Split Gate Trackers or both. It is also compatible with ambiguous and unambiguous pulse repetition frequencies.

5.4.1 Transmitters. - Several types of pulse transmitters were examined for the possible pulse radar configurations. In this survey, transmitters were studied with the following parameter bounds:

Peak power:	2 to 100 KW (single frequency) 1 to 2 KW (chirp)
Pulse width:	50 to 100 nanoseconds (single frequency) 10 microseconds (chirp)
Pulse repetition rate:	100 pps (unambiguous ranging) 1000 to 5000 pps (ambiguous ranging)
Frequency:	9 to 16 GHz

The frequency range was chosen for the following reasons. For a given antenna area, the received power is directly proportional to the square of frequency. This frequency choice permits the antenna to have high gain with a size compatible with the spacecraft dimensions and altitude stability. Furthermore, there is a large selection of off the shelf transmitters of suitable size and weight in this frequency r' ge. The bandwidth necessary for the required range resolution can be easily achieved at X-band and at these frequencies the range error caused by transmission through the ionosphere is negligible.

At the high end of the frequency range, the attenuation and echoes from rain storms are increased. An analysis indicates that the sea return is sufficiently high to permit rejection of the "weather" echoes in the detector circuits, however, the attenuation suffered at 16 GHz, when transmitting through heavy rainfall, is great enough to give the 10 GHz a definite advantage. The transmitter block diagrams are given in Figures 6 through 10. The five basic transmitter designs shown there were considered with respect to the Geos C

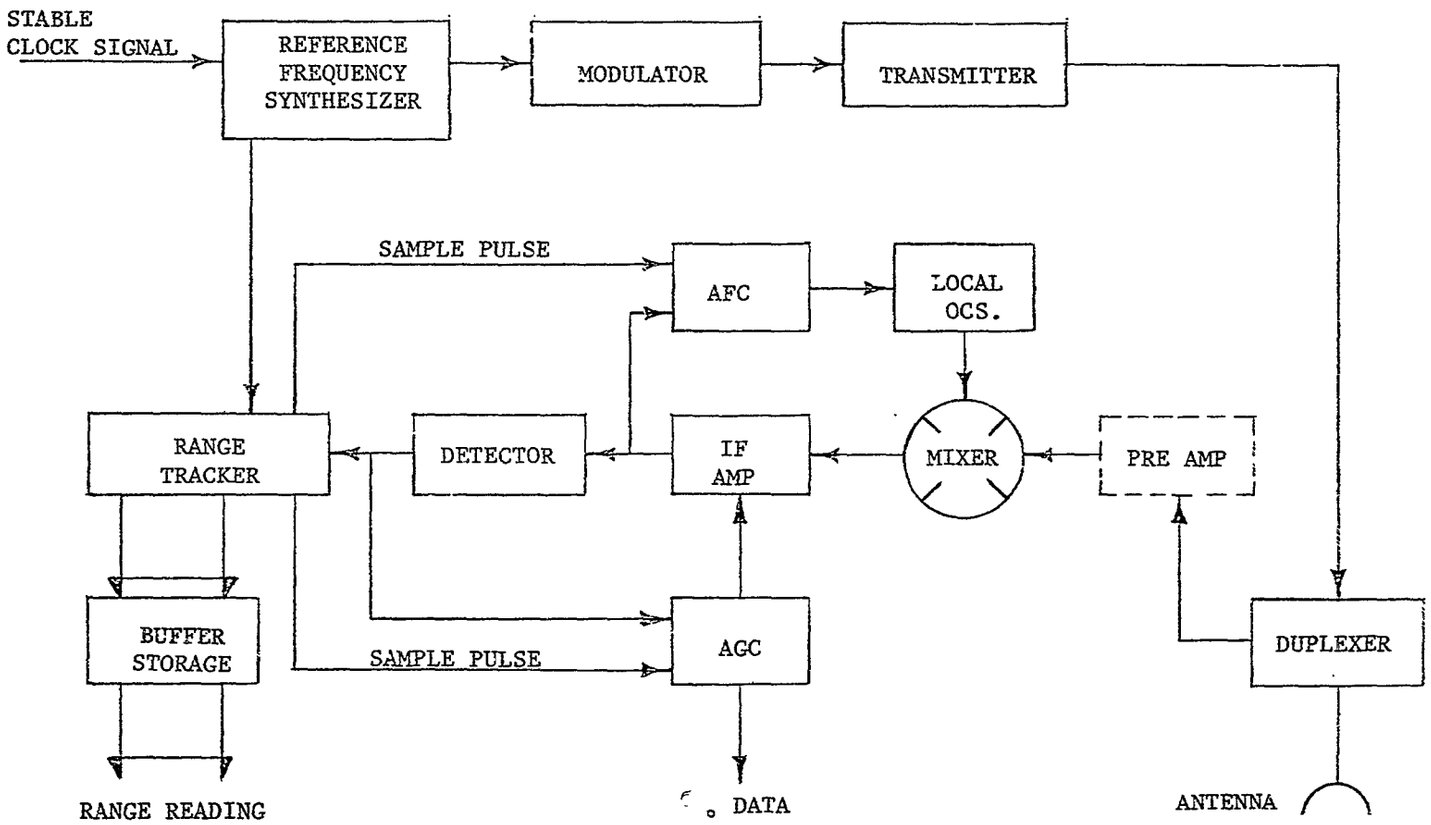

FIGURE 5 PULSE RADAR ALTIMETER BLOCK DIAGRAM

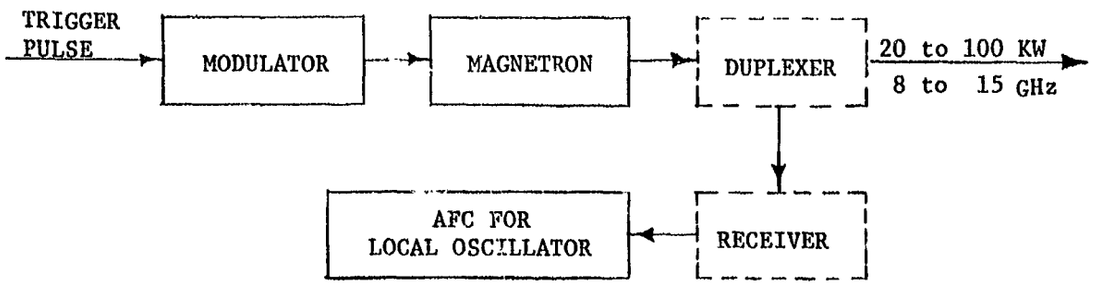

FIGURE 6 MAGNETRON TRANSMITTER (HIGH AND LOW POWER)

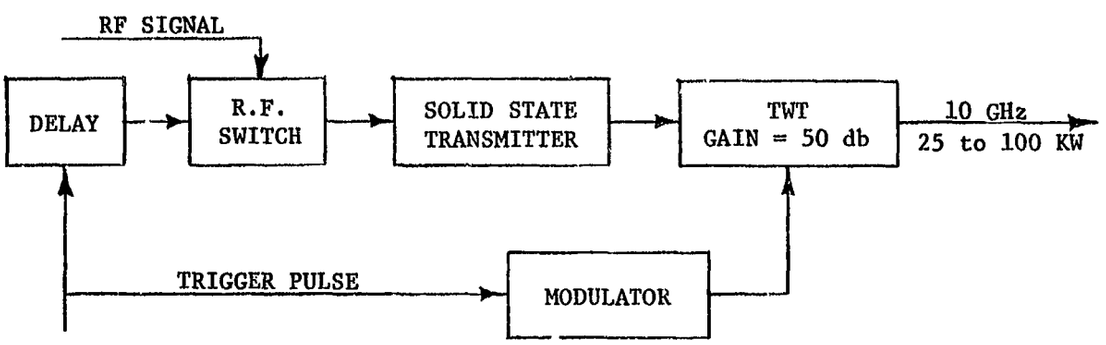

FIGURE 7 TRAVELING WAVE TUBE TRANSMITTER (HIGH POWER)

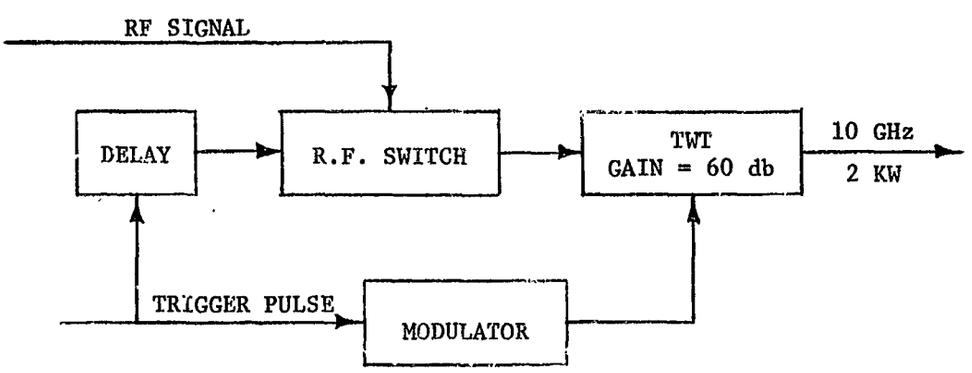

FIGURE 8 TWT TRANSMITTER (LOW POWER FOR HIGH REP RATE)

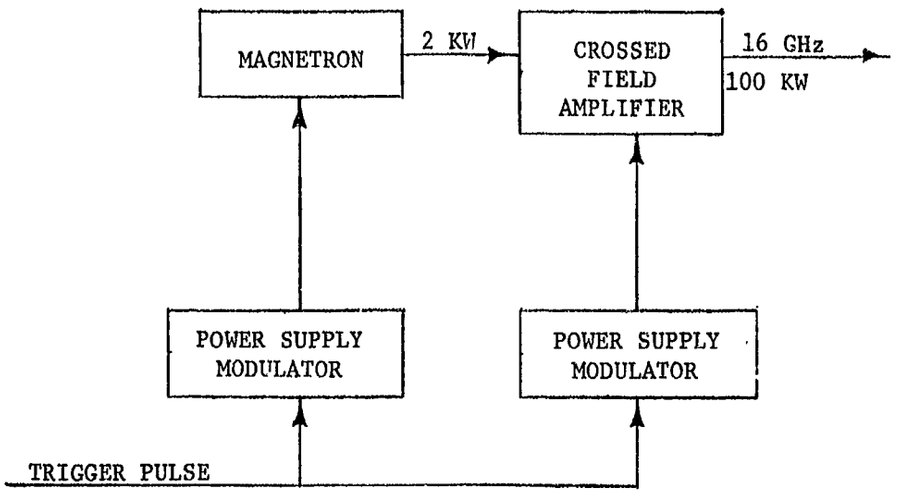

FIGURE 9 CFA TRANSMITTER

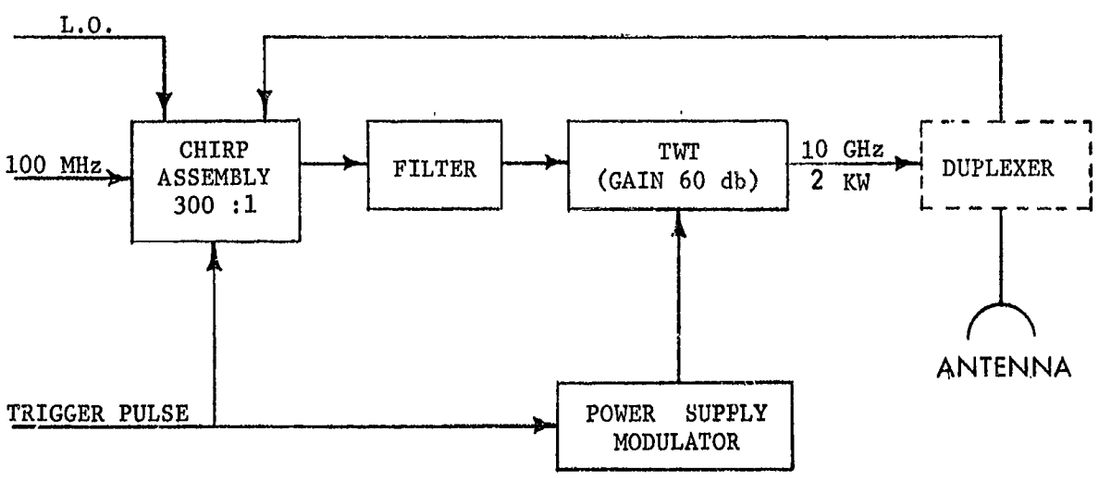

FIGURE 10 CHIRP TRANSMITTER

constraints. They include the high and low power magnetrons, high and low power traveling wave tube amplifiers (TWT) and the cross-field amplifier. The data necessary for weight and power trade-offs is provided in Table VIII. These can be related to the candidate designs of Table VII. The weight and power data includes the high voltage power supply, modulator and transmitter tube.

5.4.1.1 Magnetrons. - A survey of several magnetron vendors including Litton, Varian, Hughes, Sperry, Microwave Associates and Raytheon was made to investigate the performance characteristics of applicable devices. High power magnetrons in the 70 to 100 KW range were considered for the 100 pulse per second radar while low power magnetrons in the 4 to 25 KW range were considered for the high pulse repetition frequency radar.

The low power transmitters exhibit better waveform stability and require less filament power than the high power transmitters. The waveform stability is comprised of two basic variables, the frequency stability (during the pulse and between pulses) and the stability of the rise and fall times Although the low power magnetrons have a definite superiority in terms of stability, they do not provide sufficient power for the threshold detection receiver at an altitude of 850 nautical miles as the high power transmitters do. Available magnetrons in both classes will supply an RF pulse with a 10 to 20 nanosecond rise time, an 80 nanosecond pulse width and a 20 to 40 nanosecond fall time.

For the high power magnetron transmitter block diagram, Figure 6, a Ku-band tube was found that requires less filament power than its X-band counterpart. However, the power advantage was not enough greater to offset the additional propagation losses and increase in receiver noise figure at the higher frequency. Typical magnetrons in the X-band and Ku-band range, with peak output powers of 70 to 100 KW, require filament powers of 20 to 50 watts and are designed for higher duty cycles and wider pulse widths than desired for the altimeter application. The required filament power is proportional to the product of duty cycle and peak power. By using a different filament material and cathode structure tube filament power requirements can be substantially reduced, for low duty cycle and narrow pulse width operation. Frequency change during the pulse is related to the modulator pulse flatness, where frequency changes as large as 70 KHz per ampere are possible. Measurements made by manufacturers on high power Ku-band pulse magnetrons showed that 83% of the RF pulses were within 20 KHz of each other. It is expected that the combined frequency drift during and between pulses will be less than 250 KHz at Ku-band. Similar results are predicted for X-band tubes.

TABLE VIII
TRANSMITTER/MODULATOR CONFIGURATIONS

Type	Peak Power (kilowatts)	Pulse Rate (pps)/ Pulse Width (nsec)	Frequency (X or Ku)	Weight (lbs)	Power Requirements (watts)
Magnetron/CFA	100	100/100	Ku	24.5(22.5)*	18.3(11.5)
High Power Magnetron	100	100/100	Ku X	14.0(11.5) 14.0	20.2(11.2) 20.2
TWT	25-100	100/100	X	35.5	31.0(24.0)
TWT	1-2	5000/100	X	16.5	31.0(27.0)
TWT	1-2	2000/100	X	14.5	19.0(15.0)
Magnetron	8	5000/100	X or Ku	13.4	33.2(30.0)
Magnetron	8	2000/100	X or Ku	9.4	18.2
Magnetron	4	5000/100	X	9.4	21.7(19.0)
Magnetron	20-25	1000/100	X or Ku	12.75(10)	19.6(17.6)

*Optimistic value

On rare occasions a pulsed magnetron will not oscillate normally when the output from the modulator is applied, and the result is a missing pulse. The missing pulse rate will be approximately 0.001%, where a missing pulse is defined as a transmitted pulse with less than 70% of normal energy. Missed pulses can be detected and telemetered to allow data processing on the ground to virtually eliminate the resulting range error.

5.4.1.2 Traveling wave tube transmitter. - Traveling wave tubes (TWT's) are available that have a high reliability rating in a space environment and will amplify the fast, narrow RF input pulse. To conserve power, the TWT would be gated on slightly before the start of the RF input pulse and gated off after the RF pulse ended. The TWT input RF pulse can be generated by feeding a CW radio frequency signal through a fast diode switch. One hundred nanosecond pulses can be generated at peak power levels up to one watt using diode switches.

A survey of available TWT's with peak output powers in the range of 25 KW to 100 KW show them to be large, with weights of 15 to 25 pounds, and filament power drains of 30 to 50 watts. These tubes are designed for duty factors of 0.5% to 1%, which is considerably larger than that required for the altimeter application.

One vendor feels that by using a different cathode material the filament power requirement for tubes can be reduced to 10 to 15 watts for the altimeter low duty factor requirement. The vendor has not built tubes like this but has investigated and proposed such tubes for other customers.

Although the TWT transmitted pulse would be well controlled and of ideal shape, the requirement for associated subassemblies such as the power supply and modulator result in combined size and weight figures which exceed the bounds set for the entire altimeter.

TWT transmitters in the one to two kilowatt power range were found to have acceptable weights but still are considerably heavier and less efficient than magnetrons in the same power range. These are suitable for the Chirp and high prf systems considered.

5.4.1.3 Pulse magnetron plus cross-field amplifier. - The Cross-Field Amplifier (CFA) is an efficient microwave power amplifier that operates at relatively low voltage. Some CFA's operate with cold cathodes, making them attractive because filament power is not required. CFA's are normally large and heavy, and have gains of 10 to 20 db. The X-band units weigh from 30 to 50 pounds and more.

Since the cold cathode tube draws power only during pulse amplification, over-all efficiencies in the range of 30% to 60% are possible. The CFA will also sharpen the rise time of an RF pulse because it does not draw current during the first 80% of the applied pulse. The fall time of the RF pulse out of the CFA should be faster than the output of a pulse magnetron because it has no stored energy.

The reliability of the CFA is not well established since the device is just becoming widely used. However, the low duty factor associated with the altimeter application should result in the longest possible life.

Varian Associates manufacturers a CFA operating in Bu-band (Type SFD-236) that may be utilized in an altimeter transmitter. Since the tube is designed for a higher duty factor, the tube weight may be reduced to about 13 pounds by removing some of the cooling fins. This CFA requires a minimum input RF pulse of 2 KW peak, which can be supplied by a low power pulse magnetron. This magnetron will be small, light weight and will require considerably less dc power than the higher-powered versions discussed previously.

In the near future a possible replacement for the pulse magnetron required to drive the CFA would be the Limited Space Accumulation (LSA) diode pulse generator. The LSA generator along with the CFA would result in a complete RF source that does not require filament power. A Ku-band unit with 2 KW peak output power is not available now, but probably will be available in one to two years. Cayuga Associates, Inc. sells X-band LSA diode pulse generators with a pulse length of 100 nanoseconds which generate 500 watts at 60 pulses per second. In addition, they have achieved 1.2 KW peak power at X-band The present units operate over a small temperature range about room temperature. Work on extending the operating temperature range is progressing but more development is required before the LSA device can be used for this application Hence the LSA diode will not be considered for the Geos C altimeter application.

5.4.2 Duplexer. - The transmitter duplexer consists of a three-port circulator with a gas TR tube and a solid state limiter.

The circulator provides 20 db of isolation between the transmitter and antenna and when used as part of the duplexer results in a unit with lower transmitter insertion loss than an arc type gas switching duplexer in which the insertion tends to increase as pulse width decreases. The receiver protection circuit consists of a TR tube and a two stage diode limiter. This configuration limits the spike leakage to 0.02 ergs and the flat leakage to 50 milliwatts which is sufficient to protect a tunnel diode preamplifier, if one is used. A keep-alive voltage of 1 kilovolt at 0.150 microamperes is required by the TR tube. If a tunnel diode amplifier is not used and the signal is applied

directly to a mixer, then the duplexer design can be simplified by using a single stage diode limiter which will reduce the receiver insertion loss from 1.3 db to 0.9 db at Ku-band. For X-band frequencies the receive insertion loss would be approximately 0.2 db lower.

5.4.3 Preamplifier. - A single stage Tunnel Diode Amplifier (TDA) may follow the duplexer to amplify the received signal, either at X- or Ku-band. To achieve maximum gain the TDA bandwidth would be restricted to about 60 MHz. Should the tunnel diode or bias voltage source fail, the signal will pass through the amplifier with only slight attenuation. The TDA will have 15 db gain and 6 db maximum noise figure. The output power at the 1 db compression point is -25 dbm, and when saturated is -18 dbm. The TDA includes a multiport circulator for proper isolation. A two stage TDA may be used resulting in approximately 30 db gain with an additional 10 ma current drain.

The operating temperature range of the TDA's is 0°C to +65°C. Below 0°C the circulator changes characteristics significantly, altering the TDA gain, thus causing parametric oscillations. Normally, heaters are required for satisfactory operation at the lower temperatures. For the expected altimeter environment of -12°C to +47°C a heat source is required to guarantee proper operation.

Use of a TDA will also require additional front end protection against possible strong signal levels. As a result the duplexer loss will be increased somewhat so that the resultant signal to noise improvement over an integrated receiver RF assembly is not expected to exceed 2 db. This is not considered an acceptable tradeoff against the additional heating source requirements imposed. Hence the TDA is not considered in the proposed design.

5.4.4 Detector and Range Tracker. - Three types of detectors were considered for the receiver design and tests on the performance of each were made using the Sea Return Pulse Simulator. The detectors considered were the square law detector, half wave detector and the peak detector (i.e., fast charge-slow discharge).

A fourth detector approach, the synchronous detector, has been suggested as a possible means of improving accuracy versus signal to noise ratio by J. Morris in Reference 11. An evaluation of this approach was suggested as a topic for further study on pages 4-40 and 4-44 of Reference 11.

A preliminary investigation of the design of this detector approach indicates that it requires a significant increase in hardware over the simple diode detectors considered. Consequently, it is not treated further in the synthesized designs since its possible merits are unproven.

No significant difference in hardware is required for the three detectors considered, hence a final choice depends on the accuracy results obtained from the Sea Return Pulse Simulator and computer analysis.

The synthesis of the range tracker loops concentrated on two basic approaches, the hybrid servo and the analog servo. The analog servo derives the range gate from a voltage controlled oscillator which is phase locked to the time error signal generated by the range tracker loop. The range counter is then used to measure the oscillator period which is proportional to the altitude. This type of processor lends itself to ambiguous and unambiguous transmitted pulse repetition frequencies.

The hybrid servo approach derives the range gate from the high frequency counter. To accomplish this, the error signal is converted to digital form and after appropriate manipulation and averaging is used to set state recognition logic in the range counter. The hybrid servo is compatible with a fixed, unambiguous pulse repetition rate. Both servo loops are compatible with an Early/Late Gate form of tracker or a Leading Edge Threshold tracker.

Analysis of the combined detector, range tracker performance requires that the transmitter operating mode must be considered, since performance will differ between ambiguous and fixed pulse repetition frequency operation. As a result, receiver systems can be synthesized by selecting combinations made up of either an ambiguous or a fixed transmitter PRF an analog or a hybrid range servo loop and a Threshold or Early/Late Gate tracker. In the process of making hardware comparisons of the two basic servo approaches, it is assumed that the signal to noise ratio is at least 3 db. To minimize circuit complexity a +10 db signal to noise ratio was also assumed to allow a simple acquisition procedure using a threshold detector.

The three basic approaches resulting from the design synthesis are given in Figures 11, 12 and 13. The first is an Early/Late Gate tracking loop which compares the integrated video signal from two portions of the returned waveform and servos on the error voltage generated from their weighted difference. The second is a Leading Edge Threshold tracking loop in which an early tracking gate is used to reduce the false alarm probability to an acceptable level. Both of these approaches use the range counter to generate the range gate. (This is equivalent to making a voltage controlled one-shot with crystal oscillator timing accuracy.) The third approach is a Voltage Controlled Oscillator (VCO) tracking loop which is compatible with either a Leading Edge Threshold or Early/Late Gate time error detector. The design synthesized here uses a threshold detector for acquisition and switches to the Early/Late Gate tracker after acquisition. This approach is compatible with an ambiguous pulse repetition rate and the Figure 13 depicts the case where there are 6 pulses perround trip time period.

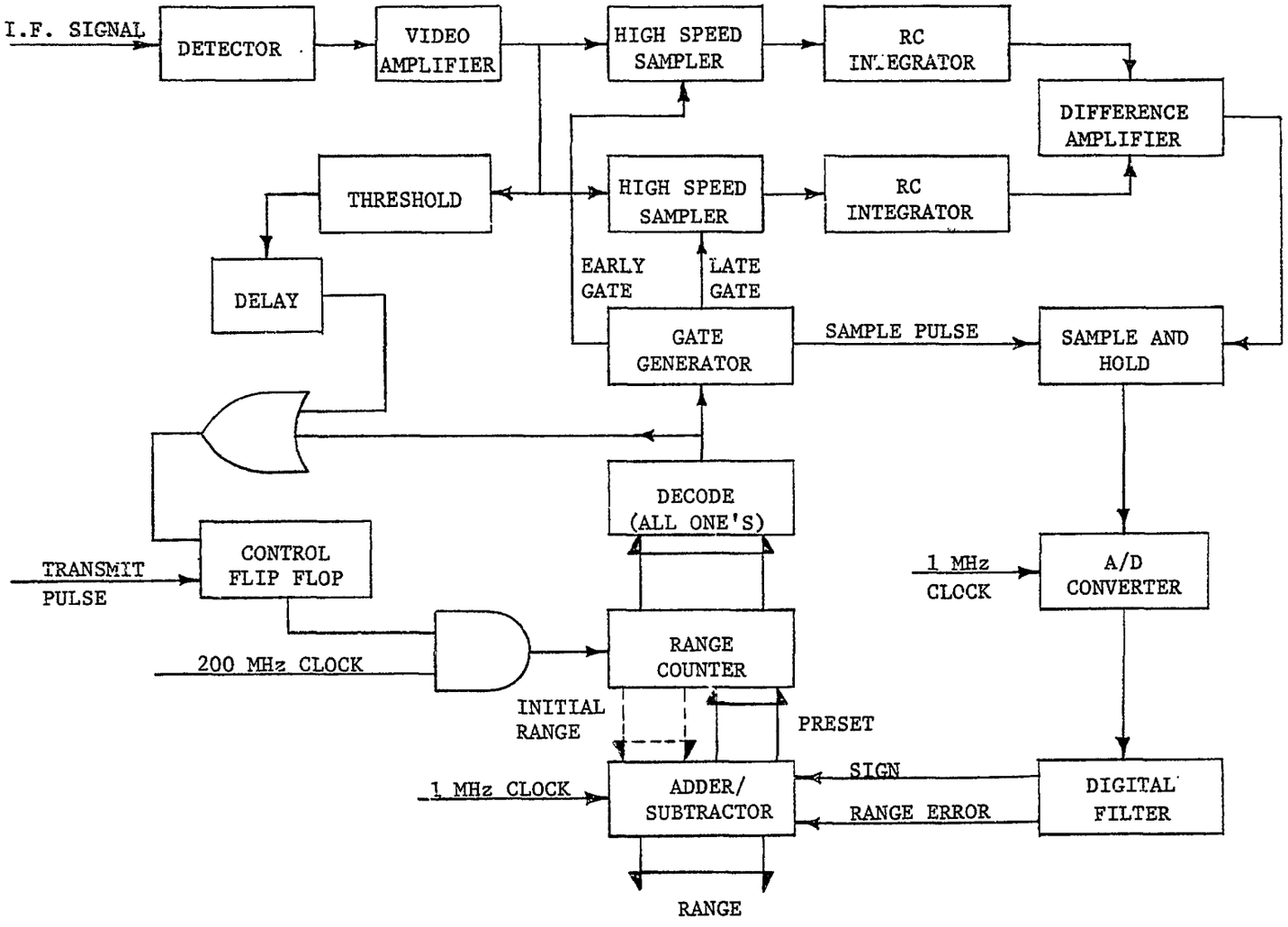

FIGURE 11 EARLY - LATE GATE TRACKING LOOP

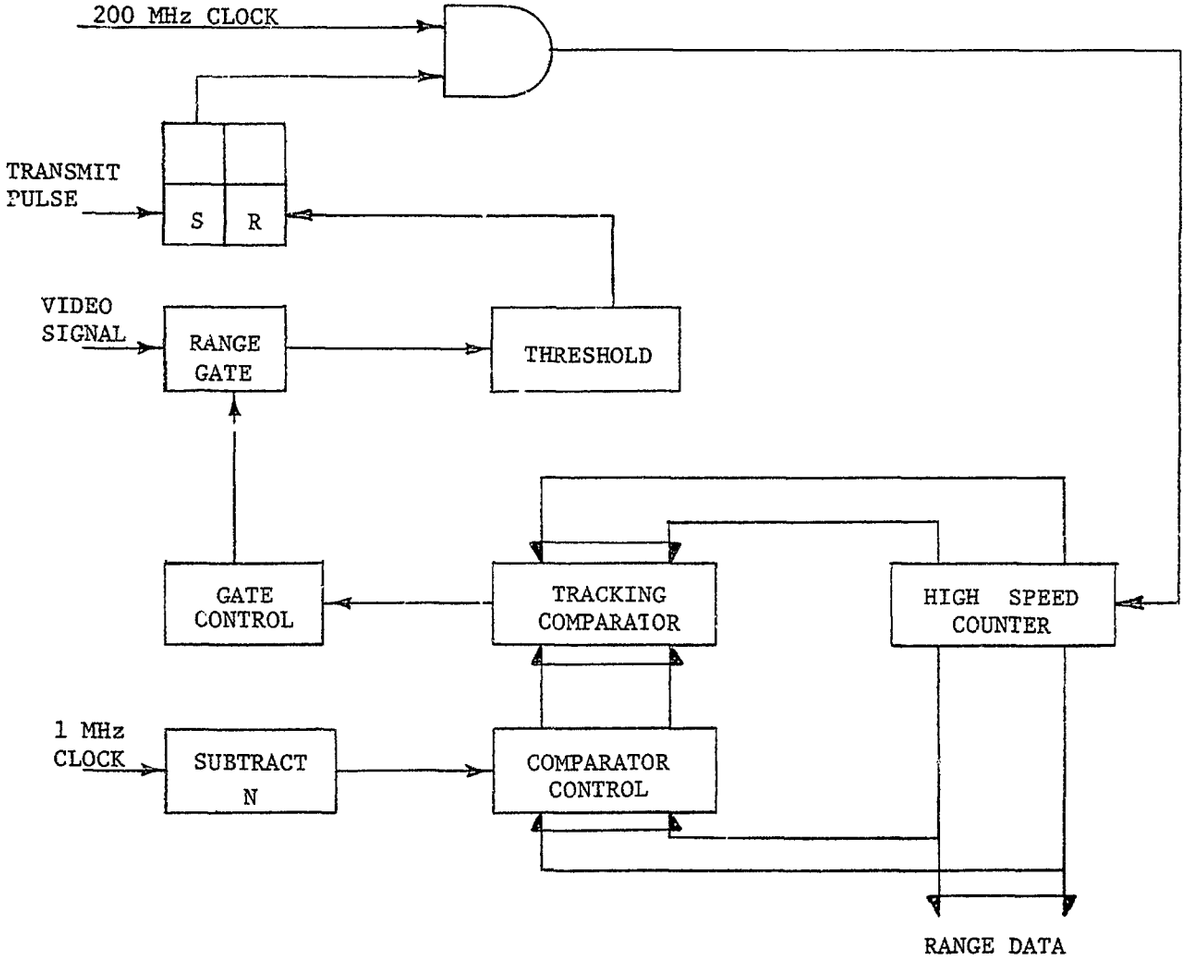

FIGURE 12 THRESHOLD TRACKING LOOP

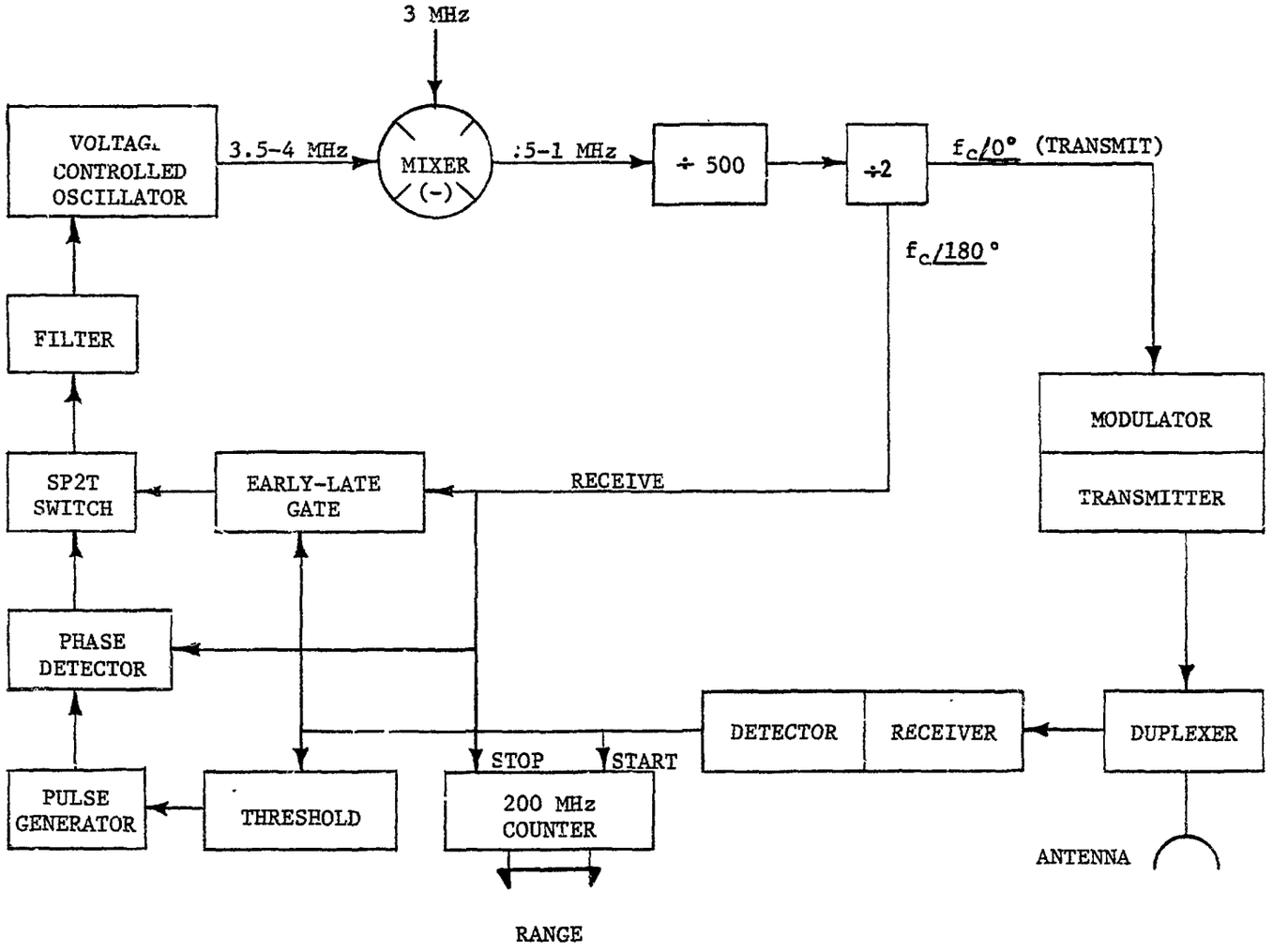

FIGURE 13 VOLTAGE CONTROLLED OSCILLATOR TRACKING LOOP

Detailing the three basic designs leads to the following conclusions. The three tracking loop approaches considered can be implemented within the Geos C time schedule. However the Leading Edge Threshold is by far the simplest from a hardware point of view. Also, utilizing a 10 db signal to noise ratio simplifies the acquisition problem. More supporting test data is also available on the unambiguous ranging system than the high repetition rate system.

5.4.5 Local oscillator and IF amplifier. - The local oscillator is essentially the same for all the design approaches considered. It consists of a solid state voltage tuned oscillator operating at a frequency of approximately 1 GHz and a diode multiplier to extend the frequency into X-band or Ku-band. In a coherent system using a TWT the oscillator is phase locked to a reference signal from the frequency synthesizer. In a noncoherent system, it would be frequency locked to the sampled IF discriminator output. Operation at Ku-band compared to X-band requires more dc power and is somewhat less reliable because of the additional electronics required.

The IF amplifier design emphasizes simplicity to insure stability of its transient and delay characteristics. An automatic gain control is used to maintain an optimum level at the detector circuit. The delay through the receiver varies with the AGC, hence its level must be used to correct the altitude data. The dynamic range of the receiver is approximately 45 db which is more than adequate to control the signal level variations caused by changes in altitude and sea state.

Since the frequency and operating conditions of the altimeter allow a relaxation of the image and spurious response specifications, a simple single conversion receiver is used with a center frequency in the 60 to 85 MHz range. The filter would be either single pole or two pole with a final choice dependent upon the results of characteristics tests with the Sea Return Pulse Simulator. The bandwidth is approximately equal to the reciprocal of the pulse width and the mean receiver delay time is in the 100 to 150 nanosecond range.

For the chirp radar case, the IF amplifier would be purchased as an entire assembly matched to the dispersive delay line.

5.4.6 AFC and AGC. - Automatic frequency control and automatic gain control are used to maintain the frequency and amplitude of the received signal centered in the receiver pass band so as to optimize detection and minimize delay variations.

Automatic frequency control is required for local oscillator tracking of the transmitter frequency in the noncoherent systems. The AFC loop is made fast to track the maximum frequency drift rate of a magnetron transmitter. In fact

the solid state local oscillator can be slewed fast enough to implement a rapid tune approach in which the AFC servo essentially acquires the signal on every pulse. A survey of applicable transmitter tubes indicates that the rate of drift is sufficiently low, compared to the IF bandwidth, to permit the loop to average over approximately 0.1 second, reducing the pulse to pulse frequency jitter to a small additive random delay error.

The automatic gain control circuit is designed so that the AGC sample is taken on the relatively long, flat portion of the ocean return pulse. With a closed loop time constant of at least 0.1 second, the AGC servo action tends to look at the average of 10 or more pulses.

5.4.7 Reference frequency synthesizer. - The reference frequency synthesizer accepts the stable reference frequency from the spacecraft and synthesizes the required frequencies for the altimeter subassemblies by means of the direct techniques of multiplication, division and mixing.

5.4.8 Power supply and power budget. - The power supply consists of a combination of switching regulators and chopper type converters, as shown in Figure 14. Switching regulators are used where possible to take advantage of the high efficiency they offer. In cases that require voltage step up or polarity inversion, the chopper type converter will be employed. An average efficiency of 85% can be achieved if the battery supply is well behaved from an audio susceptibility point of view and series regulators are not required. Similar power supplies, designed and manufactured for other aerospace programs by the General Electric Company, displayed efficiencies of 85% when series output regulators were not required.

Table IX is a tabulation of the power budgeted for each section of the system. The major variation in total required input power is caused by the different transmitter-modulator candidates considered.

5.5 Output Data Requirements

Satisfactory performance of the satellite altimeter in any designated mission requires that information generated by the altimeter be available for telemetering to the ground. This information falls into two classes, altitude measurement data and general housekeeping data.

5.5.1 Altitude data. - The raw altitude information, for altitudes to 10.5×10^6 feet, is presented as a 22 bit digital work with a least significant bit value of 2.5 feet. This information is computed and available once each transmitted pulse interval for sampling by the telemetry or data storage system.

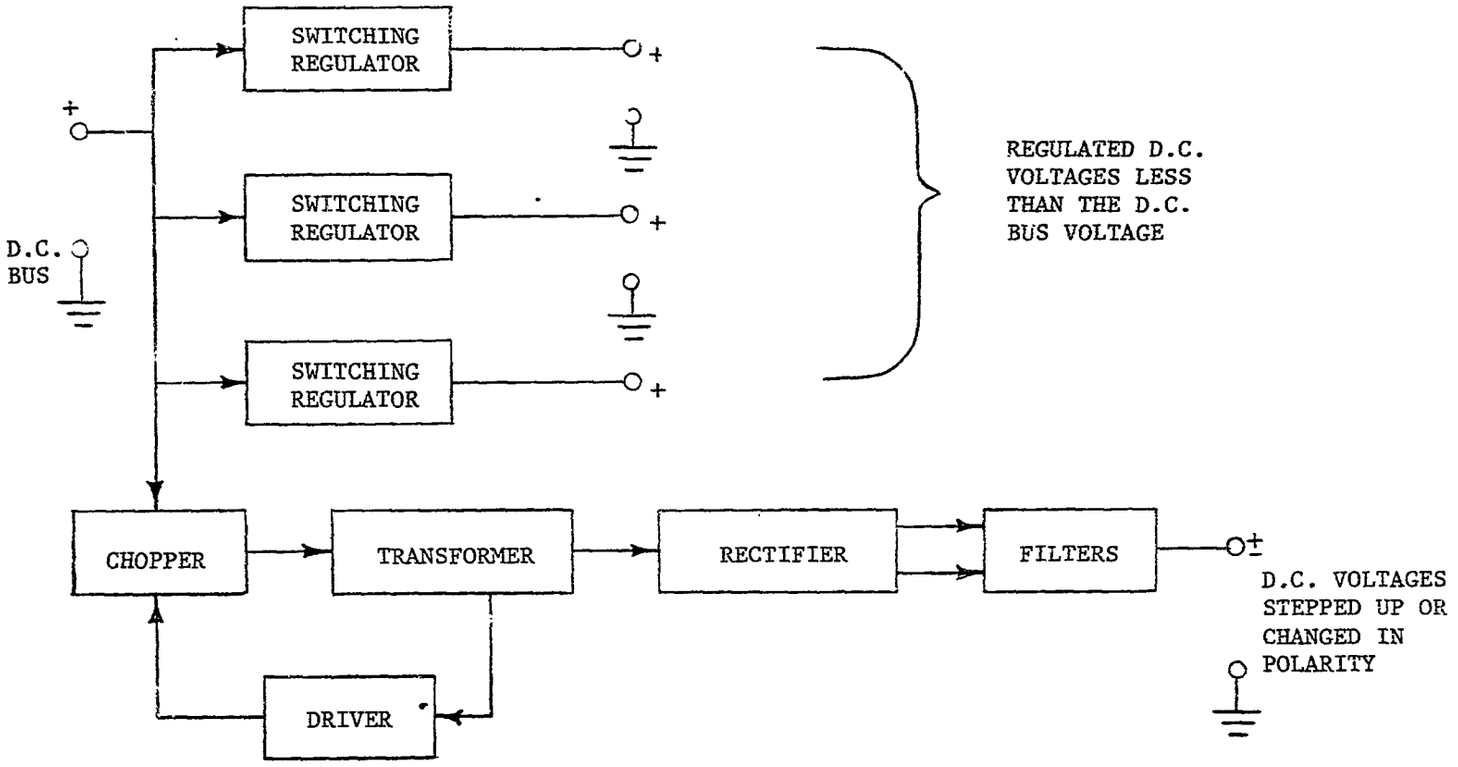

FIGURE 14 POWER SUPPLY BLOCK DIAGRAM

TABLE IX
POWER BUDGET

System Element	Pulse Width Rate	Power Estimate (watts)
Receiver		1.268
Local Oscillator		3.0
Range Tracker		4.5
Reference Frequency Synthesizer		0.5
Type of Transmitter/Modulator		
Pulse Magnetron/ Cross Field Amplifier	100/100	18.3(11.5)*
High Power Magnetron	100/100	20.2(11.2)
25-100 KW TWT	100/100	31.0(24.0)
2 KW TWT	5000/100	31.0(27.0)
8 KW Magnetron	5000/100	33.2(30.0)
4 KW Magnetron	5000/100	21.7(19 0)
20-25 KW Magnetron	1000/100	19.6(17.6)
Power Supply		15% Load Power

*Denotes an optimistic value.

For circular orbits or elliptical orbits with eccentricities of 0.03 or less, the combination of geoid altitude variations and radial velocity amplitudes which occur from one transmitted pulse period to another (assuming a worst case PRF of approximately 100 pulses per second) result in changes in the ten least significant bits only. Hence it is possible, if the data storage or data transmission channels are limited, to only sample the ten least significant bits on a regular basis and sample the complete 22 bit word at a lower rate. It is always possible that the altitude data word may be such that it will vary about a value of all ones which extends beyond the ten least significant bits. As a result, variations in the altitude word may extend beyond the suggested 10 bits. As long as the complete altitude word is sampled frequently enough, however, it is always possible to deduce the total altitude word from the ten bits sent.

In addition to the raw altitude data already discussed, certain additional data must also be transmitted, at a low data rate, to permit a continual measurement of the changing bias errors inherent in the altimeter. These characteristics include:

1. Automatic gain control (AGC) voltage

2. Component temperatures

3. Transmitted power

The AGC voltage, which is developed by integrating ten or more received pulses, varies at a frequency proportionally lower than the pulse repetition frequency. It must be used to correct the altitude measurement, because of receiver delay variations associated with the signal level in the IF amplifier.

Component temperature, which tends to stabilize once the altimeter has been on for 30 minutes or more, is also influenced by the length of time the satellite is in sunlight or dark. Hence temperature variations tend to be exponential in nature with a time constant of about 10 minutes, or approximately sinusoidal with a period equal to the orbit period.

The characteristics of the transmitted pulse, such as rise time, peak power, pulse width and fall time cannot be readily measured without using the complex sophisticated test equipment available in a laboratory. Consequently the telemetered signal will be a measure of the average power transmitted. Individual pulse transmissions will be indicated on the telemetry output making it possible to monitor missing pulses. As a result, the transmitted power should vary at the transmit pulse repetition frequency.

In order to maximize the overall accuracy of the altimeter, calibration curves will be made of each telemetered output.

The telemetry outputs will be in the standard range of zero to five volts, to be compatible with commonly available telemetry systems. One percent accuracy over this range will provide the information needed to match the values of AGC voltage, component temperature and transmitted power to the calibration curves needed to remove bias errors from the raw altitude data.

5.5.2 Housekeeping data. - In addition to the raw altitude data and the associated calibration signals, a number of other points must be monitored in a new design in order to isolate the causes of possible failures. These include:

1. Turn ON/turn OFF command
2. Local oscillator output
3. Frequency multiplexer inputs
4. Voltage converter outputs
5. Detector crystal current
6. Logic control signals
7. Automatic frequency control output

The exact functions monitored will vary depending upon the design chosen. The first two functions, turn ON/turn OFF command and local oscillator output will be monitored for all possible designs. So will the altimeter voltage converter outputs, but the number of monitoring points will vary with the design. Only two or three points will be needed if a magnetron transmitter is used. A TWT transmitter on the other hand, with its more complex voltage converter, would require at least three more monitoring points.

The 200 megahertz reference frequency is generated from a stable lower frequency reference supplied by the spacecraft. Since this signal is a key part of the range measurement technique used in all designs, both the input reference signal and the high frequency output will be monitored.

If a biased detector is used, detector crystal current will be instrumented to monitor detector performance. Allowance must be made for selecting a number of logic control signals, not to exceed ten, to determine the

performance of any of the designs selected. These signals which will be discrete in nature will vary somewhat, depending upon the design selected.

As with the altitude data outputs previously discussed the telemetered housekeeping outputs will be available in the standard zero to five volts dc range. In general, the turn ON/turn OFF command, voltage converter outputs, detector crystal current, frequency multiplexer output, local oscillator output and the automatic frequency control output can be expected to vary at a low frequency rate, thus permitting the outputs to be sampled a few times per second. A more exact determination of the occurrence of the turn ON/turn OFF command signals or detection of voltage converter transients suggests sampling at a rate of 100 to 1000 times per second.

Sampling of the logic control signals must be performed at a rate considerably higher than the transmitted pulse PRF, unless a flip-flop or other memory circuit is used to remember the short duration signals generated from the 200 MHz logic.

5.6 Mechanical Design

Since a variety of possible design approaches are presented in Table IX, some of which are incompatible with the design bounds discussed in Section 2.0, only those candidate designs recommended in Table IX, are treated here.

A sample design of a pulse altimeter was detailed to verify that the designs discussed could be satisfactorily packaged.

The configuration shown in Figure 15 applies to the high power magnetron approach, which requires the largest size package of all three proposed transmitter types. The selection of any other physically smaller transmitter design would not significantly alter the configuration of Figure 15.

5.6.1 Structural. - The volume available for an altimeter in one of the octants of the Geos C spacecraft can best be utilized by a trapezoidal shaped package having major dimensions that conform with those of the octant walls. This type of radar altimeter package configuration is shown in Figure 15. Structurally the design consists of a baseplate, approximately 0.30 inches thick which provides the mounting surface for all components. With all components mechanically secured to a common structural plate, only a thin, lightweight cover is required to serve as protection against normal ground environments. The estimated weight of a chassis having the dimensions shown

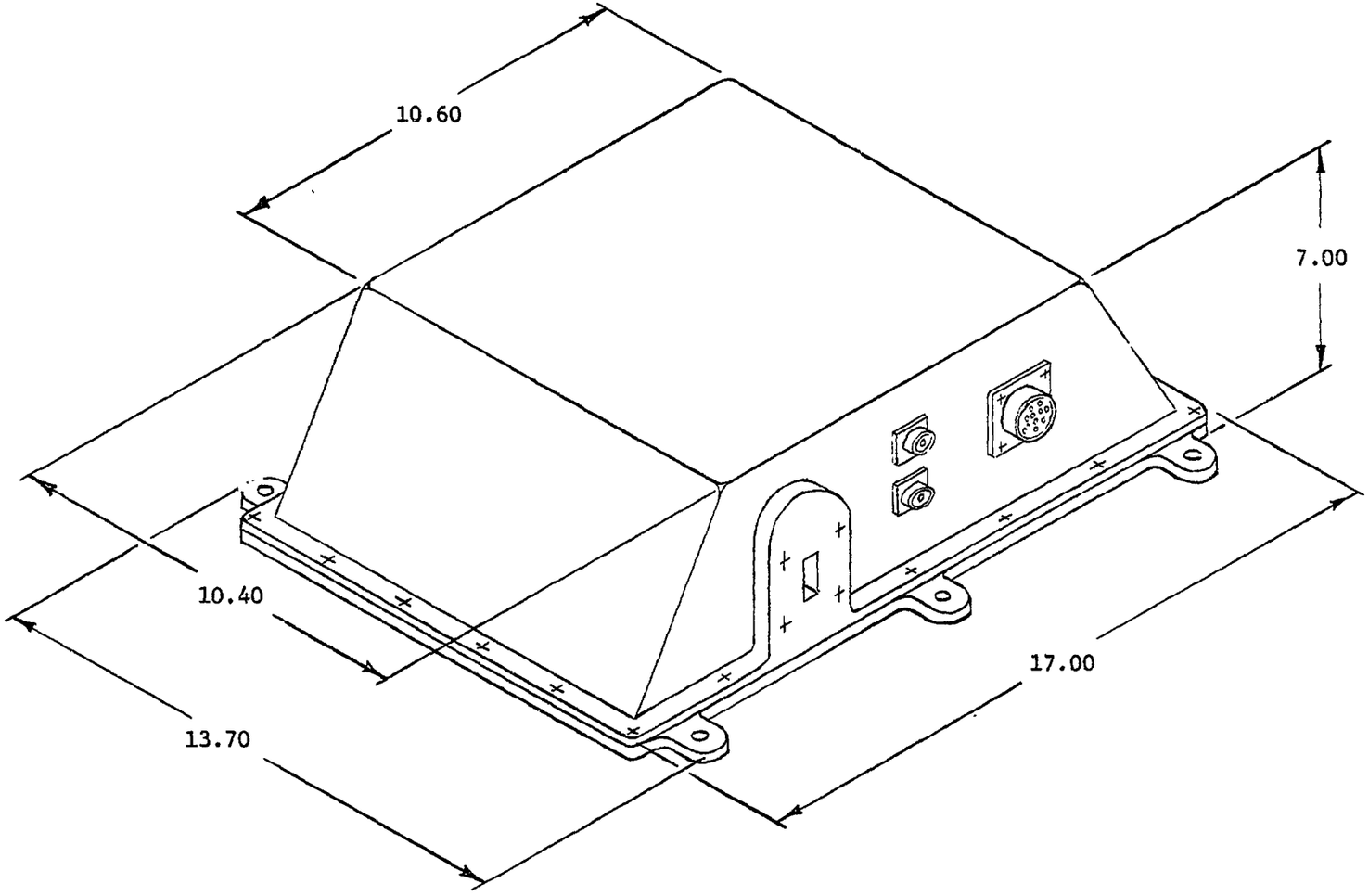

FIGURE 15 RADAR ALTIMETER ISOMETRIC VIEW

in Figure 15 is 7.90 pounds with 5.80 pounds attributed to the baseplate. Since an unpressurized package is used to permit rapid internal pressure equalization, no protection is provided for continuous corrosive environments.

5.6.2 Component packaging. - The components making up the transmitter section will be packaged in a planar configuration thereby making each component accessible without disrupting other components. This approach, in addition to providing excellent accessibility, offers the following major advantages:

1. It is a relatively simple, straightforward approach and does not require any special manufacturing techniques.

2. The baseplate is used as a common reference plane for dimensioning to all waveguide flanges and therefore misalignment of mating flanges due to a buildup of mechanical tolerances is avoided.

3. Because brackets and additional structures normally required for stacking in the "Z" direction are unnecessary in this planar approach, the equipment is lightened considerably from a weight standpoint.

The physically smaller sections of the altimeter such as the receiver, detector and logic circuitry will be packaged in planar modular form as shown in Figure 16.

5.6.3 Module description. - Components were mounted on a planar epoxy glass board which in turn were mounted in a thin wall aluminum subchassis. Component leads were terminated at terminals which fed through to the back plane or wiring side of the board. Interwiring of components were made with point to point hard wire connections. To provide for quick removal of a module from the altimeter assembly, input and output wires terminated at a multipin connector located at the module bulkhead. This modular approach is particularly attractive from both a producibility and reliability standpoint because it is based on proven, state-of-the-art techniques. The reliability and producibility risks characterized by designs using multilayer printed circuit technology were avoided because of the short schedule and low production expected.

To optimize the altimeter packaging density, the smaller modules were mounted on structural plates and stacked in the "Z" direction.

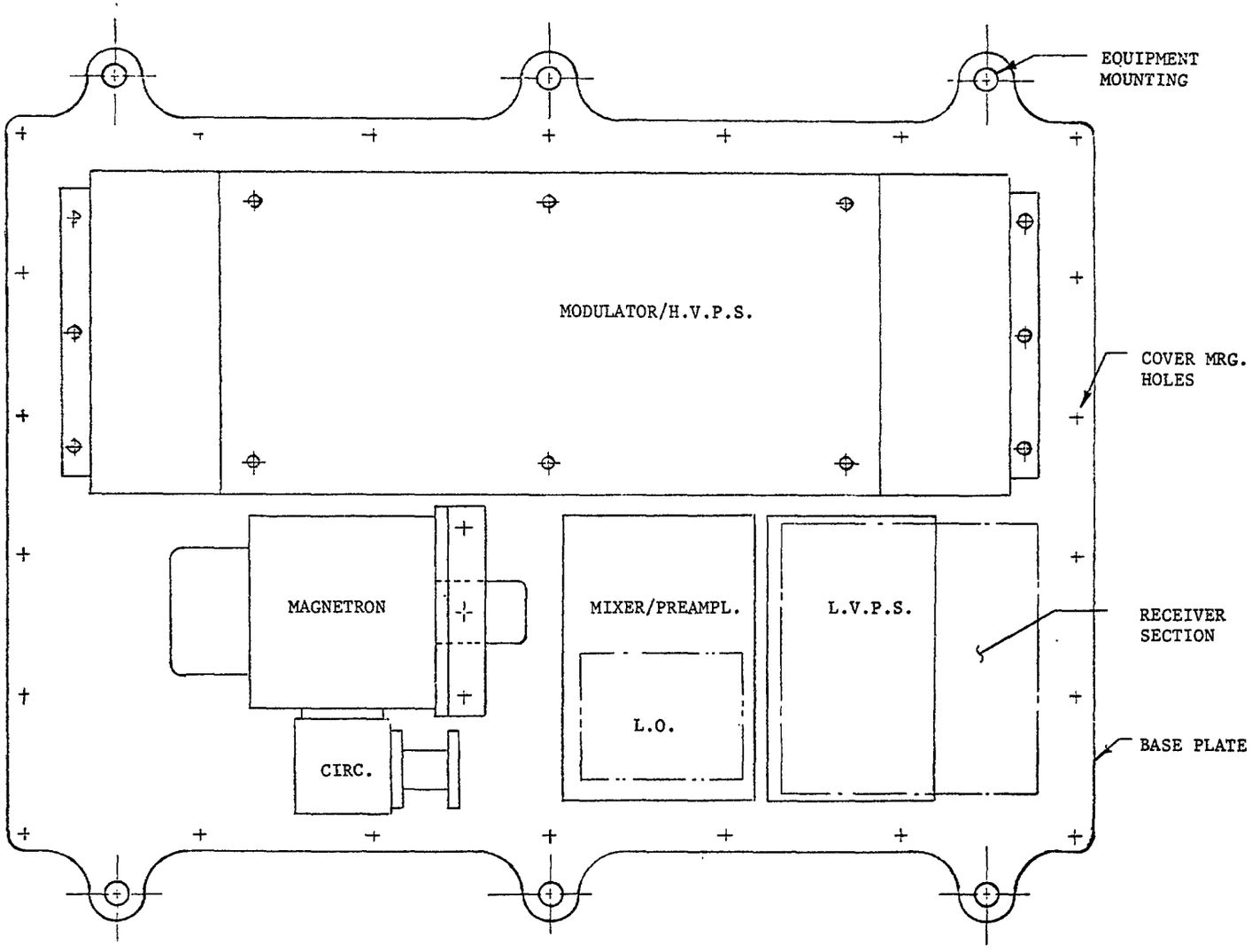

FIGURE 16. RADAR ALTIMETER - COVER REMOVED

Connections between modules were made by prefabricated laced cable assemblies which were secured to the major structure at various points to prevent oscillation of the cables during vibration.

TABLE X
SIZE, WEIGHT AND POWER CHARACTERISTICS

Transmitter Section	Weight (lbs)	Size	Volume
Magnetron	4.00	-	-
Modulator/HVPS	10.00	-	-
Circulator	0.12	-	-
Limiter	0.12	-	-
Tunnel Diode Amplifier	0.30	-	-
	14.54	-	-
Receiver Section	2.50	-	64.0
Low Voltage Power Supply	1.50	4.0x3.0x2.0	24.0

5.6.4 Vehicle mounting. - The design of the baseplate provides integral mounting tabs or feet around its perimeter and can be adapted to the vehicle structure with either rails or a flat plate. With the altimeter in its installed position, the bottom of the baseplate is located adjacent to an outside wall making it easily accessible for assembly and disassembly without disturbing the other components.

The altimeter's antenna waveguide port is located on a wall corresponding to the forward direction of the vehicle. Assuming that the antenna is to be located at the intersection of the X and Y axes, a waveguide transmission line path of approximately 2 feet is required.

5.6.5 Environmental performance. - The radar altimeter is mechanically designed to successfully survive the dynamics of launch and ascent and to perform reliably during the orbital phase of the mission. A brief analysis

of altimeter performance with respect to the various environments encountered is outlined below.

5.6.6 Vibration. - Since the baseplate is used to structurally support all altimeter components, it is important that the various resonant frequencies and mode shapes be identified so that coupling with component frequencies can be avoided. Components are physically mounted on nodal lines at those resonant frequencies where coupling is liable to occur. The natural or resonant frequency of the baseplate is determined by the following equation:

$$f_n = \frac{d}{a^2} \alpha \sqrt{\frac{E_y}{\rho (1 - \gamma^2)}} \qquad (4)$$

where

f_n = Natural or resonant frequency (Hz)
α = Parameter determined by edge restraint and mode shape
d = Plate thickness (inches)
a = Plate width (inches)
E_y = Young's modulus (PSI)
ρ = Density of material (lbs/cu in.)
γ = Poisson's ratio (0.33)

For a 0.30 inch thick aluminum plate, the initial f_n is determined to be 215 Hz with the last occurring at approximately 1300 Hz. The resonant frequencies of the smaller components are considerably higher than this and coupling does not occur. Those components having an f_n falling within this 215-1300 Hz bandwidth can be located on or near baseplate nodal lines.

5.6.7 Shock. - Similarly designed equipments produced at GE/AE have successfully withstood shock levels as high as 100 g. The highest levels to be encountered during the mission probably occur at booster separation and usually are substantially below 100 g. However, a situation can exist where the frequency of the shock pulse will coincide with the resonant frequency of the equipment thereby causing excessive transmissibilities. According to the equation

$$f_p = \frac{1}{2t_r} \qquad (5)$$

where

f_p = the shock pulse frequency

t_r = the rise time of the pulse

A coupling of frequencies occurs when t_r = 2.3 milliseconds. Rise times are usually slower (8 to 11 milliseconds) thereby putting the shock pulse frequency below the equipment resonant frequency.

5.6.8 Thermal. - If rails are used to mount the altimeter to the vehicle, the primary mode of of heat transfer is by radiation. Assuming the highest ambient temperature is +110° F, the temperature rise within the unit based upon a power dissipation of 30 watts is determined by the following equation:

$$Q = \sigma_s F_e F_a A (T_r^4 - T_c^4) \qquad (6)$$

where

Q = Power dissipation (BTU/hr)

σ_s = Stefan-Boltzmann constant (0.173×10^{-8})

F_e = Emissivity factor

F_a = View factor

A = Unit surface area

T_r = Temperature of radiating surface (°R)

T_c = Temperature of ambient surroundings (°R)

The temperature rise is calculated to be 12.5° F which results in component operating temperatures of 122.5° F. This is well within the limits required for reliable operation.

5.6.9 Pressure. - Extended exposure to low atmospheric pressure can be considered hostile because of its effect on non-metallic materials. Certain materials can lose a considerable amount of weight in a years time due to sublimation. Because of this phenomenon special attention will be given to choosing materials with low sublimation rates.

Electrical breakdown due to low atmospheric pressure is not considered to be a problem. Since the altimeter package is unpressurized the positive pressure differential within the package during ascent will bleed off rapidly and will reach equilibrium with the surrounding outside environment before orbit is achieved.

5.6.10 Other environments. - Additional adverse environmental conditions such as humidity and saline atmosphere are considered to be less critical. Enclosing the equipment with a cover is usually sufficient to protect the internal components from corrosive atmospheres including high relative humidity.

5.6.11 Summary. - The environmental requirements as specified in the Performance Specification for Geos B Spacecraft[12] will be well within the maximum limits of the radar altimeter design and therefore, no problems are anticipated in this area.

REFERENCES

1. Schooley, A. H. ; Upwind-Downwind Ratio of Radar Return Calculated from Facet Size Statistics of Wind Disturbed Water Surface, Proceedings of IRE, April 1962.

2. F. J. Janza, R. K. Moore, B. D. Warner; Radar Cross Sections of Terrain near Vertical Incidence at 415 Mc, 3800 Mc and Extension to X-Band, Technical Report EE-21, University of New Mexico, 1959.

3. Ruze, John; Antenna Tolerance Theory - A Review; Proceedings of the IEEE, April 1966.

4. Zucker, H. ; Gain of Antennas with Random Surface Deviations; The Bell System Technical Journal; Vol. 47, No. 8, October 1968.

5. Greenwood, J. A. , A. Nathan, G. Neumann, W. J. Pierson, F. C. Jackson, T. E. Pease, May 1967: Radar Altimetry from a Spacecraft and its Potential Applications to Geodesy and Oceanography. New York University, Geophysical Science Laboratory, New York, New York, TR-67-3.

6. Pierson, W. J. ; The Effect of Waves on Radar Altimetry from a Spacecraft, A Preliminary Draft of a note for future publication.

7. "Continuous Orbital Guidance System", General Electric LMED proposal, July 1964.

8. Lee, H. L. ; Range Error Statistics for Splitgate Altimeter: Part I, Technical Memorandum 112-3, Center for Research, Inc. , University of Kansas, April 1968.

9. Lee, H. L. ; Range Error Statistics for Splitgate Altimeter: Part II, Technical Memorandum 112-4, Center for Research, Inc. , University of Kansas, April 1968.

10. "Space Rated Altimeter Study", Third Monthly Report, NASA Contract NAS 12-683, October 1968; General Electric Company.

11. Raytheon Company; Space Geodesy Altimetry Study, NASA Contract NA SW-1709, October 1968.

12. Performance Specification for Geos B Spacecraft, The Johns Hopkins University, Applied Physics Laboratory; S4S-0-199, 31 May 1967.

13. "An Analysis of Atmospheric Refraction Errors of Phase Measuring Radio Tracking Systems", Gordon D. Thayer. A technical report to Space Technology Laboratories, NBS Project 83485; and to General Electric Company, NBS Project 83488, 15 December 1961.

BIBLIOGRAPHY

1. Barton, D. K.; Radar System Analysis, Prentice-Hall, Inc., New Jersey, 1964.

2. Communications Systems, Inc.; Plan of Operations for the Geos B Spacecraft, Report No. R-4035-45-2, Falls Church, Virginia, October 1967.

3. Cooper, J. A.; Comparison of Observed and Calculated Near Vertical Ground Return Intensities and Fading Spectra, Technical Report EE-10, University of New Mexico, 1958.

4. Edison, A. R., Moore, R. K., Warner, B. D.; Radar Return at Near Vertical Incidence, Technical Report EE-24, University of New Mexico, 1959.

5. Ewing, Gifford C., Editor; Oceanography from Space, Woods Hole Oceanography Institution, Woods Hole, Massachusetts.

6. Frey, E. J., Harrington, J. V., and von Arx, W. S.; A Study of Satellite Altimetry for Geophysical and Oceanographic Measurement; XIV IAF Congress, September 1965, Athens, Greece.

7. Godbey, T. W.; Oceanographic Satellite Radar Altimeter and Wind Sea Sensor, Proceedings of Conference on the Feasibility of Oceanographic Explorations from Aircraft, Manned Orbital and Lunar Laboratories, Woods Hole, Massachusetts, August 1964.

8. Grant, C. R. and Yaplee, B. S.; Back Scattering from Water and Land at Centimeter and Millimeter Wavelengths, Proceedings IRE, Volume 45, 1957.

9. Klauder, J. R., Price, A. C., Darlington, S.; Albersheim, W. J.; The Theory and Design of Chirp Radars, The Bell System Technical Journal, Volume XXXIX, July 1960, Number 4, pp 745-808.

10. Lundquist, C.A.; The Interface Between Satellite Alimetry and Orbit Determination, Smithsonian Astrophysical Observatory, Cambridge, Massachusetts.

11. Moore, R.K., and Williams, C.S., Jr.; Radar Terrain Return at Near Vertical Incidence, Proceedings IRE, Volume 45, pp 228, 1957.

12. Moore, R.K.; Resolution of Vertical Incidence Radar Return into Random and Specular Components, Technical Report EE-6, University of New Mexico, 1957.

13. Neumann, G., and Pierson, W.J., 1966; Principles of Physical Oceanography, Prentice-Hall, Inc., Englewood Cliffs, New Jersey.

14. Performance Specification for the Geos B Spacecraft, 31 May 1967, Applied Physics Laboratory, John Hopkins University, S4S-0-199.

15. Price, C.F.; Signal Processing in a Satellite Radar Altimeter, Massachusetts Institute of Technology, August 1968.

16. Skolnik, M.I.; Introduction to Radar Systems, McGraw-Hill Book Company, New York, 1962.

17. Wiltse, J.C., Schlesinger, S.P., Johnson, C.M.; Back Scattering Characteristics of the Sea in the Region from 10 KMc to 50 KMc, Proceedings IRE, Volume 45, 1957.

APPENDIX A
THE CHARACTERISTIC OCEAN RADAR RETURN AT SATELLITE ALTITUDES

1. Flat, Lambertian Scattering Ocean from Satellite Altitudes

The radar return per unit area, $\sigma(\theta_i)$, as a function of angle of incidence from a flat Lambertian scattering surface is shown in Figure A-1.

The radar geometry, showing the build up of radar area from satellite altitude, h, is shown in Figure A-2.

$$P_R = \frac{P_T G^2 \lambda^2 A_T \sigma_T}{(4\pi)^3 R^4} \qquad \text{(A-1)}$$

where:

P_R = Received power
P_T = Transmitted power
λ = Wavelength
A_T = Area intercepted
R = One way range
σ_T = Scattering cross section

The reflection from satellite altitude from a flat Lambertian ocean is then:

$$P_R = \frac{k_1 A_T \sigma_T}{R^4} \quad \text{where } k_1 = \frac{P_T G^2 \lambda^2}{(4\pi)^3} \qquad \text{(A-2)}$$

Using the nomenclature of Figures A-1 and A-2 for t' 0 the radar altimeter equation then becomes:

$$P_R = \frac{k_2 c t'}{h^3} \left(1 - \frac{7c t'}{4h}\right) \qquad 0 \leq t' < T_p \qquad \text{(A-3)}$$

and

$$P_R = \frac{k_2 \, c \, T_p}{h^3} \left(1 - \frac{2ncT_p}{h}\right) \qquad T_p < t' < nT_p \qquad \text{(A-4)}$$

where

$$k_2 = \frac{P_T \, G^2 \, \lambda^2}{2(4\pi)^2} \qquad \text{(A-5)}$$

Figure A-3 is a plot of the detected radar altimeter signal from satellite altitudes of 600 and 850 nautical miles. This figure shows the altitude dependence of the receiver signal amplitude, V_R, using a square law detector. Note that this signal is proportional to the received power, P_R. Figure A-4 shows the characteristic radar altimeter return when an envelope detector is used. This signal is proportional to the square root of the received power. Note that amplitude change as a function of altitude is not as great as for square law detection.

Also observe that if a simple, fixed threshold detector is used to stop an altitude counter there would be an altitude error generated as a function of altitude, but that this error would be less for the envelope detected signal than for the square law detected signal.

2. Spherical, Lambertian Scattering Ocean from Satellite Altitudes

The ocean surface is not flat but spherical. Figure A-5 shows the radar geometry for a satellite borne altimeter operating over the earth's oceans. Also shown on Figure A-5 are the equations for radar area build up as a function of time over a spherical ocean surface. Note that the primary effect of the spherical ocean surface is to reduce the radar area by the amount

$$\frac{1}{\frac{1+h}{r_e}}$$

where h is satellite altitude and r_e is the radius of the earth. Figures A-6 and A-7 show this effect for both square law and envelope detected radar returns. Of particular interest is the fact that the shape of the returns is no different from that obtained over a flat ocean.

Figures A-8 and A-9 indicate that by using an automatic gain control the effects of altitude on the return signal are eliminated such that a simple threshold detector would not develop any altitude dependent error. This then gives two preferred modes of receiver operation:

(1) Square law detection with AGC on the return.

(2) Envelope detection with AGC on the return.

3. Effect of Ocean Waves on Pulse Radar Altimeter Returns

The earth's oceans, beside being a spherical surface, also have significantly different wave heights, $H_{1/3}$, depending on the past history and geometry of the wind fields over the particular stretch of ocean observed.

Figure A-10 illustrates the case of real ocean as a radar scattering cross-section generator. It indicates that the real ocean surface consists of many reflectors of different sizes at different heights above and below mean sea level, each pointing in a different direction.

Figure A-11 relates the probability density distribution of reflecting ocean area, above and below the mean sea level value, to the significant wave height $H_{1/3}$, of oceans.

From the work of Schooley[1] it is clear that effective radar backscattering area will be encountered at any surface on the ocean.

Thus, the convolution of the probability distribution of surface Figure A-11 onto the radar signal return from a flat surface Figure A-8 will show the effect of ocean waves on pulsed radar altimeter returns.

Pierson[6] has recently derived this convolution integral and solved it for the effect of seas with significant wave heights, from $H_{1/3} = 2$ meters to $H_{1/3} = 20$ meters, on a 50 nanosecond altimeter pulse. This is considered a sufficient range of sea states, since the highest waves ever recorded had a significant wave height of $H_{1/3} = 18.5$ meters.

In the process of this study Godbey arrived at exactly the same results as Pierson's convolution integral using a numerical integration approach. Using this numerical integration approach, the effect of the largest sea state ever measured on pulses of 10 nanoseconds, 50 nanoseconds (coincides with Pierson's results) and 200 nanoseconds was determined. The resultant effect upon these pulses is shown in Figure A-12.

Since the rounding effect of sea state on the radar altimeter return is smaller for longer transmitted pulse widths, T, a sufficiently long pulse is necessary to avoid tracking wave tops. Using threshold tracking, a pulse length of 50 nanoseconds appears acceptable.

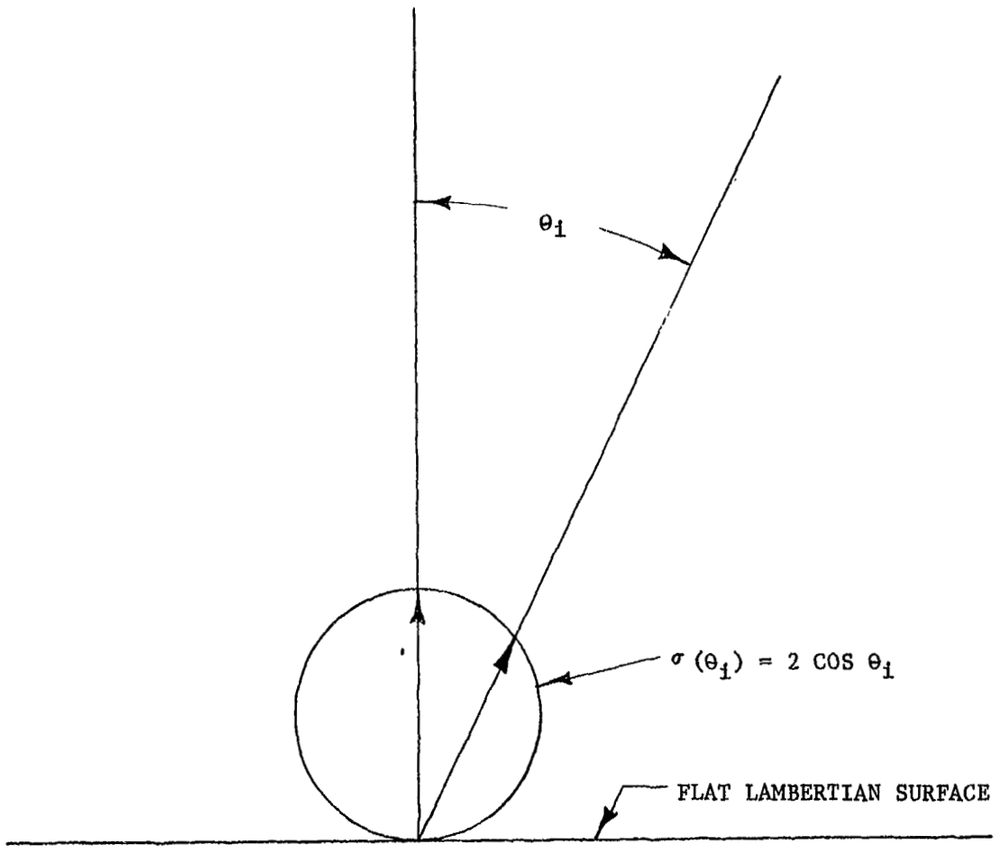

RADAR POWER RETURN FROM A FLAT, LAMBERTIAN SCATTERING OCEAN

FIGURE A-1

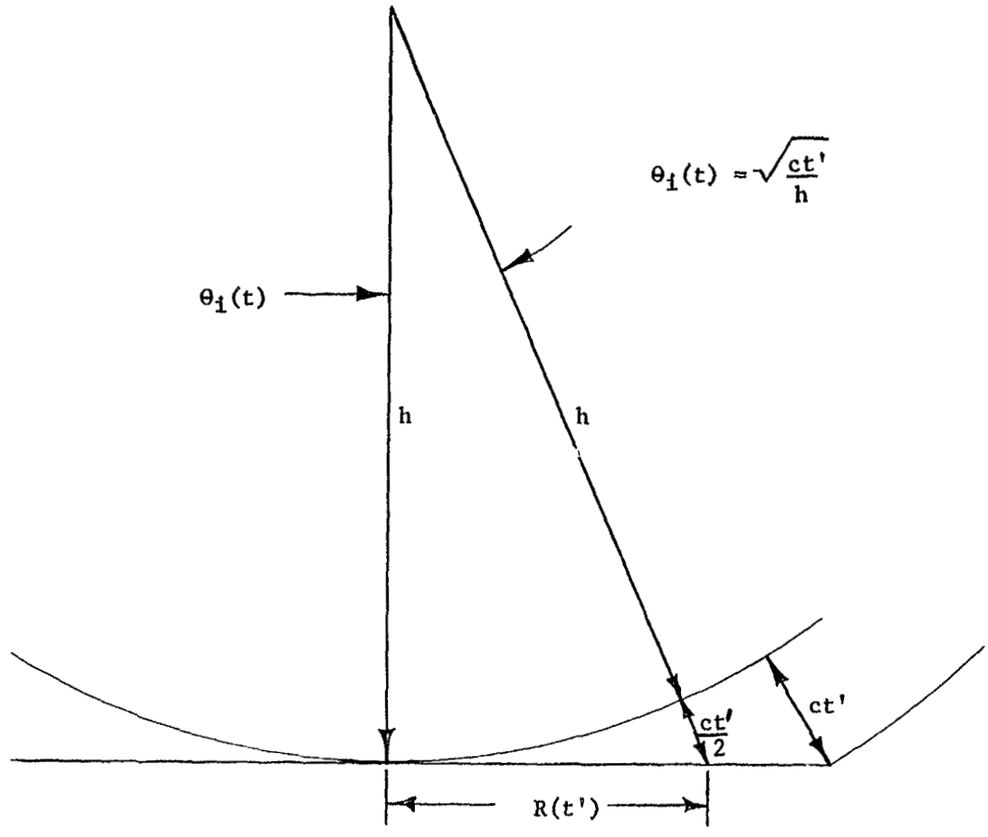

$$A(t') = o \; ; \quad t' < 0 \text{ where } t' = t - \frac{2h}{c}$$

$$A(t') = R(t')^2 = \pi[(h+\frac{ct'}{2})^2 - h^2] = \pi \; ct'h(1 + \frac{ct'}{4h}); \; o \leq t' < T$$

$$A(t') = \pi \; [R(nT)^2 - R[(n-1)T]^2] = \pi \, cTh(1 + \frac{(2n-1)cT}{4h}) \; ; T < t' < nT$$

GEOMETRY OF RADAR TARGET AREA, A(t), BUILD UP AS A FUNCTION OF TIME, t, FROM RADAR TRAMSMISSION

FIGURE A-2

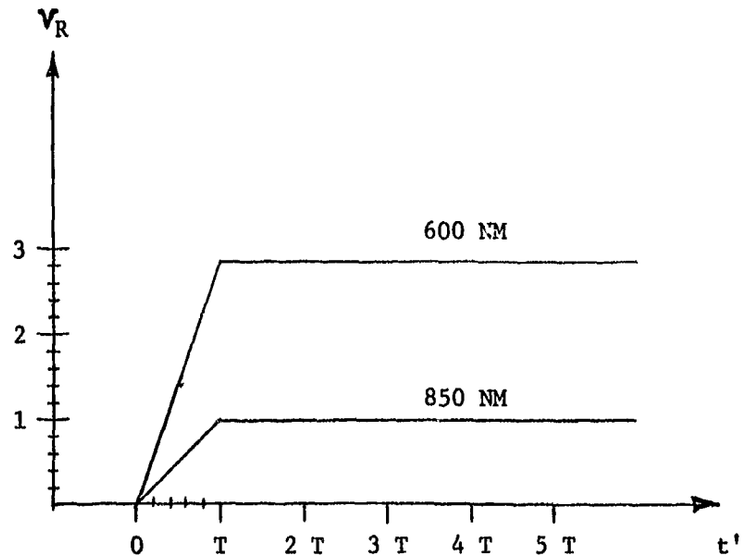

CHARACTERISTIC RADAR ALTIMETER RETURN FROM FLAT, LAMBERTIAN SCATTERING OCEAN (SQ LAW DETECTION NO AGC)

FIGURE A-3

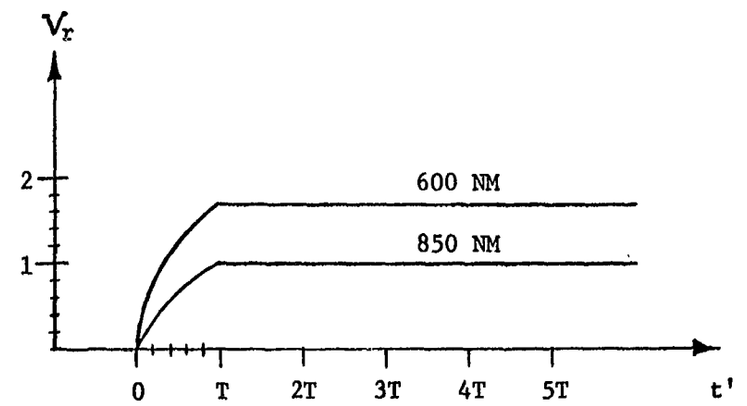

CHARACTERISTIC RADAR ALTIMETER RETURN FROM FLAT, LAMBERTIAN SCATTERING OCEAN (ENVELOPE DETECTION NO AGC)

FIGURE A-4

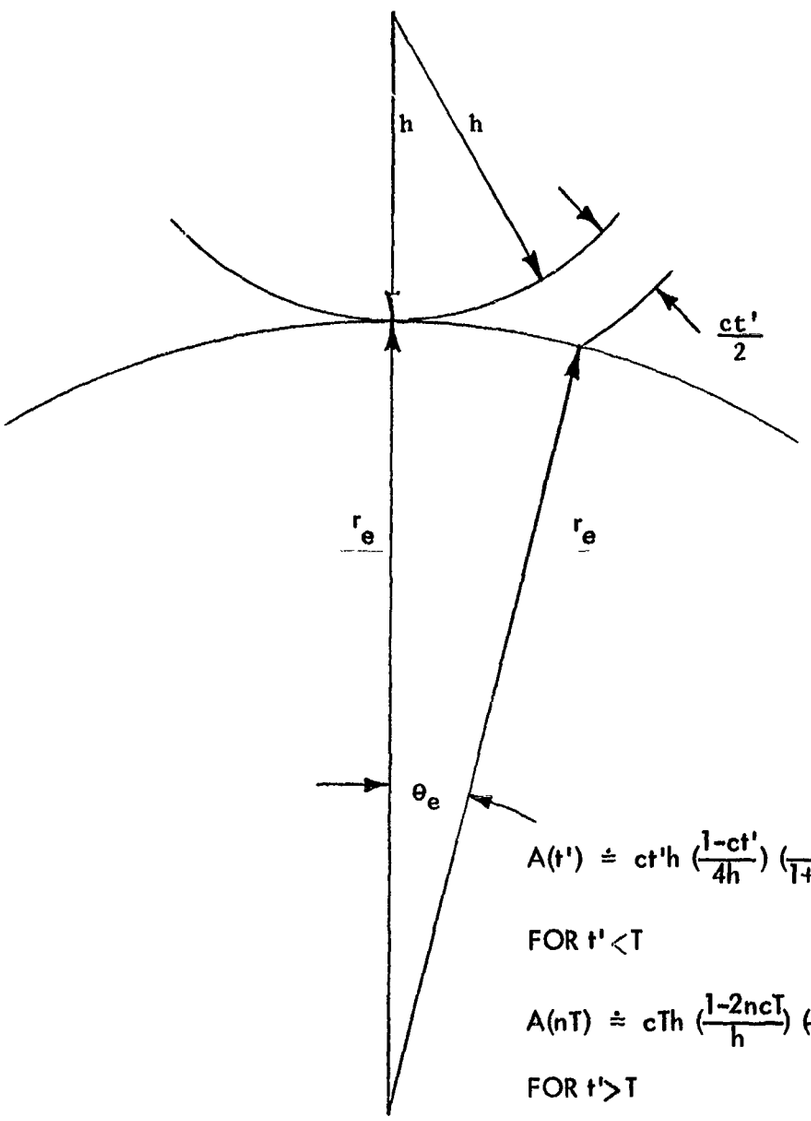

GEOMETRY OF SATELLITE RADAR ALTIMETER
RETURN FROM SPHERICAL OCEAN SURFACE

FIGURE A-5

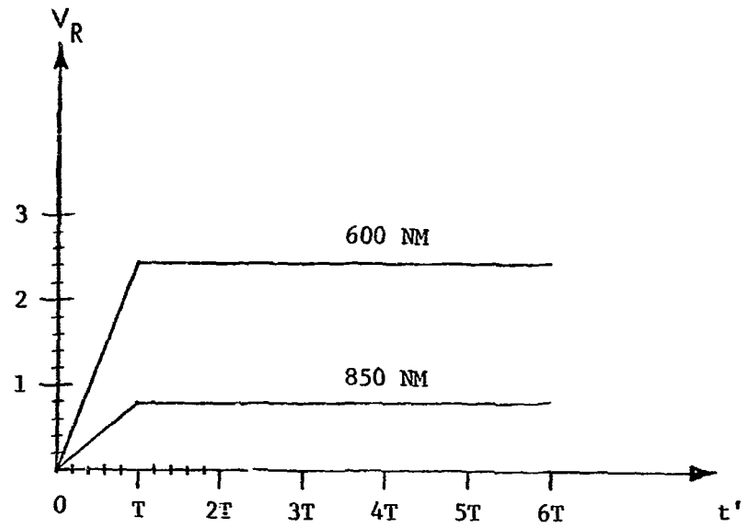

CHARACTERISTIC RADAR ALTIMETER RETURN FROM SPHERICAL LAMBERTIAN SCATTERING OCEAN (SQ LOW DETECTION, NO AGC)
FIGURE A-6

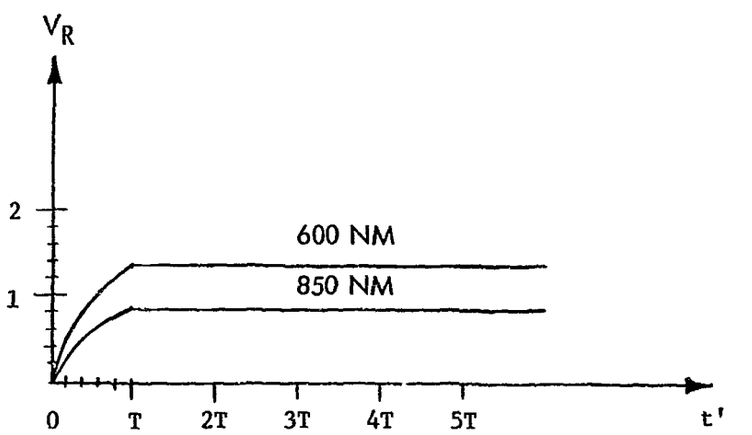

CHARACTERISTIC RADAR ALTIMETER RETURN FROM SPHERICAL LAMBERTIAN SCATTERING OCEAN (ENVELOPE DETECTION, NO AGC)
FIGURE A-7

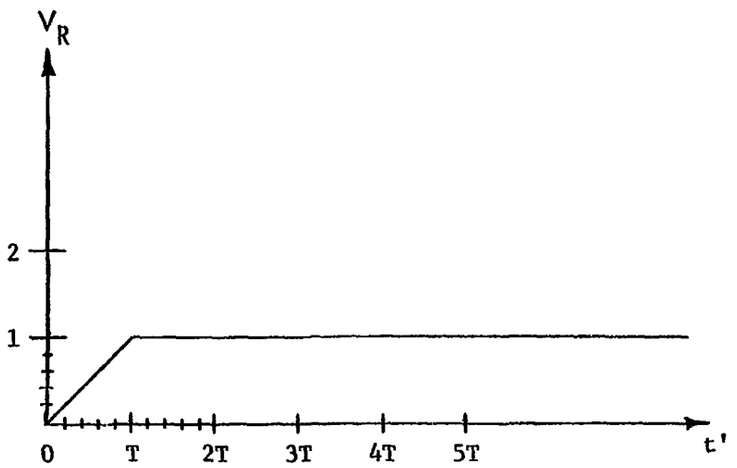

CHARACTERISTIC RADAR ALTIMETER RETURN FROM SPHERICAL LAMBERTIAN SCATTERING OCEAN (SQUARE LAW DETECTION, AGC ON RETURN)

FIGURE A-8

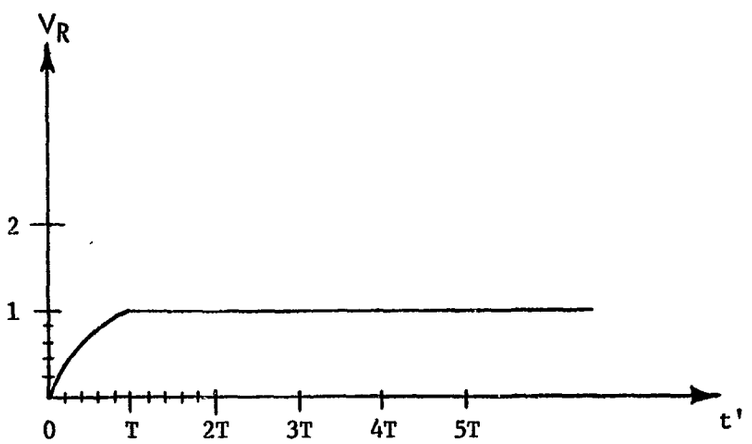

CHARACTERISTIC RADAR ALTIMETER RETURN FROM SPHERICAL LAMBERTIAN SCATTERING OCEAN (ENVELOPE DETECTION, AGC ON RETURN)

FIGURE A-9

ILLUSTRATION OF REAL OCEAN AS A RADAR SCATTERING
CROSS SECTION GENERATOR
FIGURE A-10

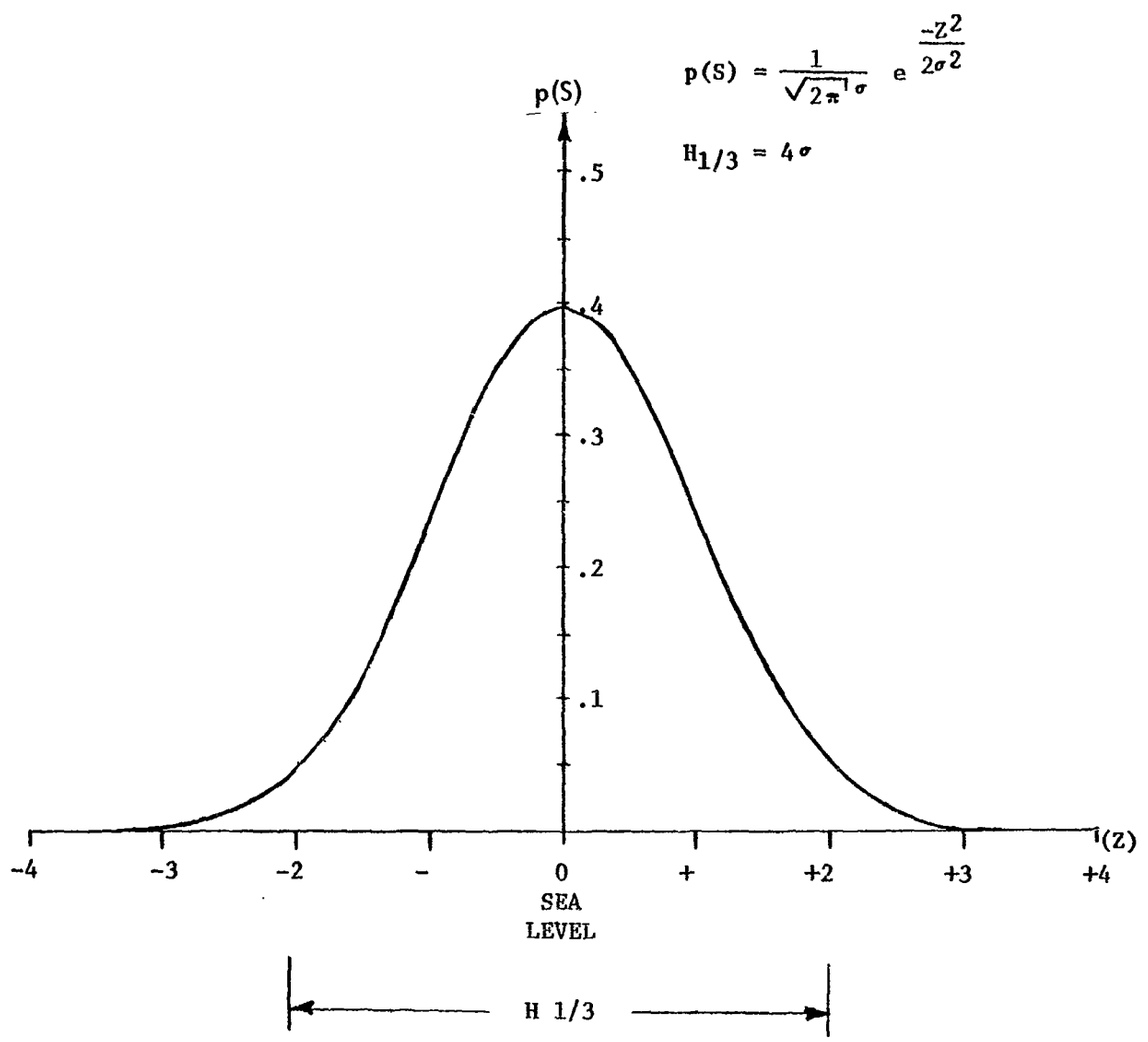

PROBABILITY DENSITY FUNCTION OF SEA AREA (S) AS A FUNCTION OF DISTANCE (Z) FROM MEAN SEA LEVEL FOR A SIGNIFICANT WAVE HEIGHT H 1/3

FIGURE A-11

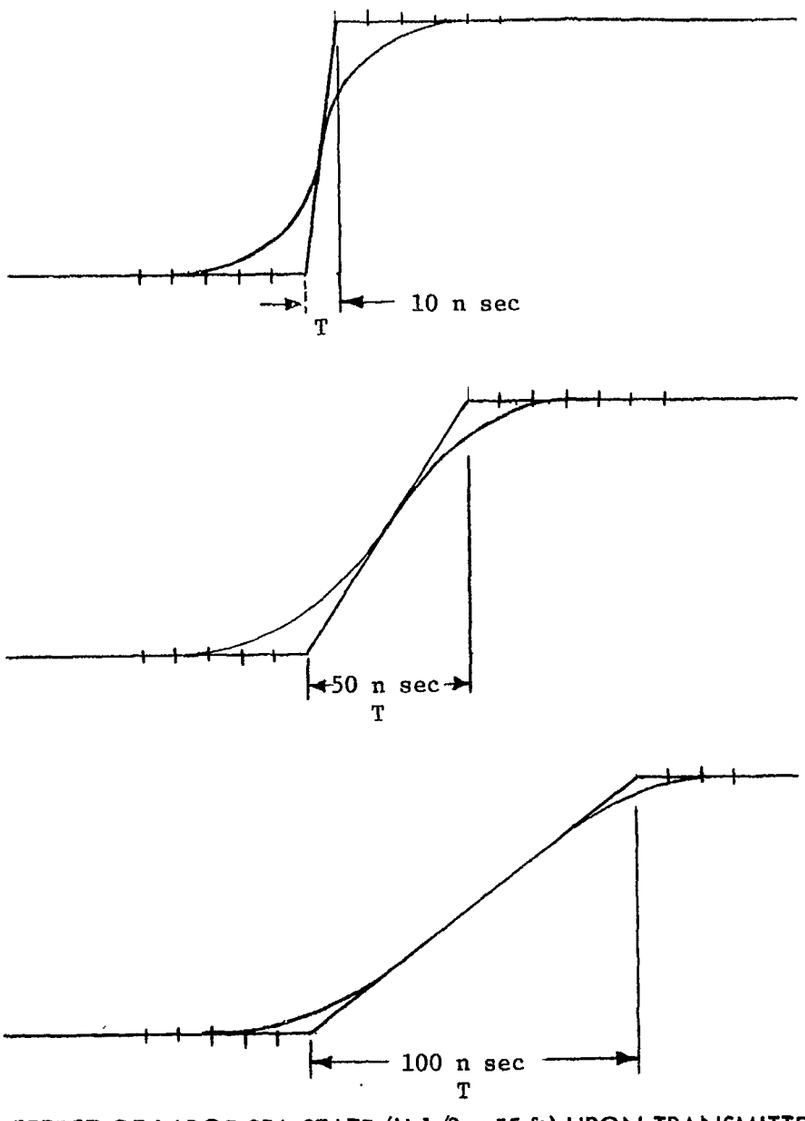

EFFECT OF LARGE SEA STATE (H 1/3 = 55 ft) UPON TRANSMITTED PULSE WIDTH FOR SQUARE LAW DETECTED SEA RETURNS

FIGURE A-12

APPENDIX B
THE OCEAN RADAR RETURN NOISE CHARACTER AND SIGNAL PROCESSING

1. Noise Character of Radar Return from Ocean

The noise character of the radar return from the ocean is a consequence of the fact that the envelope of the received voltage waveform will have a Rayleigh probability density function as described in Section 5.1. The statement of statistical stability due to the very large number of scattering elements comprising each part of the ocean means that the Rayleigh probability density distribution and no other probability density distribution will be observed.

The return from ocean of a transmitted square pulse can be represented as:

$$V(t') = 0; \qquad t' < 0$$

$$V(t') = \sum_{k\ t=1}^{N} (a_k \cos \omega_c t + b_k \sin \omega_c t) \qquad 0 \leq t' < T_p \qquad \text{(B-1)}$$

V(t') represents the ocean return pulse signal; an increasing function of time. a_k and b_k are normally distributed constants with a mean of zero and a variance of one. ω_c = transmitted carrier radial frequency. The linear detected envelope of this signal is:

$$x = \sqrt{\left(\sum_{k\Delta t=1}^{N} a_k\right)^2 + \left(\sum_{k\Delta t=1}^{N} b_k\right)^2} \qquad \text{(B-2)}$$

Which is a Rayleigh noise distribution whose mean value is:

$$M(x) = \sigma \sqrt{\pi t'/2} \qquad \text{(B-3)}$$

With variance about the mean of:

$$S^2(x) = (4-\pi)\, t'\, \sigma^2/2 \qquad \text{(B-4)}$$

The signal to standard deviation ratio of the detected envelope is:

$$\frac{M(x)}{S(x)} = \sqrt{\frac{\pi}{(4-\pi)}} = 5.63 \text{ db} \qquad \text{(B-5)}$$

At this point in the analysis the fact that the signal is Rayleigh distributed must be considered. That is, the signal cannot be treated as a classical radar signal since signal to noise statistics for each case differs.

Figure B-1 shows the probability density functions of noise and signal plus noise for envelope detection in the ordinary radar case. The classical radar problem is to select the detection threshold with respect to the receiver noise level, σ_n, to minimize the false alarm probability and maximize the target detection probability. In the radar problem a signal to noise ratio of 14 db is considered sufficient for accurate range tracking while the tracking error due to receiver noise is considered negligible when signal to noise is greater than about 20 db.

The expected signal and noise statistics for the altimeter problem is shown in Figure B-2. In the altimeter problem, during the rise time of the return signal, the probability density function of the signal plus noise increases linearly from just receiver noise to noise with 20 db more power. Thus if a threshold is chosen high enough to reduce false alarm probability to a negligible amount, for example $4\sigma_n$, then even when the ocean return plus noise power reaches 20 db above the receiver noise, there is only an 85% probability that the return is detected.

Square law detection is one method investigated for use in the altimeter receiver. The probability density functions of square law detected receiver noise and sea return plus noise are:

$$p(y) = \frac{1}{2\sigma_n^2} e^{(-y/2\sigma_n^2)} \qquad \text{for receiver noise} \qquad \text{(B-6)}$$

and

$$p(y) = \frac{1}{2(\sigma_s^2 + \sigma_n^2)} e^{(-y/2(\sigma_s^2 + \sigma_n^2))} \qquad \text{(B-7)}$$

for sea return plus noise

where σ_n = Standard deviation of receiver noise

σ_s = Standard deviation of ocean return

2. Pre-Detection Filtering, Detection and Post-Detection Filtering of Radar Sea Return Noise

The characteristics of an IF Amplifier which affect the noise statistics of radar altimeter returns are bandwidth and saturation or limiting. The IF bandwidth acts as a pre-detection filter to decrease the probability of very large signal excursions. IF saturation further reduces the probability of large signals.

The simple diode detector characteristic which affects the noise statistics of radar altimeter returns is the breakdown threshold. The breakdown threshold acts as a lower limiter and specifically can be biased so that detection does not occur until radar signal plus receiver noise exceeds a selected value. This condition results in non-linear envelope detection, or non-linear square law detection and greatly decreases the probability of a detected signal output due to receiver noise only.

Post detection filtering consisting of a simple resistor and capacitor integrator can greatly reduce the noise envelope of the radar altimeter detector return. As a result the signal out of the post detection filter is made to more nearly approximate the signal plus noise probability distribution obtained with targeting radar. The penalties paid for using post detection filtering are the introduction of an additional time delay element (on the order of 400 nanoseconds) and creation of a longer rise time on the leading edge of the return. Figures D-6 and D-7 show this series of processes applied with non-linear envelope detection. Figures D-8 and D-9 show the time dispersion of detected signals after post detection filtering.

Analysis of this signal detection dispersion shows that the average delay time of the detected signal is about 370 nanoseconds after t_o, and the standard deviation of the delay time is ±80 nanoseconds for a radar return to receiver noise level of 10 db.

Hence if only threshold detection is used for altitude ranging and the altitude measurements are averaged over one second, the resulting altitude value would have a residual sea return noise error of about ±1.2 meters RMS for a radar pulse repetition rate of 100.

By using less post detection filtering, the average delay time can be improved to a limit of about 130 nanoseconds after t_0 with a standard deviation of ±20 nanoseconds. Thus it is experimentally determined that with about 20 db signal to noise ratio, one simple, easy to implement, altitude detection circuit is adequate to achieve a one meter standard deviation satellite altimeter.

The experiment also shows that the signal out of the detector crosses the same signal detection threshold earlier in every case than it does with post-detection filtering. Thus we need not fear that signal threshold detection without post-detection filtering would give a condition of no-detection so long as the detection gate is at least 400 nanoseconds long.

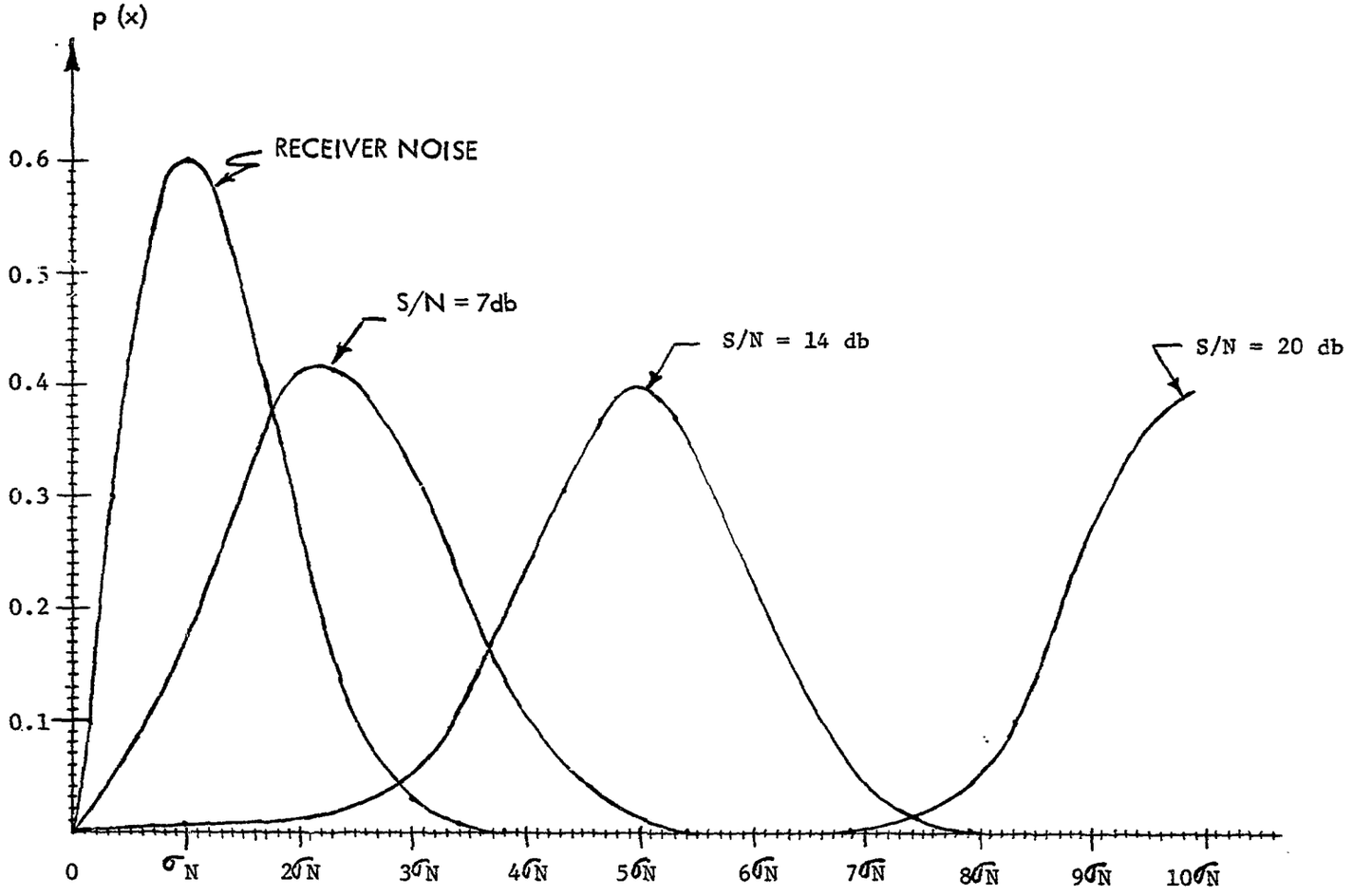

PROBABILITY DENSITY FUNCTIONS OF NOISE & SIGNAL PLUS NOISE
(ENVELOPE DETECTION) THE CLASSICAL RADAR PROBLEM

FIGURE B-1

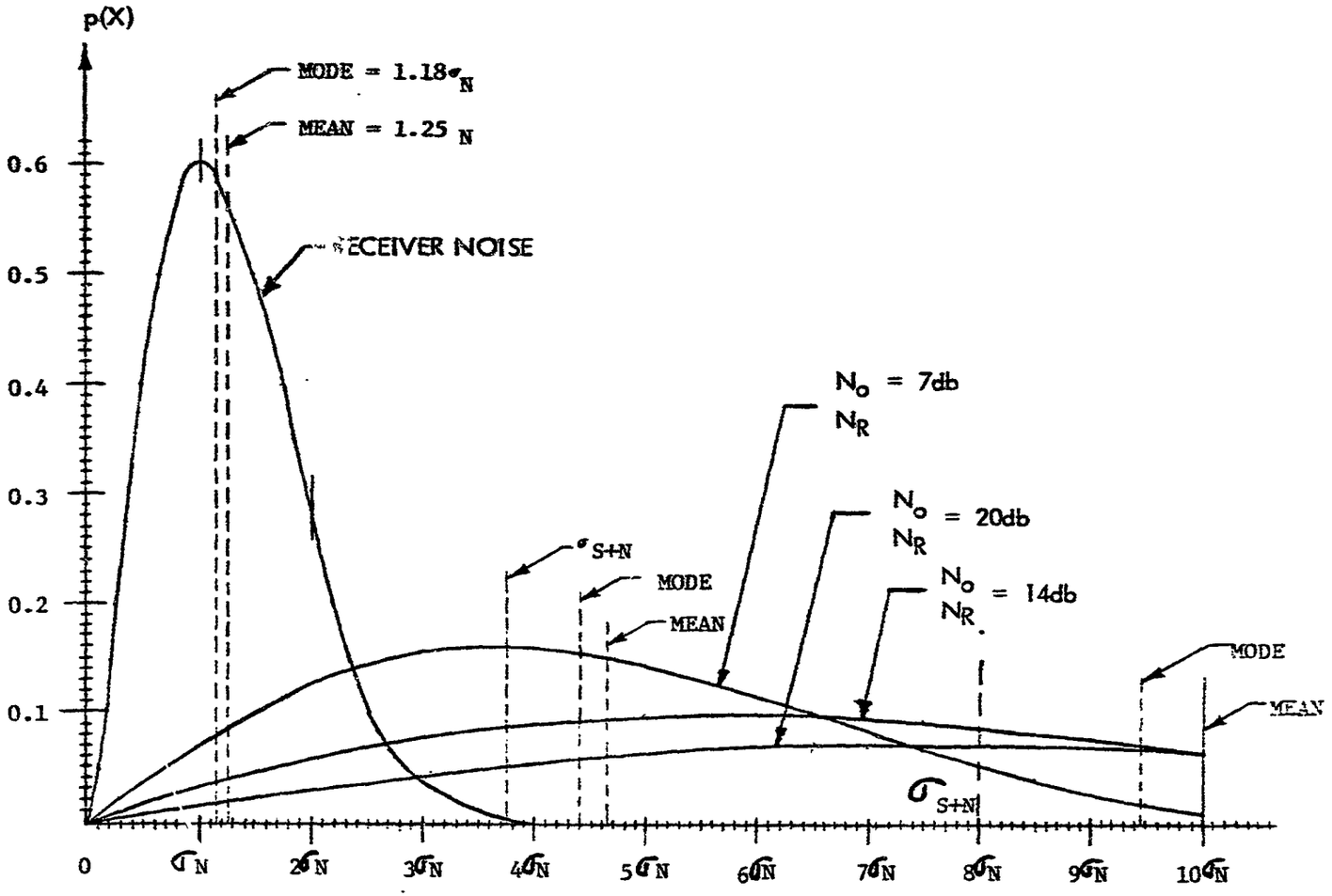

PROBABILITY DENSITY FUNCTIONS OF NOISE & OCEAN RETURN PLUS NOISE (ENVELOPE DETECTION) THE SATELLITE RADAR ALTIMETER PROBLEM

FIGURE B-2

APPENDIX C
PROPAGATION ERRORS

Mr. Gordon Thayer of the National Bureau of Standards[13] has studied and measured atmospheric propagation errors for radars at all elevation angles. Tests have been conducted all over the world, at all times of the year. The result of this work is a complete set of equations for the correction of propagation range error through the total atmosphere which take into account both geographical location and the day of the year.

For a satellited altimeter in the X to Ku band range, propagation on a vertical path through the entire atmospheric results in a mean altitude error of about +4.5 meters. Using the National Bureau of Standards equations to correct for atmospheric propagation range delay results in a residual standard error of less than 0.1 meters.

It is recommended that these equations be employed for the correction of satellite altimetry data because their demonstrated accuracy makes it unnecessary to conduct atmospheric refraction measurements.

APPENDIX D
SEA RETURN PULSE SIMULATOR

A Sea Return Pulse Simulator test set was constructed, using material and equipment available within the General Electric Company, to permit a practical evaluation of typical receiver components and detectors. The block diagram of the Sea Return Pulse Simulator, Figure D-1, shows how a sinewave or noise pulse is generated and then detected using linear, peak, or square law detection. The Rayleigh envelope and characteristic rise time of the return pulse from the sea are produced by a pulsed narrowband Gaussian process. The first order effects of various receiver structures were studied using this design tool. Primarily, the performance characteristics of detectors, AGC, IF, and low pass filters, integrators and threshold circuits with different detector configurations were investigated and measured using the simulator to provide an input signal. The following nomenclature is used in discussing the results:

N_o - Ocean Return Signal

N_r - Receiver Noise

S - Sine Wave Signal

A series of tests were performed with different configurations using several different ocean noise to receiver noise ratios and sinewave signal to noise ratios.

A most important result was obtained from these Sea Return Pulse Simulator tests. Analysis of threshold detection crossing times obtained from photographs of linear detection of simulated radar altimeter ocean returns indicate that at N_o/N_r ratios in excess of 10 db a threshold detector would give one sigma altitude accuracies on the order of one meter.

Photographs of the key test results are given in Figures D-2 through D-12 of linear detection, linear detection with integration and square law detection. Figure D2 shows the output of an unbiased linear detector with two superimposed signals; the first an ocean return with N_o/N_r = 20 db and the second a sine wave signal of the same RMS value. The dc level produced by the

sine wave signal is greater than the mean value of the ocean return signal, consequently the leading edge of the sine wave signal is not the mean of the ocean return leading edge. This would not be true if AGC were used to maintain the pulse top at the ocean return mean value, as is shown in Figure D-5.

In Figure D-5, the lower photo shows the leading edges of 50 Linearly Detected Pulses with sine wave modulation. The sine wave signal to receiver noise ratio of 16 db produces a probability spread of leading edge threshold detection times. At a threshold level of 0.1 volts, corresponding to one third the mean peak voltage maintained by the AGC, the mean threshold detection time is centered at about +35 n sec from the start of the pulse with a spread from +20 n sec to +55 n sec. The standard deviation of detection time calculated for a Gaussian like distribution is then approximately 6 n sec. The residual standard deviation after averaging one hundred measurements would be approximately 0.6 n sec which translates to an altitude standard deviation of approximately 0.1 meters. These results are representative of the expected return from a clean radar target. The returns produced by the ocean on the other hand, are more nearly represented by the upper photo of Figure D-5 which has the same mean value as the sine wave signal. The 20 db value of N_O/N_r, 4 db better than the sine wave signal to noise ratio, is much noisier in voltage excursion and threshold crossing time dispersion. Each of the fifty individual pulses can be seen in the photo. A photo analysis of the initial detection time for a leading edge threshold set at 0.1 volts yields a mean of about +65 n sec with a spread from +10 to +130 n sec. The associated standard deviation is then about 25 to 30 n sec and the residual standard deviation after averaging one hundred measurements is about 2.5 to 3 n sec or 0.38 to 0.45 meters in terms of altitude. The principal effect of the noisy ocean return is to increase threshold detection noise statistics as just shown and as evidenced in the photograph of Figure D-5.

Figure D-3 shows the unbiased linear detector output resulting from six input pulses with N_O/N_r = 20 db. The wave form of each of the six output pulses can be identified in the photograph. Figure D-4 is the output of a linear unbiased detector at N_O/N_r = 10 db and under this condition it appears impossible to use a leading edge threshold technique because of the uncertainty in the position of the detected pulse. This situation is improved by biasing the detector, as is shown in Figures D-5 and D-6 for ocean returns of N_O/N_r = 20 db, N_O/N_r = 10 db and a sine wave signal with S/N_r = 16 db, with an AGC to maintain the same average pulse top value.

An integrator can be used to reduce the magnitude of the pulse amplitude variation and produce a waveform more acceptable to the threshold circuit. Figure D-7 shows the output for an input sine wave signal with a 16 db signal to noise ratio and an ocean return of N_O/N_r = 10 db.

Analysis of the time statistics of the ocean return signal of Figure D-7 gives an average crossing time at the 0.1 Volt threshold of about +370 n sec after the start of the pulse, with a spread from approximately +120 n sec to +620 n sec. For Gaussian statistics, with a standard deviation of about 80 n sec, the residual standard deviation after averaging one hundred measurements would be about 8 n sec or 1.2 meters in altitude. Note that the integrated sine wave signal of Figure D-7 has about the same average crossing time at the 0.1 Volt threshold as with the noisy ocean return. The integration time constant used was on the order of 800 n sec. An initial analysis indicates that an optimum integration time constant somewhere between 100 and 1000 n sec will yield the best tradeoff between the detection time statistics of a threshold tracking system and control of the additional delay time introduced by the integration time constant.

The output of a threshold circuit, after detection and integration of the input signal, is shown in Figures D-8 and D-9 for N_O to N_r ratios of 10 and 20 db and for a sine wave signal to noise ratio of 16 db with AGC. The peak-to-peak time variation for 50 pulses is 400, 200 and 40 n sec respectively. It should be noted in Figure D-8 that when AGC is used, the mean value of the ocean return leading edge appears at the same time as the sine wave signal.

The output of a square law detector, with a receiver AGC is shown in Figures D-10 through D-12 for N_O to N_r ratios of 10, 20 and 30 db. The increased value of receiver noise corresponding to lower N_O to N_r ratios can be seen on the oscilloscope trace before the first pulse appears. The photos indicate that the square law detector used has a tendency toward the fast rise time, slow fall time action of the pulse detector. This property changes the statistical behavior of the square law detection from the theoretical. The result is a tendency to produce a monotonically increasing signal probability, limit rapid voltage excursions from high to low, and if enhanced and used in conjunction with IF amplifier high voltage limiting should give an engineering method of affecting a significant decrease in the noise content obtained in each gate of the square law detection Early/Gate Gate Tracking servo described in Appendix E.

Similar techniques can be used to improve noise statistics and improve the tracking accuracy of the envelope detection, Early/Late Gate Tracking servo also described in Appendix E.

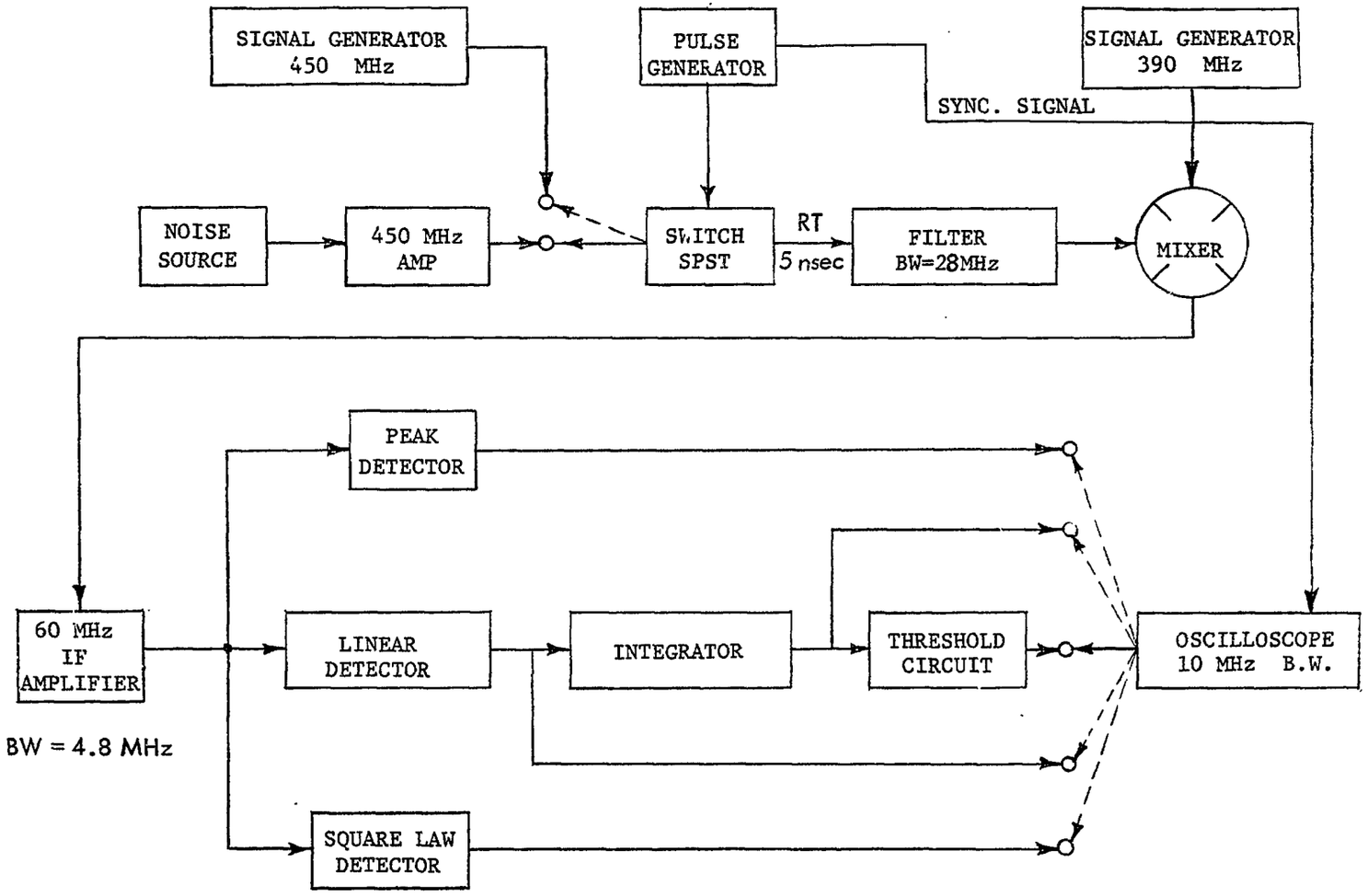

FIGURE D-1 SEA RETURN PULSE SIMULATOR BLOCK DIAGRAM

LINEAR DETECTOR OUTPUT WAVEFORMS

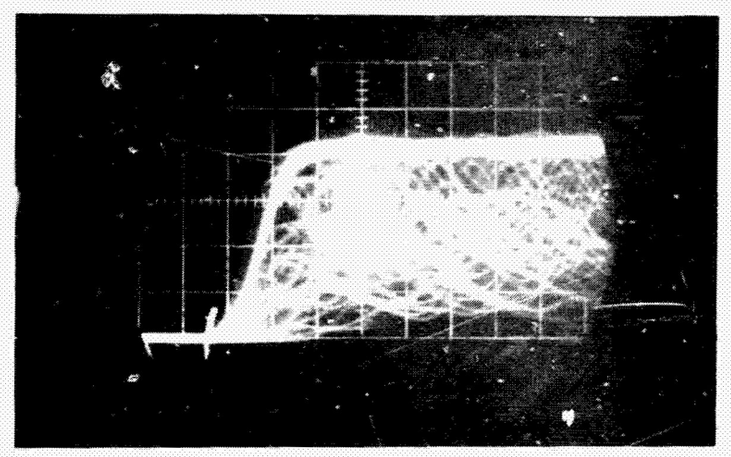

FIGURE D-2
DETECTOR OUTPUT
(NO BIAS)
OCEAN RETURN WITH
THE SAME RMS VALUE
OF SINE WAVE SIGNAL
SUPER-IMPOSED
NO AGG
N_o/N_r = 20 DB
50 PULSES
0.5 V/CM
40 N SEC/CM

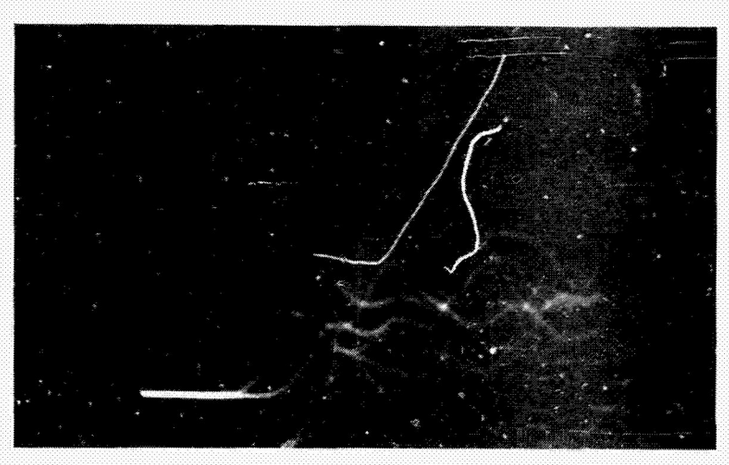

FIGURE D-3
DETECTOR OUTPUT
(NO BIAS)
OCEAN RETURN
NO AGG
6 PULSES
N_o/N_r = 20 DB
0.5 V/CM
40 N SEC/CM

LINEAR DETECTOR OUTPUT WAVEFORMS

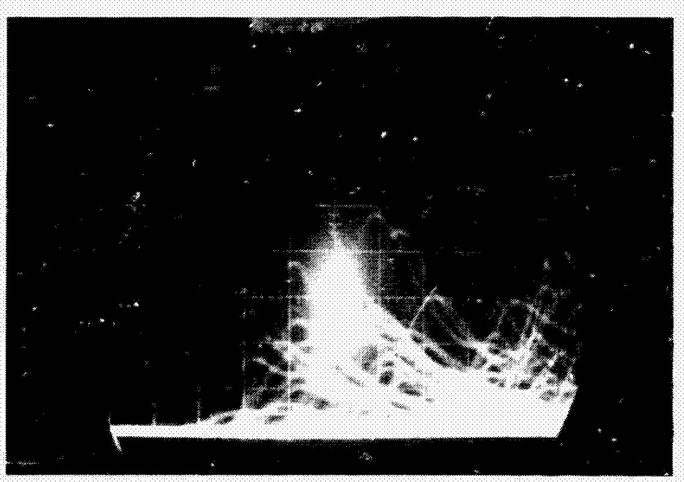

FIGURE D-4
DETECTOR OUTPUT
(NO BIAS)
OCEAN RETURN
N_o/N_r = 10 DB
50 PULSES
NO AGC
0.5 V/CM
40 N SEC/CM

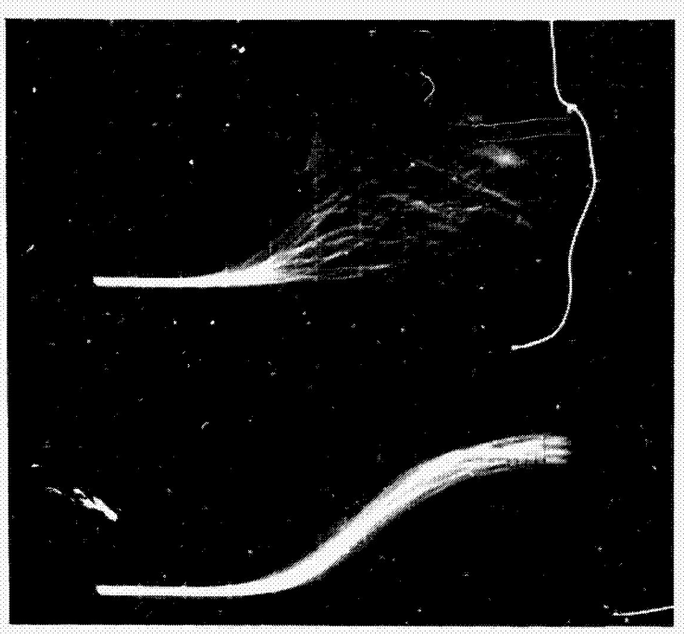

FIGURE D-5
DETECTOR OUTPUT
OCEAN RETURN (TOP)
N_o/N_r = 20 DB
SINE WAVE SIGNAL (BOT)
S/N_r = 16 DB
AGC OPERATING
DETECTOR BIASED
50 PULSES
0.1 V/CM
20 N SEC/CM

LINEAR DETECTOR OUTPUT WAVEFORMS

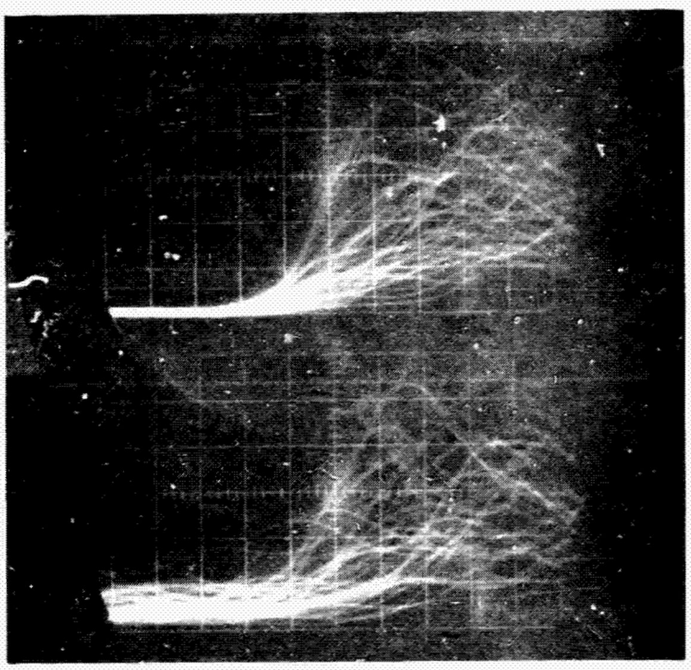

FIGURE D-6
DETECTOR OUTPUT
(WITH BIAS)
OCEAN RETURN
N_o/N_r = 20 DB (TOP)
N_o/N_r = 10 DB (BOT)
AGC OPERATING
50 PULSES
0.1 V/CM
40 N SEC/CM

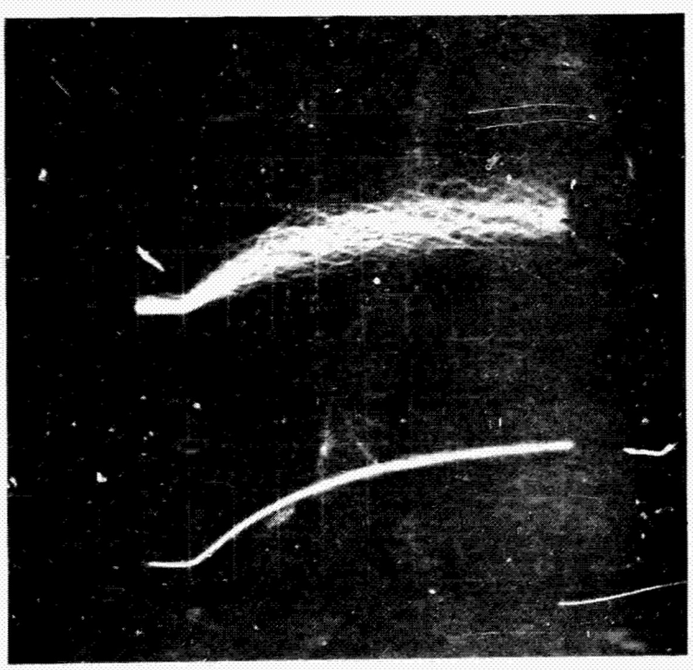

FIGURE D-7
INTEGRATOR OUTPUT
OCEAN RETURN
N_o/N_r = 10 DB
SINE WAVE SIGNAL (TOP)
S/N_r = 16 DB (BOT)
AGC OPERATING
DETECTOR BIASED
50 PULSES
0.1 V/CM
400 N SEC/CM

LINEAR DETECTOR OUTPUT WAVEFORMS

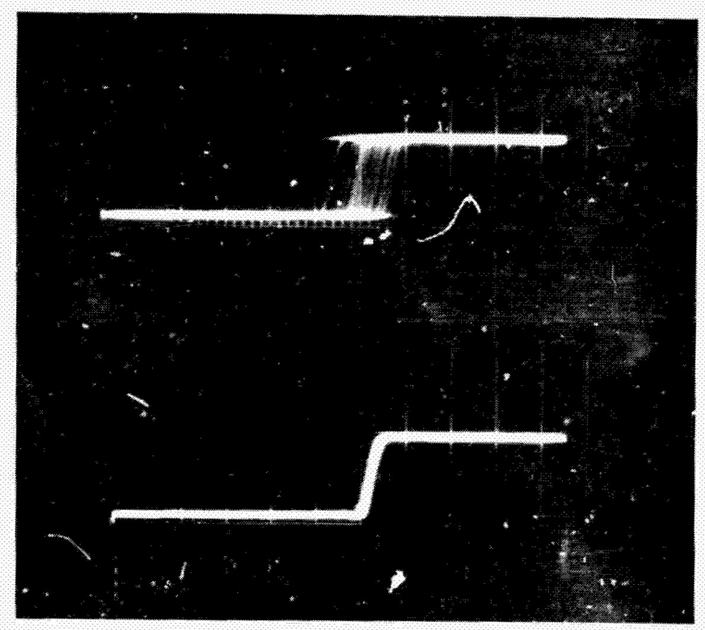

FIGURE D-8
THRESHOLD CKT. OUTPUT
OCEAN RETURN
N_o/N_r = 20 DB (TOP)
SINE WAVE SIGNAL
S/N_r = 16 DB (BOT)
AGC OPERATING
DETECTOR BIASED
DETECTOR OUTPUT
INTEGRATED
50 PULSES
0.5 V/CM 100 N SEC/CM

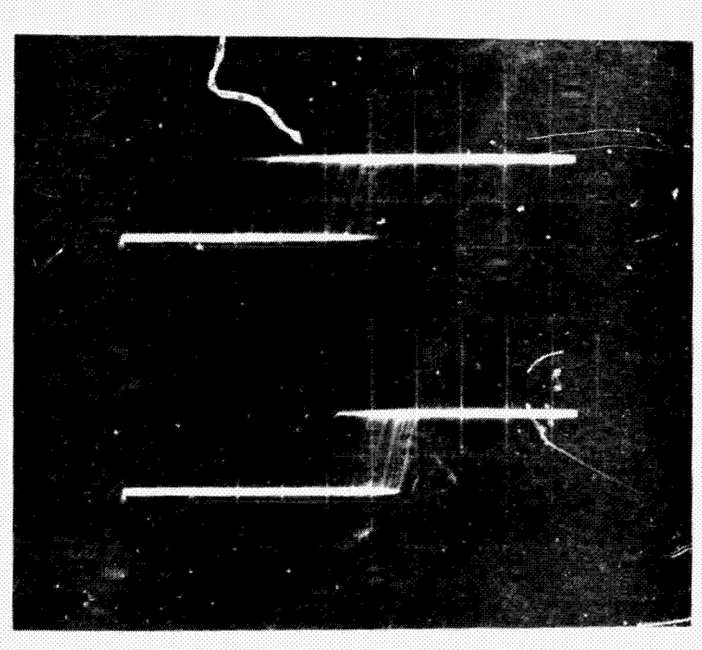

FIGURE D-9
THRESHOLD CKT. OUTPUT
OCEAN RETURN
N_o/N_r = 10 DB (TOP)
N_o/N_r = 20 DB (BOT)
AGC OPERATING
DETECTOR BIASED
50 PULSES
DETECTOR OUTPUT
INTEGRATED
0.5 V/CM
100 N SEC/CM

SQUARE LAW DETECTOR OUTPUT WAVEFORMS

AGC OPERATING
50 PULSES
40 SEC CM
5 MV/CM

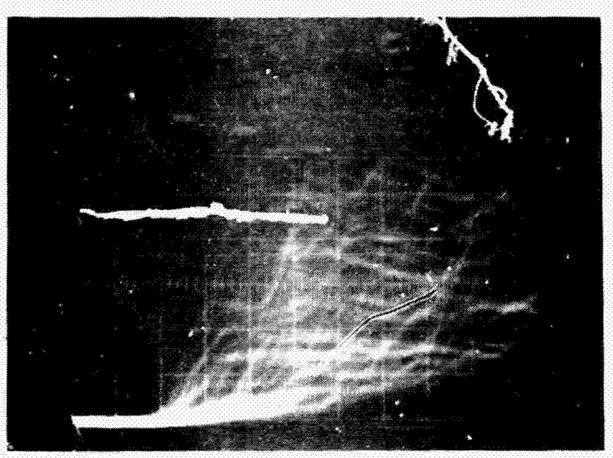

FIGURE D-10

N_o/N_r = 30 DB

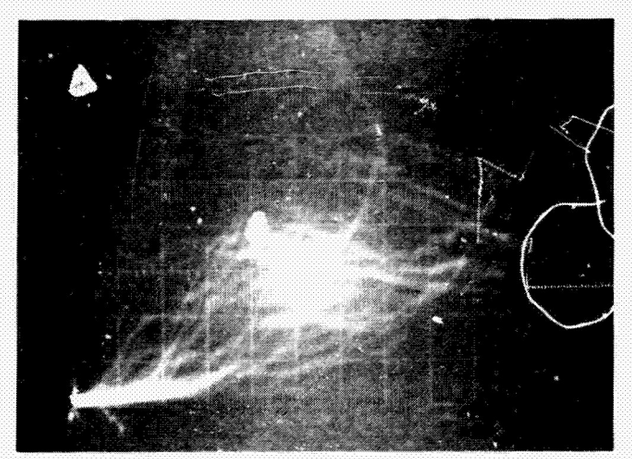

FIGURE D-11

N_o/N_r = 20 DB

SQUARE LAW DETECTOR OUTPUT WAVEFORMS

AGC OPERATING
50 PU.SES
40 SEC/CM
5 MV/CM

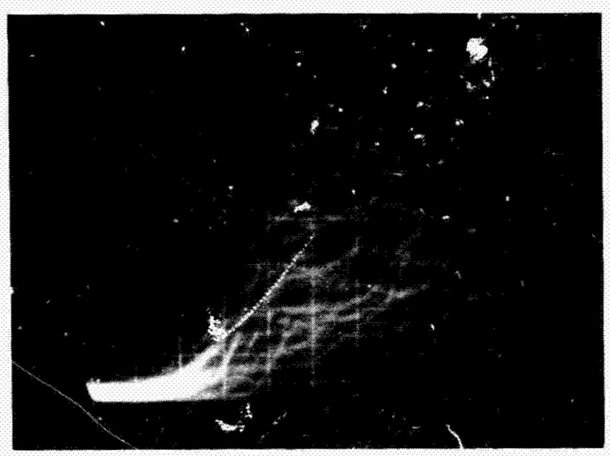

FIGURE D-12

N_o/N_r = 10 DB

APPENDIX E
EARLY/LATE GATE TRACKING

1. Early/Late Gate Tracking of Square Law Detected Sea Returns

When one examines Figure E-1, which shows the characteristic return if square law detection is used, and the effect of sea state on the characteristic return, it becomes evident that an early gate starting at $t = t_o$ and ending at $t = t_o + T_p$ will on the average contain one half as much energy as the average energy in a late gate starting at $t = t_o + 2T_p$ and ending at $t = t_o + 3T_p$. The reason for positioning the late gate at $t_o + 2T_p$ is to preclude the possibility of sea state affecting the average energy in the late gate.

Square law detection of the return gives more noise per return than envelope detection since in square law detection the signal standard deviation is equal to the signal expected value, V_{agc}, while in envelope detection the signal standard deviation is equal to 52.3% of the signal expected value, V_{agc}.

2. Control Function for Early/Late Gate Tracking of Square Law Detected Sea Returns

The relative positions of the early and late gates are fixed. Each gate has a width of T_g seconds and there is a separation between the gates of T_g seconds. When correctly positioned on the square law detected returns the expected value of the integral of voltage in the early date is $(V_{agc}\ T_g)/2$ and the expected value of the integral of voltage in the late gate is $V_{agc}\ T_g$.

The control function of Figure E-2 is generated if one half the integral voltage in the late gate is subtracted from the integral voltage in the early gate and then the early gates leading edge position is shifted from $t_o - 4T_g$ to $t_o + 4T_g$. Antenna beamwidth limiting will cause the return to go to zero some microseconds after t_o so that the control function will go from positive to zero and remain there when displaced past the beam limiting time.

Note in Figure E-2 that the effect of sea state on the control function is to decrease slightly the gain (i.e., the slope of the wave) at t_o position. A large change of gain would make implementation of the tracking servo difficult, but the gain change evidenced is too small to cause concern in that respect. This

servo should track at mean sea level even with the highest sea states expected, but at these high sea states there is a slightly greater error contribution than with very small sea states.

3. Expected Square Law Detection Tracking Error

The use of Early/Late Gate tracking on a square law detected return is attractive in a high pulse repetition frequency (i.e., ambiguous range) radar system. Specifically with a PRF of about 5000 per second the time to acquire the return signal is less than five seconds. The time constant of the tracking loop can be set to average about 100 returns for both acquisition and tracking control.

With this time constant the RMS error voltage after filtering per gate will be:

$$\sigma_{VRMS} = \pm \frac{V_{agc}\, T_g/2}{\sqrt{100}} \qquad T_g = T_p \qquad \text{(E-1)}$$

The RMS time error caused by this RMS voltage error will be:

$$\sigma_{tRMS} = \pm \frac{\sqrt{2}\,\sigma_{VRMS}}{G_{CF}} \qquad \text{(E-2)}$$

where

G_{CF} = Control function gain at zero error position

The control function gain at and near zero error position is:

$$G_{CF} = V_{agc} \frac{\text{(volt seconds)}}{\text{(seconds)}} \qquad \text{(E-3)}$$

Substituting values into equation (E-2) from equations (E-1) and (E-3) gives the RMS time error of the tracking loop as:

$$\sigma_{tRMS} = \frac{T_p}{\sqrt{2}\ \sqrt{100}} = 0.0707\ T_p \text{ (seconds)} \qquad \text{(E-4)}$$

At a PRF of 5000, where 50 altitude time counts are averaged to give an output altitude time once every second, there is a further reduction of the time error so that:

$$\sigma^{*}_{tRMS} = \frac{\sigma_{tRMS}}{\sqrt{50}} = 0.01T_p \qquad \text{(E-5)}$$

With a pulse width, T_p, of 100 nanoseconds the RMS time error due to tracked return noise would be ±0.152 meters.

4. Early/Late Gate Tracking of Envelope Detected Sea Return

The characteristic return when envelope detection is used and the effect of sea state on the characteristic return is shown in Figure E-3. The characteristic return itself is not symmetrical about $T_p/2$. Also note that the effect of a larger sea state is to produce a considerable signal preceeding $t = t_o$. It is apparent that sea state will cause Early/Late Gate tracking of envelope detected returns to be biased toward the wave tops. That is the position of the zero crossing of the control curve will move in the minus t direction. The actual zero shift of the control curve depends on the ratio of the transmitted pulse length, T_p, to the sea state characteristic wave height, $H_{1/3}$.

When the transmitted pulse width is chosen to be 50 nanoseconds, Figure E-4 shows the control function for an Early/Late Gate tracker in which the gate durations and relative positions are the same as those for the square law detector described in Figure E-1. Figure E-5 shows in finer detail the effect of sea state on the zero crossing of this control function.

Note that for a sea state with significant wave heights of 18.5 meters, the time shift of the control function zero crossing is approximately 12 nanoseconds which translates to an altitude bias error of about 2 meters.

5. Expected Envelope Detection Tracking Error

If the time constant of the tracking loop is set to average 100 returns for both acquisition and tracking control, the expected value of the integral of voltage in the early gate is $(2/3)V_{agc}\,T_p$. The control function is established by subtracting 2/3 the integral of voltage obtained in the late gate.

The RMS error voltage per gate will be:

$$\sigma_{VRMS} = \frac{\sqrt{\frac{4-\pi}{\pi}}\ \frac{2}{3}\ V_{agc}\ T_p}{\sqrt{100}} \qquad \text{(E-6)}$$

The RMS time error caused by this error per gate will be:

$$\sigma_{tRMS} = \frac{\sqrt{2}\ \sigma_{VRMS}}{G_{CF}} \qquad \text{(E-7)}$$

where

G_{CF} = Control function gain at zero error position

The control function gain at, and near, zero error position is:

$$G_{CF} = V_{agc}\ (\frac{\text{volt seconds}}{\text{second}}) \qquad \text{(E-8)}$$

Substituting values into equation (E-7) gives the RMS time error of the tracking loop as:

$$\sigma_{tRMS} = 0.0495T_p \qquad \text{(E-9)}$$

At 5000 PRF, 50 altitude time counts are averaged to give an output altitude time once every second. This gives a further reduction of time error to a value of:

$$\sigma^*_{tRMS} = \frac{\sigma_{tRMS}}{\sqrt{50}} = 0.007T_p \qquad \text{(E-10)}$$

With a pulse width, T_p, of 100 nanoseconds the RMS time error would be ±0.7 nanoseconds which translates to an RMS altitude error of 0.107 meters.

6. Gated Envelope Detection Sea State Measurement

Examination of Figure E-3 shows that the return expected before t_o is a function of wave height, $H_{1/3}$. This suggests the possibility that a gate, T,

seconds long immediately preceeding the early gate will have a volt-time integral content which is a function of wave height. Figure E-6 shows approximately the amount of energy in the sea state gain obtained as a function of significant wave height, $H_{1/3}$ using a transmitted pulse length, T_p, of 50 nanoseconds.

The combined effect of increasing the pulse length to 100 nanoseconds and maintaining the level of V_{agc} is to reduce this curve by 1/2, and also to reduce the sea state bias error of Figure E-5 by 1/2.

The expected accuracy of estimation of sea state significant height using this sea state gain approach is arrived at by the same process used in analyzing the early-late gate tracking accuracy.

Assume a PRF of 5000 and an averaging time constant for the sea state gate of one second. Then the error on a sea state measurement will be:

$$VSS = \frac{\sqrt{\frac{4-\pi}{\pi}}\, V_{SS}}{\sqrt{5000}} = 0.0074\, V_{SS} \qquad \text{(E-11)}$$

That is we could expect to measure the sea state voltage to an RMS accuracy of approximately ±1% due to return noise alone if the sea state gate stayed perfectly positioned during the total time.

Gate positions, however, are constantly moving with respect to the perfect position, t_0, and would generate dc errors equivalent to about 1 meter sigificant wave height, with an RMS jitter of about one meter significant wave height.

Thus measurement of significant wave heights less than about 2 meters is not to be expected, but measurement of wave heights from 5 to 20 meters to an accuracy of ±1 meter RMS looks feasible using a sea state gate.

The sea state altitude bias error shown in Figure E-5 can be corrected to less than one meter using this sea state measurement.

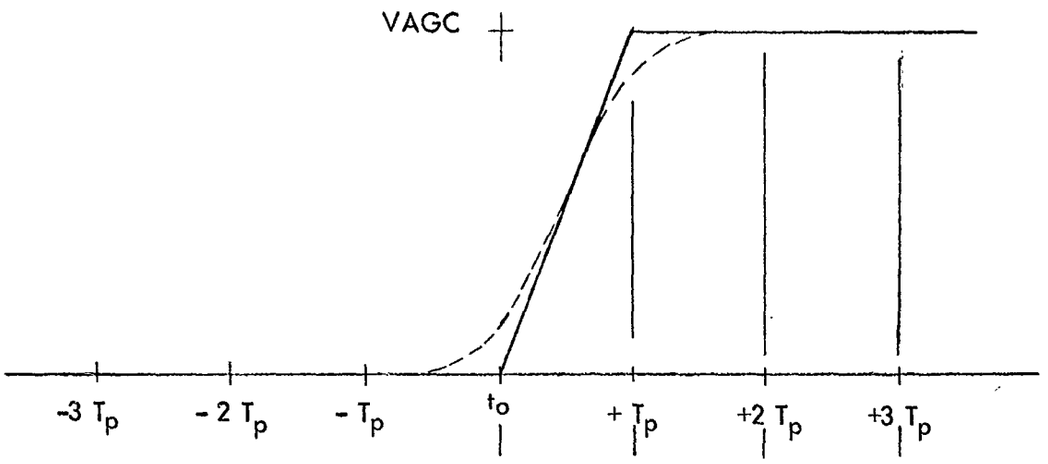

CHARACTERISTIC OCEAN RETURN WITH SQUARE LAW DETECTION
LOW SEA STATE (SOLID LINE) HIGH SEA STATE (DASHED LINE)

FIGURE E-1

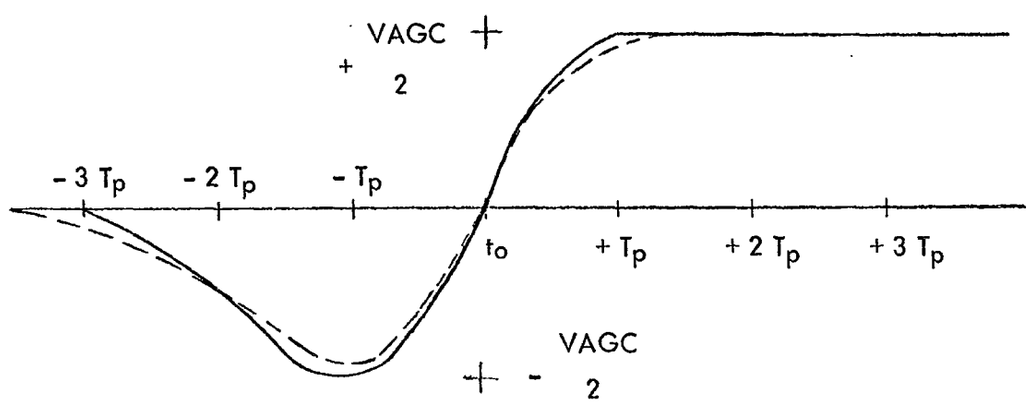

EARLY/LATE GATE CONTROL FUNCTION SQUARE LAW DETECTION
LOW SEA STATE (SOLID LINE) HIGH SEA STATE (DASHED LINE)

FIGURE E-2

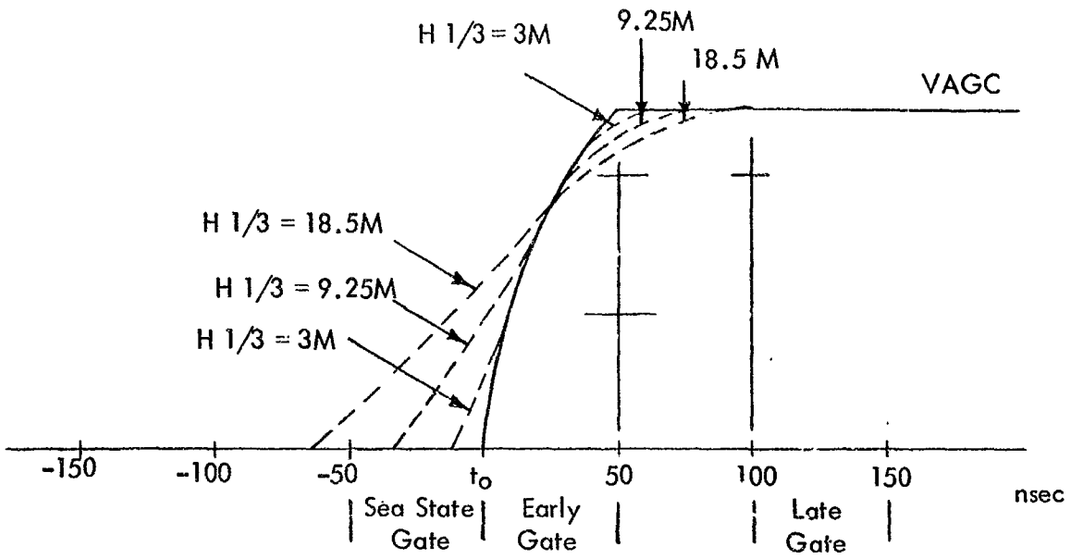

CHARACTERISTIC OCEAN RETURN WITH ENVELOPE DETECTION LOW SEA STATE (SOLID LINE), SEA STATES FROM H 1/3 = 3 TO 18.5 METERS(DASHED LINE)

FIGURE E-3

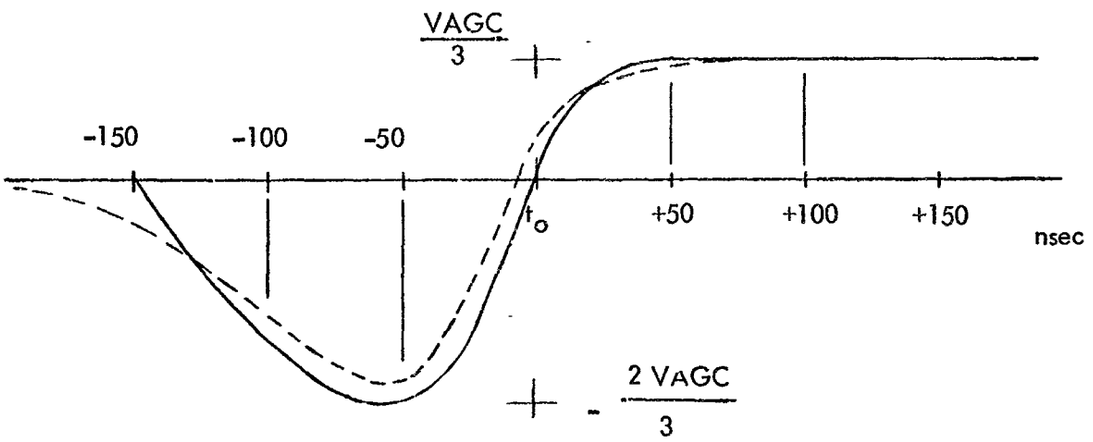

EARLY/LATE GATE CONTROL FUNCTION, ENVELOPE DETECTION LOW SEA STATE (SOLID LINES), HIGH SEA STATE H 1/3 = 18.5 METERS (DASHED LINES)

FIGURE E-4

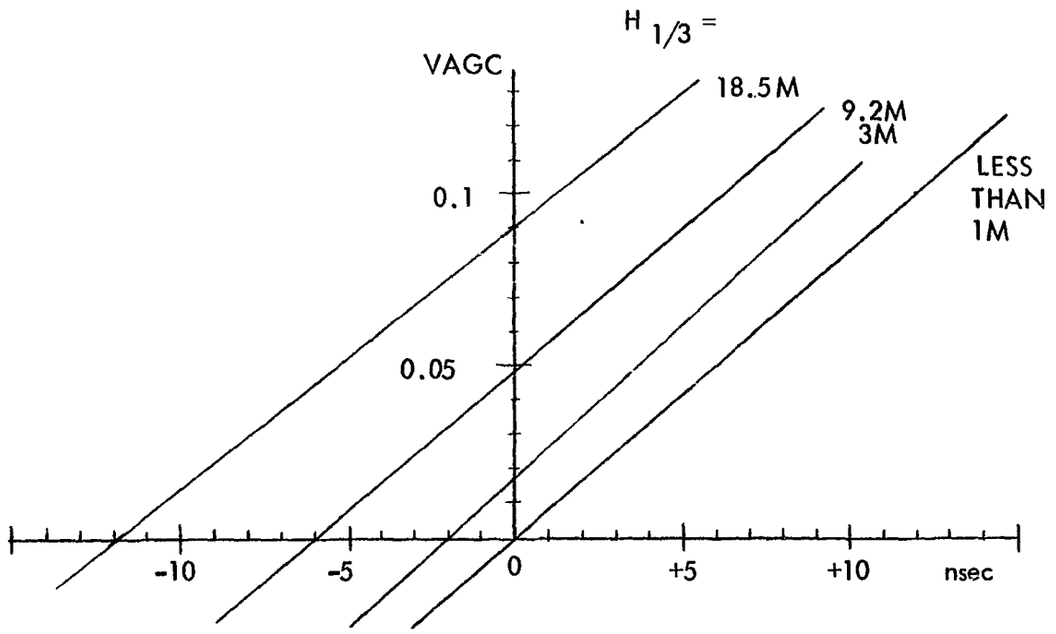

EFFECT OF SEA STATE UP TO $H_{1/3}$ = 18.5 METERS ON EARLY/LATE GATE, ENVELOPE DETECTION CONTROL FUNCTION ZERO CROSSING POINT

FIGURE E-5

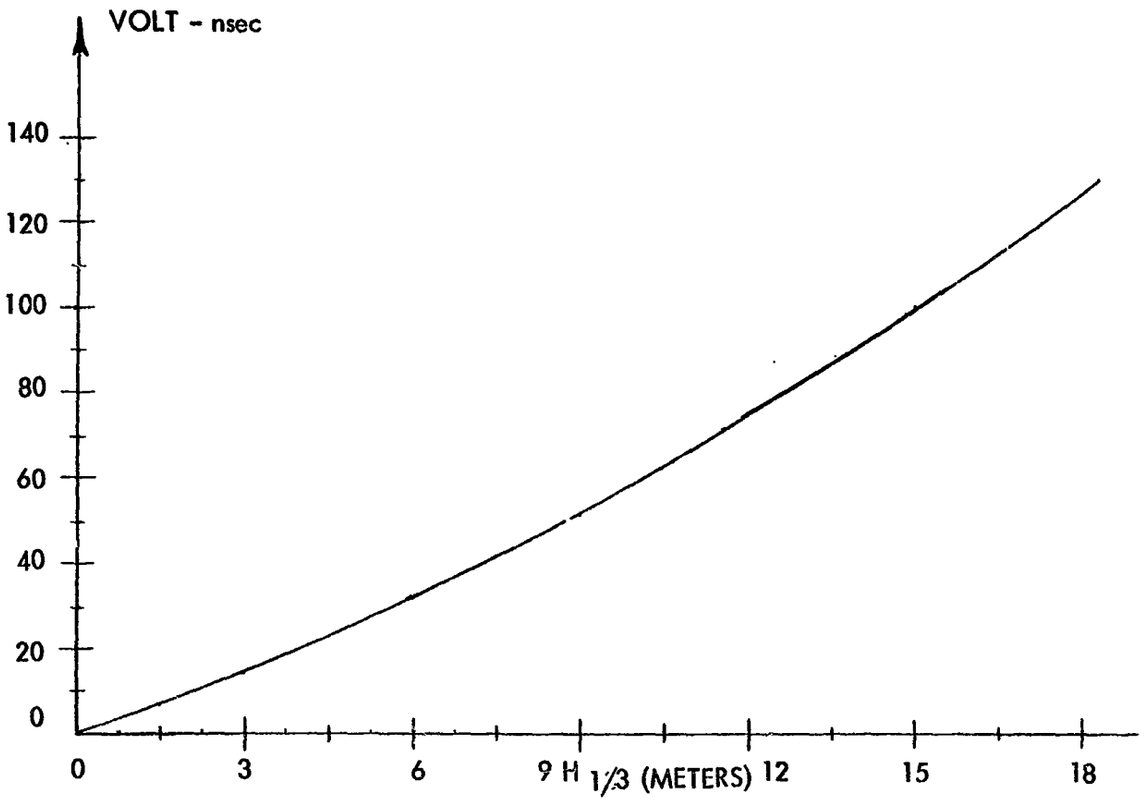

AVERAGE VOLT - nsec ENERGY IN SEA STATE GATE VERSUS
SIGNIFICANT WAVE HEIGHT ($H_{1/3}$) IN METERS

FIGURE E-6

APPENDIX F
METEOROLOGICAL ECHOES AND ATTENUATION

An analysis of the meteorological effects on the signal propagation show that weather echoes can be handled in the X-Band to Ku-Band range, but the rainfall attenuation effects make the X-Band frequency preferable.

1. Meteorological Echoes and Attenuation

Antenna size and transmitter availability considerations lead to a choice of frequency in the 8 to 16 GHz range. Since the backscatter cross sections of rain and clouds become significant at these short wavelengths, an analysis of the expected returns is necessary to determine the weather echoes.

To accomplish the analysis, the following assumptions are made:

1. The satellite altitude is 6×10^5 meters.
2. The altitude of rain storms is 10^3 meters.
3. Heavy storm centers have a radius of 5×10^2 meters.
4. The thickness of rain storms or clouds is 10^3 meters.
5. The antenna beamwidth does not limit the return (A 6° x 6° antenna would limit the return for cloud thickness greater than 10^3 meters.)
6. The cross section per unit area (σ_0) of the ocean is 3 db (worst case).

First the range cells for the ocean surface and rain storms will be computed. The backscatter cross section of the rain is estimated from Figure 12.10, Reference 1. The backscatter cross section for clouds and fog is much less than that of moderate rain, hence echoes from them will only be computed if the echoes from moderate rain are significant.

2. Range Resolution Cells

The geometry of the ocean return is shown in Figure F-1. The maximum pulse width under consideration is 100 nanoseconds. Consequently, at a range of 6×10^5 meters, the radius of the resolution cell is less than 5×10^3 meters.

For the geometry under consideration, the average received power rises to the following value in T_p seconds after the first returned energy is received.

$$P_R = \frac{P_T G^2 \lambda^2 c T_p \sigma_o}{4(4\pi)^2 R^3} \qquad \text{(F-1)}$$

where

P_T = Transmitted power
G = Antenna gain
λ = Wavelength
R = Altitude or one way range
c = Speed of light
T_p = Pulse width
σ_o = Radar cross section per unit area

The geometry of the large storm or cloud return is given in Figure F-2. From an altitude of 6×10^5 meters, the volume is approximated by a pill box of thickness $c\,T_p/2$. The radius of the pill box for the heavy storm center is given by the radius of the storm center itself. In the case of large moderate storms, the radius is calculated from knowledge of the thickness (D) of the storm. In either case, the volume of the resolution cell V_M is:

$$V_M = \pi R^2 \theta^2 \frac{c T_p}{2} \qquad \text{(F-2)}$$

where θ is specified in Figures F-2 and F-3. The target cross section for storms is then given by

$$\sigma = \pi R^2 \theta^2 \frac{c T_p}{2} \Sigma_i \sigma_i \qquad \text{(F-3)}$$

where $\Sigma_i \sigma_i$ is the cross section per unit volume and is plotted as a function of wavelength and rainfall rate in Figure 12.10 of Reference 1.

3. Storm Echoes

The echo received from a rain storm can be determined by substituting equation (F-3) in the range equation (F-1):

$$P_R = \frac{P_T G^2 \lambda^2 \sigma}{8(4\pi)^2 R^2} \qquad \text{(F-4)}$$

This gives

$$P_{R(STORM)} = \frac{P_T G^2 \lambda^2 \theta^2 c T_p \Sigma_i \sigma_i}{8(4\pi)^2 R^2} \qquad \text{(F-5)}$$

Since the ratio of the ocean echo to the storm is of interest, it is convenient to take the ratio of equations (F-1) and (F-5).

$$\frac{P_R}{P_{R(STORM)}} = \frac{2\sigma_o}{k R \theta^2 \Sigma_i \sigma_i} \qquad \text{(F-6)}$$

where σ_o is assumed to be 3 db, R is 6×10^5 meters and k accounts for the rain attenuation of the ocean return. The value for the backscatter cross section in Figure 12.10, Reference 1, is given in cm^2/m^3 by dividing by 10^4 or subtracting 40 db. Performing this scaling and converting equation (F-6) to decibel form gives the signal to storm echo ratio

$$\frac{P_R}{P_{R(STORM)}} = -12 + (-20) \log \theta - 10 \log S - 10 \log k \qquad \text{(F-7)}$$

where S is the value from Figure 12.10, Reference 1. The rain attenuation factor is obtained from Figure 15.4, Reference 2. For a large storm with a moderate rainfall rate (5mm/hr.), θ is approximately 0.05 radians and S is 10^{-2}. The signal to storm echo ratio is

$$\frac{P_R}{P_{R(STORM)}} = -12 + 26 + 20 - 1 = 33 \text{ db} \qquad \text{(F-8)}$$

for λ approximately equal to 2 cm.

Likewise, for a heavy rainfall rate (20mm/hr.) and a storm radius of 500 meters, the signal to storm echo ratio is

$$\frac{P_R}{P_{R(STORM)}} = -12 + 62 + 0 - 3 = +47 \text{ db} \qquad \text{(F-9)}$$

Note that the ratios computed in equations (F-8) and (F-9) were based on a 2 cm wavelength of 15 GHz signal. The graph of Figure 12.10 Reference 1 indicates that a significant improvement can be achieved by using X-Band, however, the ratios computed are sufficiently high for reliable operation under the assumed conditions.

4. Cloud Echoes

Since cloud echoes are much smaller than rain echoes (typically one-millionth), it is not necessary to compute their intensity for the altimeter application.

5. Rain Attenuation

The rain attenuation factor was introduced in the storm echo analysis. From Figure 15.4 of Reference 2, the attenuation in heavy rain (16mm/hr.) is 3 db per mile for a 2 cm wave and 1 db per mile for a 3 cm wave (referred to the two way range). For this reason, the X-Band frequency is definitely preferred over the Ku-Band frequency.

6. Attenuation Due to Oxygen and Water Vapor

To evaluate the atmospheric attenuation of a signal transmitted from a spacecraft to earth due to natural oxygen and water vapor, the results of Figure 1, Reference 3 can be used. These results indicate that the two way attenuation is 0.2 db at 9 GHz and 0.4 db at 15 GHz.

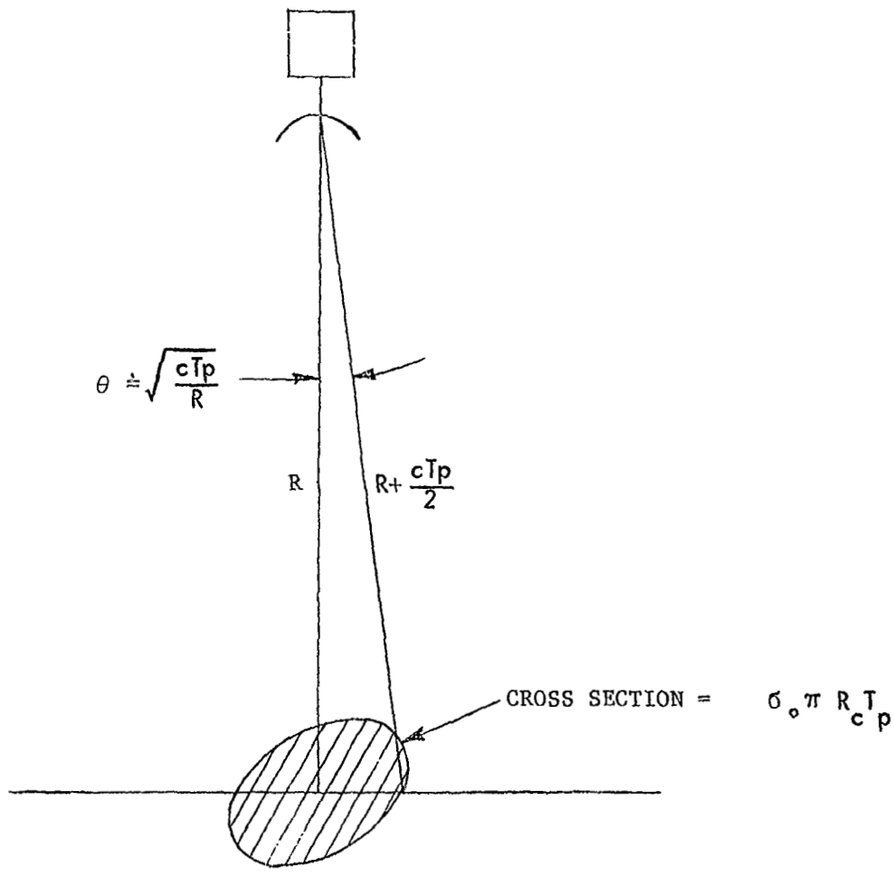

FIGURE F-1 GEOMETRY OF THE OCEAN RETURN

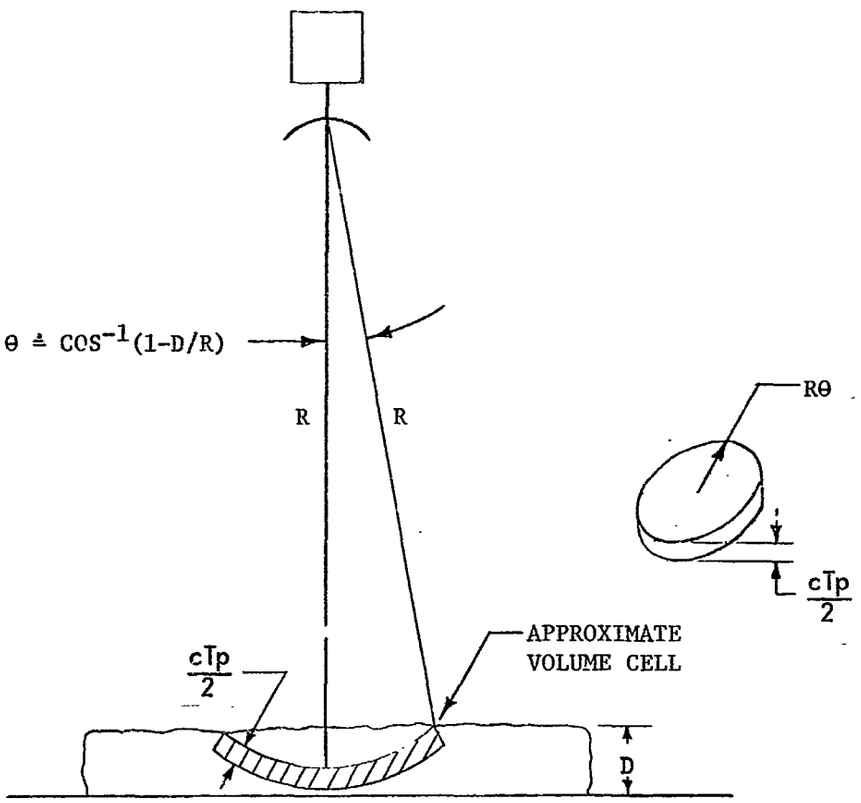

CROSS SECTION OF THE VOLUME OF THE RESOLUTION CELL FOR A STORM RETURN

FIGURE F-2

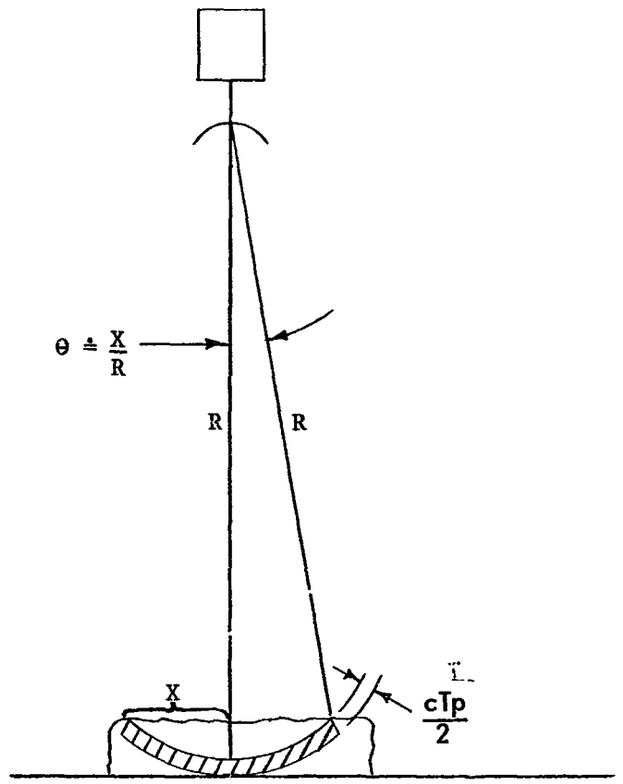

FIGURE F-3 RETURN FROM A HEAVY STORM CENTER